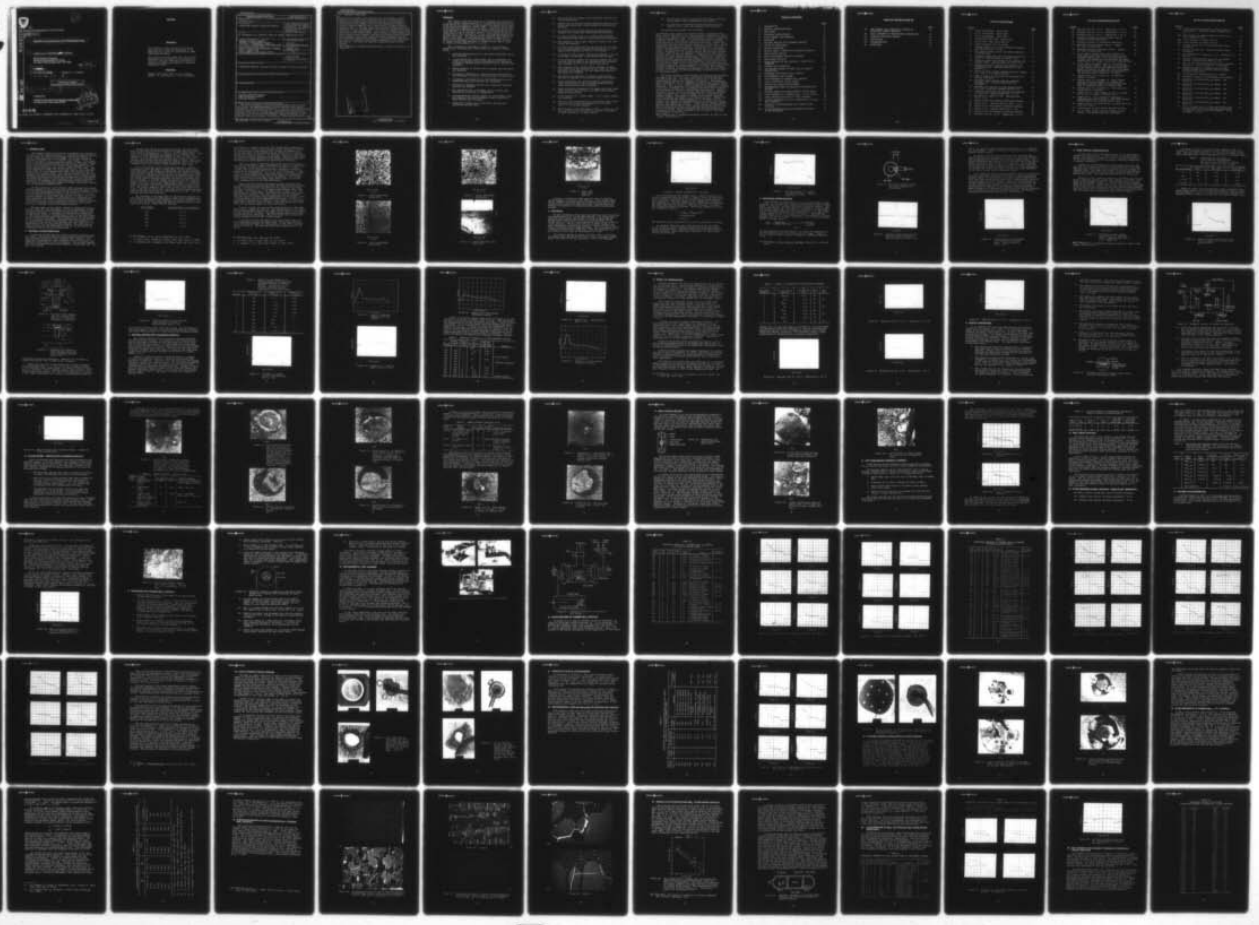
AD-A047 732 GENERAL ELECTRIC CO SCHENECTADY N Y RESEARCH AND DEV--ETC F/G 9/1
PROTECTIVE COAXIAL SWITCHING DEVICES.(U)
OCT 77 L M LEVINSON, H R PHILIPP, G A SLACK DAAB07-76-C-1331
UNCLASSIFIED SRD-77-158 ECOM-76-1331-F NL

1 OF 2
AD
A047 732



AD A047732

DDC FILE COPY

(12) 25

(11) Research and Development Technical Report

ECOM-76-1331-F

(18)

(6) # PROTECTIVE COAXIAL SWITCHING DEVICES,

(10) L.M. Levinson, H.R. Philipp [redacted] G.A. Slack

General Electric Company
Research and Development Center
P.O. Box 8, Schenectady, New York 12301

(12) 193 p.

(11) Oct [redacted] 77

(9) Final Technical Report. 76 June 15 — 77 June 14

15 Jun 76 – 14 Jun 77,

DISTRIBUTION STATEMENT
Approved for public release; distribution unlimited

(15) DAABØ7-76-C-1331 (16) 1S762705AH94 (17) W3

Prepared for

UNITED STATES ARMY ELECTRONICS COMMAND
Fort Monmouth, New Jersey 07703

DDC
RECEIVED
DEC 16 1977
A

ECOM

US ARMY ELECTRONICS COMMAND FORT MONMOUTH, NEW JERSEY 07703

149440

(14) SRD-77-158

NOTICES

Disclaimers

The findings in this report are not to be construed as an official Department of the Army position, unless so designated by other authorized documents.

The citation of trade names and names of manufacturers in this report is not to be construed as official Government indorsement or approval of commercial products or services referenced herein.

Disposition

Destroy this report when it is no longer needed. Do not return it to the originator.

UNCLASSIFIED

SECURITY CLASSIFICATION OF THIS PAGE *(When Data Entered)*

REPORT DOCUMENTATION PAGE		READ INSTRUCTIONS BEFORE COMPLETING FORM
1. REPORT NUMBER ECOM-76-1331-F	2 GOVT ACCESSION NO.	3. RECIPIENT'S CATALOG NUMBER
4. TITLE *(and Subtitle)* PROTECTIVE COAXIAL SWITCHING DEVICES		5. TYPE OF REPORT & PERIOD COVERED FINAL TECHNICAL REPORT 76 JUNE 15 - 77 JUNE 14
		6. PERFORMING ORG. REPORT NUMBER SRD-77-158
7. AUTHOR(s) L.M. LEVINSON, H.R. PHILIPP, AND G.A. SLACK		8. CONTRACT OR GRANT NUMBER(s) DAAB07-76-C-1331
9. PERFORMING ORGANIZATION NAME AND ADDRESS GENERAL ELECTRIC COMPANY RESEARCH & DEVELOPMENT CENTER P.O. BOX 8, SCHENECTADY, NEW YORK 12301		10. PROGRAM ELEMENT, PROJECT, TASK AREA & WORK UNIT NUMBERS 6-27-05-A 1S762705 AH94 W3 014
11. CONTROLLING OFFICE NAME AND ADDRESS UNITED STATES ARMY ELECTRONICS COMMAND ATTN: DRSEL-TL-MD FORT MONMOUTH, NEW JERSEY 07703		12. REPORT DATE OCTOBER 1977 13. NUMBER OF PAGES 89
14. MONITORING AGENCY NAME & ADDRESS*(if different from Controlling Office)*		15. SECURITY CLASS. *(of this report)* UNCLASSIFIED 15a. DECLASSIFICATION/DOWNGRADING SCHEDULE

16. DISTRIBUTION STATEMENT *(of this Report)*

DISTRIBUTION STATEMENT Approved for public release; distribution unlimited

17. DISTRIBUTION STATEMENT *(of the abstract entered in Block 20, if different from Report)*

18. SUPPLEMENTARY NOTES

19. KEY WORDS *(Continue on reverse side if necessary and identify by block number)*

COAXIAL SWITCHING DEVICE
NEMP PROTECTIVE DEVICE
NIOBIUM DIOXIDE

20. ABSTRACT *(Continue on reverse side if necessary and identify by block number)*

The use and performance of both polycrystalline NbO_2 on NbO and single-crystal NbO_x chips ~~supplied by ECOM~~ in a coaxial switching device has been investigated. The polycrystalline material, ~ 10 μm thick, does exhibit switching with a delay time of less than 1 ns. The threshold switching voltage is typically 100 to 300 V. A manufacturable packaging configuration with evaporated small area contacts has been developed. Step-by-step details of all pertinent fabrication procedures, from selection of "as-received" chips to final

DD FORM 1 JAN 73 1473 EDITION OF 1 NOV 65 IS OBSOLETE

UNCLASSIFIED

SECURITY CLASSIFICATION OF THIS PAGE *(When Data Entered)*

20. ABSTRACT (CONTINUED)

mounting and wire bonding of the completed units are described. Device stability for a range of pulse lengths has also been investigated and is discussed in some detail. The electrical parameters of the as-supplied polycrystalline chips, however, do not meet the specifications listed in Technical Guidelines DAAB07-76-Q-1335, which require a threshold switching voltage of <100V. In addition, device degradation with repeated pulsing is observable, even for 3 ns pulse widths, and is markedly accelerated for larger pulse widths. Single-crystal chips, ∿ 25 μm thick, also exhibit switching at essentially the same electric field. Device stability in these thicker single-crystal samples is much improved. Switching and associated sparking phenomena were investigated in air, freon, helium, and vacuum environments, and only minor behavioral differences were observed. These studies also indicate that switching is not sensitive to the labeled stoichiometry of the "as-received" NbO_x crystals. One hundred and fifty (150) completed devices have been supplied.

*For a definition of threshold switching voltage, as used in this report, see Section 31.



SUMMARY

The present study was initiated to determine the feasibility of using niobium dioxide material in a threshold switching device which serves as a means of circuit protection against the effects of Nuclear Electromagnetic Pulses (NEMP). According to the Technical Guidelines DAAB-76-Q-1335, the device must have sufficiently high impedance in the off state to ensure minimum insertion loss (less than 0.4 db at 200 MHz), while in the on state the device voltage should never exceed 100 V with a corresponding delay time of less than 1 ns. The niobium dioxide material was supplied by ECOM in two forms: 1) polycrystalline layers of NbO_2, $\sim$10 μm thick on NbO substrates $\sim$3 mm in diameter and $\sim$0.6 mm thick and 2) single crystal NbO_x materials of various sizes with a range of labeled stoichiometry $1.87 \leq x \leq 2.00$.

The investigation proceeded according to the following (essentially chronological) steps, which are listed in summary below:

1. Material characterization of the supplied NbO/NbO_2 chips was completed.

2. A test system with cable pulser and 75 picosecond (ps) resolution sampling scope was assembled and calibrated. A system to measure device insertion loss at 480 MHz was assembled.

3. System response to various device package configurations was measured.

4. Switching of NbO/NbO_2 in a point contact configuration was evaluated to provide a reference point to prior work.

5. A packaging configuration for the NbO/NbO_2 devices with evaporated small area contacts was developed.

6. Switching of NbO/NbO_2 devices with evaporated aluminum contacts was studied.

7. The characteristics of NbO/NbO_2 coaxial devices were measured as a function of temperature.

8. A sputtered Nb/Au contact system for the NbO/NbO_2 chips was prepared, and the performance characteristics of these devices were evaluated.

9. Twenty-four mounted coaxial switching devices were fabricated and delivered.

10. Failure modes for samples with evaporated aluminum contacts were studied.

11. Samples with no foreign contact materials (back-to-back chips) were pulsed and failure modes in these devices observed.

12. An additional 26 mounted coaxial switching devices (making 50 in total) were fabricated and delivered.

13. A variety of NbO_x ($2.00 \geq x \geq 1.87$) single crystals was electroded and mounted in microwave diode packages.

14. The response of the single crystals to short rise time pulses was measured.

15. A Velonex Pulse Generator for the evaluation of switching in single-crystal niobium dioxide was set up, and samples were tested with 100 ns, 2 kV pulses.

16. A variety of NbO_x single crystals was thinned ($\sim$ 25 μm), electroded, and mounted in microwave diode packages.

17. An environmental chamber for quickly changing the pressure and type of ambient gas surrounding the microwave diode package and 50 Ω test fixture was set up.

18. The response of the thinned single crystals to short rise time pulses was measured in air, freon 12, helium, and vacuum environments, and the associated sparking phenomena were studied.

19. The electrical stability of thinned single-crystal devices to repeated 50 ns duration pulses was studied.

20. Light microscopic and scanning electron microscopic (SEM) examinations of device damage associated with pulsing and sparking were performed.

21. Light microscopic examination of damage occurring underneath the ball bond contact in pulsed single-crystal samples was performed.

22. Pulse response of a thinned NbO_2 + 5% Ti crystal sample was measured.

23. The X-ray lattice parameters of as-received NbO_x single crystals with labeled stoichiometry in the range $1.87 \leq x \leq 2.00$ were measured.

24. Metallurgical light microscopy on $NbO_{1.87}$, $NbO_{1.89}$, and $NbO_{1.90}$ crystals was performed to reveal the presence of phase separation in these samples.

25. Two different types of polycrystalline NbO_x on NbO substrate samples were prepared and pulse tested.

26. An additional 100 mounted coaxial switching devices (making 150 in total) were prepared and delivered.

The primary conclusions are as follows:

The NbO/Nbo_2 chips supplied by ECOM do exhibit switching with a delay time of less than 1 ns. The electrical parameters of these chips do not, however, meet the specifications listed in Technical Guidelines DAAB07-76-Q-1335. The threshold switching voltage* is typically 100 to 300 V and not <100 V as specified. Switching characteristics and off-state resistance are highly variable between chips and even from place to place on a single chip. Device degradation with repeated pulsing is observable for 3 ns pulse width, and degradation is markedly accelerated for larger pulse widths. Samples subjected to long (50 ns) pulses or to extensive pulsing (thousands of 3 ns pulses) exhibit deep channels through the NbO_2 layer to the NbO substrate. Samples with less severe pulsing show less physical damage, but deterioration is sometimes observed in device off-state resistance. There is no clear correlation between physical damage and device off-state resistance. The switching characteristics and degradation with pulsing of the devices do not appear to be a function of the electrode material. Polycrystalline NbO_x layers prepared by oxidizing NbO single-crystal surfaces probably have stoichiometry $x < 2.0$ when the available "oxygen" pressure is reduced, as compared to that used by Yeshiva University in preparing the NbO_2/NbO chips received at the onset of the present work.

The single-crystal devices exhibit switching at approximately the same field, 20 to 30 V/μm, as found for the NbO_2/NbO polycrystalline devices. The electrical stability of the thicker single-crystal devices is, however, much better. Switching and device degradation are not dependent on the crystal stoichiometry, NbO_x, for $1.89 \leq x \leq 2.0$. Sparking frequently accompanies device switching. This sparking is not related to the dielectric strength of the gas environment but is probably associated with a thermal volatilization of material from the NbO_x upon pulsing. Damage in the form of pits $\sim$ 25 μm in diameter and 20 μm deep is observed around the periphery of the ball bond contact in pulsed single-crystal samples. The amount of damage is correlated with the severity (number and length) of the applied pulses. Damage also occurs under the ball bond contact but is not nearly as pronounced. The switching characteristics of Ti doped (5%) single-crystal NbO_2 samples are similar to those of the undoped crystal; however, the resistance is lower. X-ray studies of as-received NbO_x single-crystal samples with labeled stoichiometries of 1.89 and 1.87 indicate they are two-phase and consist of NbO_2 with inclusions of NbO. This two-phase nature is clearly confirmed by microscopic examination.

*For a definition of threshold switching voltage, as used in this report, see Section 31.

Preceding Page BLANK - FILMED

TABLE OF CONTENTS

		Page
1.	INTRODUCTION	1
2.	MATERIAL CHARACTERIZATION	1
3.	TEST SETUP	6
4.	PACKAGING CONFIGURATIONS	8
5.	POINT CONTACT CONFIGURATION	11
6.	PACKAGING	14
7.	NbO/NbO_2 DEVICES WITH ALUMINUM CONTACTS	16
8.	EFFECT OF TEMPERATURE	21
9.	CONTACT PROCEDURES	24
10.	FAILURE MODES - SAMPLES WITH ALUMINUM CONTACTS	29
11.	BACK-TO-BACK DEVICES	35
12.	FIFTY PRELIMINARY FEASIBILITY MODELS	37
13.	NbO_x SINGLE CRYSTALS	39
14.	PULSE RESPONSE OF NbO_x CRYSTALS - CABLE PULSE GENERATOR	39
15.	VELONEX PULSE GENERATOR	40
16.	CAT WHISKER CONTACT ON THICK $NbO_{1.87}$ SINGLE-CRYSTAL CHIP	42
17.	PROCEDURE FOR THINNING NbO_x CRYSTALS	44
18.	ENVIRONMENTAL TEST CHAMBER	46
19.	PULSE RESPONSE OF THINNED NbO_x CRYSTALS	48
20.	S.E.M. STUDIES OF DEVICE DAMAGE	59
21.	EFFECTS OF CRYSTAL STOICHIOMETRY	62
22.	ENVIRONMENTAL TESTS ON NbO_2/NbO POLYCRYSTALLINE DEVICES	62
23.	FURTHER STUDIES OF SINGLE-CRYSTAL DEVICE DAMAGE	65
24.	PULSE RESPONSE OF A THINNED NbO_2 + 5% Ti CRYSTAL	68
25.	X-RAY STUDIES OF AS-RECEIVED NbO_x CRYSTALS	70
26.	SURFACE MICROSCOPY OF METALLOGRAPHICALLY POLISHED NbO_x CRYSTALS	73
27.	GROWTH OF POLYCRYSTALLINE NbO_2 LAYERS ON NbO CRYSTALS	77
28.	PULSE RESPONSE OF NbO_x POLYCRYSTALLINE LAYERS ON NbO SUBSTRATES	79

TABLE OF CONTENTS (CONT'D)

		Page
29.	ONE HUNDRED FINAL FEASIBILITY MODELS OF PROTECTIVE COAXIAL SWITCHES	81
30.	FINAL STATEMENT OF MANUFACTURING FEASIBILITY	83
31.	THRESHOLD SWITCHING VOLTAGE	83
32.	CONCLUSIONS	85
33.	RECOMMENDATIONS	85
34.	REFERENCES	88

LIST OF ILLUSTRATIONS

Figure		Page
1	S.E.M. photograph. Batch #102.	4
2	S.E.M. photograph. Batch #104.	4
3	S.E.M. photograph. Batch #105.	5
4	Cleaved NbO/NbO_2 chip. Batch #105.	5
5	Batch #105. NbO_2 layer edge on.	6
6	System response for 3 ns pulse.	7
7	Voltage across 5 Ω coaxial microwave resistor. Applied pulse 500 V, 3 ns.	8
8	Foil strip between center and outer conductor of GR-874 line.	9
9	Inductive spike from the foil shorting strip of Figure 8. Applied pulse is 250 V, 3 ns.	9
10	Inductive spike from shorted 1N-23 package (cat whisker type). Applied pulse is 500 V, 3 ns.	10
11	Switching of point contact configuration for NbO/NbO_2 device. Applied pulse 50 V, 3 ns. Sample L-7.	11
12	Switch of point contact configuration for sample L-6. 500 V, 3 ns applied pulse.	12
13	Data of Figure 12 digitized and corrected for package inductance.	13
14	Microwave diode package used for mounting NbO/NbO_2 chip. Various dimensions are available.	15
15	NbO/NbO_2 chip mounted in diode package which fits into a specially adapted GR-874 "tee."	15
16	Inductive spike from the shorted diode package of Figure 15. Applied pulse 500 V, 3 ns.	16
17	Switching in sample X-3-4B. Applied pulse 500 V, 3 ns.	17
18	Sample X-3-4B with package inductance removed.	18
19	Sample X-2-3. Applied pulse is 500 V, 3 ns.	18
20	Sample X-2-3 with package inductance removed.	19
21	Sample X-3-4. Applied pulse 500 V, 3 ns.	20
22	Sample X-3-4 with package inductance removed.	20
23	NbO_2/NbO chip No. X-3-9. Temperature = 26 °C.	22

LIST OF ILLUSTRATIONS (CONT'D)

Figure		Page
24	NbO_2/NbO chip No. X-3-9. Temperature = 83 °C.	23
25	NbO_2/NbO chip No. X-3-9. Temperature = -54 °C.	23
26	NbO_2/NbO chip No. X-3-9. Temperature = 26 °C.	24
27	Schematic drawing of sample holder used in grinding and polishing step.	25
28	Schematic drawing of sputtering apparatus.	26
29	NbO_2/NbO chip with Nb-Au contact. Sample No. X-13-4, Batch #102.	28
30	NbO_2/NbO chip with aluminum contact. Sample No. X-13-7, Batch #102.	29
31	S.E.M. photo of NbO_2 layer after removal of gold contact wires and partial etching of the aluminum contact pads. Four contact areas are visible, and regions a,b,c,d are shown at higher magnification in Figures 32,33,34,35, respectively.	30
32	S.E.M. photo of contact area "a" of Figure 31. Four pits are visible. Two are on the periphery of the contact area of the gold ball bond, the deeper pit being 6 μm deep and 13 μm in diameter. The two pits close together on the periphery of the aluminum contact area are 7 μm deep.	31
33	Contact area "b" of Figure 31. No physical damage is visible.	31
34	Contact area "c" of Figure 31. Major damage area is pit 10 μm diameter, 7 μm deep, on periphery (between edge of gold ball bond and edge of aluminum contact) of contact area.	32
35	Contact area "d" of Figure 31. This area was inadvertently scratched.	32
36	Sample X-13-8. Major damage is pit 13 μm deep, 16 μm dia. in center of contact area.	33
37	Sample X-6-1. This sample was subjected to long duration (10 μs) pulses. The crater formed extends beyond the aluminum contact area.	34
38	Sample X-6-1A. Two pits about 4 μm deep and 8 μm dia. are visible.	34
39	Construction of back-to-back NbO_2/NbO devices.	35
40	S.E.M. photo of NbO_2 surface of back-to-back device. Two damage areas are indicated.	36

LIST OF ILLUSTRATIONS (CONT'D)

Figure		Page
41a	Higher magnification photo of damage area "a" of Figure 40. The major crater is about 25 μm deep.	36
41b	Area adjacent to damage region of Figure 41a but on opposing chip.	37
42a	Pulse response of sample X-15-31.	38
42b	Pulse response of sample X-15-32.	38
43	Voltage across 200 Ω resistor-Velonex Pulse Generator.	41
44	Current through 200 Ω resistor-Velonex Pulse Generator.	41
45	Air breakdown for $V_{applied} > 2$ kV. Sample No. 2, $NbO_{1.95}$.	42
46	$NbO_{1.87}$ single-crystal chip with cat whisker contact. Applied pulse 1000 V, 3 ns.	43
47	Area of cat whisker contact after 1000 V pulses. The pit is ~ 14 μm across and ~ 20 μm deep.	44
48	Schematic drawing of lapping jig with NbO_x sample mounted on a tungsten disk surrounded by three glass shims.	45
49	Photographs of environmental test chamber.	47
50	Schematic diagram of environmental test chamber.	48
51	Switching in thinned $NbO_{1.89}$ sample. See Table 12.	50
52	Switching in thinned $NbO_{1.89}$ sample. See Table 12.	51
53	Switching in thinned $NbO_{1.90}$ sample. See Table 13.	53
54	Switching in thinned $NbO_{1.90}$ sample. See Table 13.	54
55	Switching in thinned $NbO_{1.90}$ sample. See Table 13.	55
56	Switching in thinned $NbO_{1.95}$ sample. See Table 14.	57
57	S.E.M. pictures at 14X, 350X, and 1400X of the $NbO_{1.89}$ sample after the experiments described in Table 12. The pits are of diameter ~ 30 μm and depth ~ 20 μm.	60

LIST OF ILLUSTRATIONS (CONT'D)

Figure		Page
58	S.E.M. pictures at 35X, 350X, and 1400X of the $NbO_{1.90}$ sample after the experiments described in Table 13. The largest visible pit is ~ 20 μm in diameter and ~ 22 μm deep.	61
59	Switching in a polycrystalline NbO_2/NbO sample (No. X-15-33). See Table 15.	64
60	S.E.M. pictures at 35X and 500X of a polycrystalline NbO_2/NbO sample (No. X-15-33) after the experiments described in Table 15.	65
61	Light microscope pictures at 375X and 750X of the $NbO_{1.89}$ sample after removal of the ball bond contact.	66
62	Light microscope pictures at 375X and 750X of the $NbO_{1.90}$ sample after removal of the ball bond contact.	67
63	Switching in thinned NbO_2 + 5% Ti. See Table 16.	70
64	Microscope pictures at 230X of metallographically polished NbO_x crystal surfaces for stoichiometry. (a) x = 1.90, (b) x = 1.89, and (c) x = 1.87	74
65	Microscope pictures at 1320X of metallographically polished NbO_x crystal surfaces for stoichiometry (a) x = 1.90, (b) x = 1.89, and (c) x = 1.87.	75
66	The oxygen partial pressure over the various two-phase regicns of the niobium-oxygen system as a function of temperature. The lowest line indicates the oxygen pressure in equilibrium with a mixture of niobium metal and NbO. The semiconductor-metal transition in NbO_2 occurs at T_x. The melting points are indicated by "M.P."	77
67	Schematic diagram of a two-temperature technique for oxidizing polished NbO crystal surfaces.	78
68	Switching in NbO_x layers grown by isothermal process. See Table 18.	80
69	Switching in NbO_x layers grown by a two-temperature process. See Table 19.	81
70	The response of chips No. X-15-29 to input voltage pulses of 100, 200, 300, 400, and 500 V. The device does not switch into its low impedance state until the applied voltage exceeds 400 V.	84

LIST OF TABLES

Table		Page
1	Pulse Behavior of Sample L-7 (point contact configuration). The sample was subjected to repeated pulsing at the 3 ns, 500 V level.	12
2	Pulse Behavior of Sample L-6 (point contact configuration). The sample was subjected to 500 V, 3 ns pulses.	13
3	Value of DC Resistance R at Various Points on the Chip Face for Three Nominally Identical Samples. An array of 125 μm diameter aluminum dots was evaporated on the sample face.	17
4	Behavior of Sample X-3-4 with Repeated Pulsing	19
5	Effect of Temperature Upon NbO_2/NbO Switching	22
6	Behavior of NbO_2/NbO Chip with Nb/Au Contacts	27
7	Behavior of NbO_2/NbO Chip with Aluminum Contacts	28
8	Damage Analysis - Sample X-14-1	30
9	Damage Analysis NbO_2/NbO Chips	33
10	Typical Behavior of Preliminary Feasibility Models of Coaxial Switching Device	39
11	Resistance and Maximum Applied Field for the NbO_x Single-Crystal Samples. The resistivity is computed from the resistance ignoring end effects and is only qualitatively correct.	40
12	Electrical Behavior of Thinned $NbO_{1.89}$ Crystal in Various Ambient Gases	49
13	Electrical Behavior of Thinned $NbO_{1.90}$ Crystal in Various Ambient Gases	52
14	Electrical Behavior of Thinned $NbO_{1.95}$ Crystal in Various Ambient Gases	56
15	Electrical Behavior of a Polycrystalline NbO_2/NbO Sample (No. X-15-33) in Various Ambient Gases	63
16	Electrical Behavior of Thinned NbO_2 + 5% Ti Crystal	69
17	Literature References for the Lattice Parameters of "NbO_2" at Room Temperature	72
18	Electrical Behavior of NbO_x Layers Grown By Isothermal Process	79
19	Electrical Behavior of NbO_x Layers Grown By Two-Temperature Process	80
20	Resistance Values of 100 Final Feasibility Models of Protective Coaxial Switches	82

1. INTRODUCTION

The present study was initiated to determine the feasibility of using niobium dioxide material in a threshold switching device which serves as a means of protection against the effects of Nuclear Electromagnetic Pulses (NEMP). To prevent damage to sensitive circuitry (e.g., a receiver input stage), it is necessary to provide a voltage-responsive device to shunt the incoming pulse to ground before reaching any such circuit elements. The device will normally be in a state of high impedance so as to cause minimal insertion loss in this normal, or OFF, mode. Upon being subjected to NEMP, the device must switch, with a minimum delay time, to a low impedance ON state, thus shunting and reflecting the incoming pulse. The reverse transition to the high impedance OFF state is effected by the end of the incoming pulse. Switching characteristics should be reproducible over the operating temperature range of the equipment, and the device should be capable of withstanding many rapid switching cycles under the full range of environmental conditions without significant alteration of operating characteristics.

For the purpose of this contract, ECOM furnished the niobium dioxide material in the form of thin polycrystalline layers, $\sim$10μm thick on niobium monoxide substrates and as single crystals of various labeled stoichiometries NbO_x in the range $1.87 \leq x \leq 2.00$. The work covered in this report had two main thrusts: (1) to determine whether the niobium dioxide material as supplied did exhibit switching and whether its characteristics fulfilled the requirements as set forth in Technical Guideline DAAB07-76-Q-1335, and (2) to formulate a manufacturable housing for the coaxial protective switching device with bonded contacts.

The main text of this report follows in essentially chronological order the work procedures, the tests performed, and the results achieved in the evaluation of the niobium dioxide chips as supplied by ECOM. A statement of manufacturing feasibility is also given, based on the experience gained in the fabrication of 150 niobium dioxide switching devices already delivered under terms of the work agreement. This includes step by step details of all pertinent fabrication procedures from the selection of as-received chips to the final mounting and wire bonding of the completed unit in microwave diode packages. The major conclusions of this work are summarized at the end of the report and recommendations for future studies given.

2. MATERIAL CHARACTERIZATION

A study of the NbO chips as grown by Yeshiva University has been made. These chips were melt-grown single crystals of NbO that had been cleaved and their surfaces then oxidized. The chips were approximately 3 mm in diameter and 0.6 mm thick, with substantial variations in these dimensions. We received samples from five different batches, batch numbers of which were 101, 102, 104, 105, and 110.

We have verified by X-ray powder patterns that the crystal body of the chips is actually NbO, with a cubic structure and X-ray lattice parameter of a = 4.211 ± .005 Å (sample #101). This value is in good agreement with Bowman et al,[1] Brauer and Morawietz,[2] and Anderson and Magneli[3], who all find 4.2105 ± .004 Å. We have also verified by X-ray back reflection on a cleavage face of NbO that the cleavage face is {100}. This might be expected since the NbO structure is related to[1,3], but not identical with, that of NaCl, which cleaves on {100} also.

All of the single-crystal chips were cleaved at Yeshiva University so that the large, active faces for the devices were {100} NbO faces. The chips, as cleaved but not further polished, were surface-oxidized at Yeshiva to give a thin layer of a higher niobium oxide. We have verified by an X-ray powder pattern that this layer is actually NbO_2, at least for a chip from batch #105. The recipe used by Yeshiva University for making this NbO_2 layer was as follows: 2 g of NbO chips (an average chip has a mass of about 3×10^{-2} g), plus 8 g of NbO_2 powder, plus 0.1 g of Nb_2O_5 powder are placed in a sealed, fused quartz tube 1.4 cm dia. and about 10 cm long. The air in the tube is evacuated before sealing. The tube is heated to 800 °C for 24 hrs., then 1000 °C for 2 hrs., then 900 °C for 22 hrs. The tube is then removed abruptly from the furnace and cooled to room temperature in air. All five batches were done this same way.

The thickness of the NbO_2 layer so produced was measured for each batch by cleaving the NbO along a (010) plane perpendicular to its (100) surface and then studying the fracture surface. The results with an optical microscope and a scanning electron microscope were similar. These were as follows:

Batch Number	NbO_2 Thickness in Micrometers
101	10 ± 2
102	11 ± 2
104	11 ± 2
105	11 ± 2
110	9 ± 2

1. A.L. Bowman, et al, Acta Crystallogr. 21, 843 (1966).
2. G. Brauer and H. Morawietz, Anorg. Allg. Chem. 317, 13 (1962).
3. G. Anderson and A. Magneli, Acta Chem. Scand. 11, 1065 (1957).

Some areas on a sample from batch #105 showed NbO_2 thicknesses of up to 20 μm in a region where the NbO surface possessed a series of cleavage steps. We conclude that it might be necessary to polish carefully the NbO surfaces before oxidation if a uniform thickness of NbO_2 is desired. In addition, the gross flatness of the as-cleaved chips supplied was variable. Some chips had ridges and valleys, thereby preventing good contact between a mask and the NbO_2 layer for evaporation or sputtering of contacts.

The X-ray study of some NbO_2 powder made from Nb and Nb_2O_5 in the tri-arc furnace at Yeshiva University on August 1, 1974, gave a tetragonal structure with a = 13.692 ± .003 Å, c = 5.983 ± .003 Å. This is in good agreement with literature values[4-6], which can be represented by a_o = 13.70 ± 0.02 Å and c_o = 5.980 ± .005 Å at room temperature. Our X-ray study of the NbO_2 surface layer on the NbO chips (from Batch #105) shows the same tetragonal structure with the same lattice parameters. The orientation of the c-axis of this NbO_2 layer with respect to the NbO (100) substrate has not yet been determined.

Some scanning electron microscope pictures have been made of as-received NbO chips cleaved after the NbO_2 surface layer was formed. A view looking down onto the top surface of the chips is shown in Figures 1, 2, 3 for samples from Batches #102, #104, and #105. The grain size of the NbO_2 layer is about 3 μm. The magnification is 2000 times. Note that the surface structure of each batch is different, that the surface is far from smooth, and that there are vacant pores between some of the grains. This is particularly true of the sample from Batch #104. If the top electrode of the device is about 75 μm in diameter, it will cover about 2000 different grains of NbO_2. Thus the electrical properties will be some average over all these grains.

A S.E.M. picture of the cleaved cross section of a NbO chip, Batch #105, is shown in Figure 4. The magnification is 20 times, and the rectangular piece in the center of the picture is actually 4.0 mm long by 0.7 mm thick. The NbO_2 surface layer can be seen edge-on around the periphery. The fine white lines on the face of the rectangle are the NbO cleavage steps.

In Figure 5 we see the edge-on view of the NbO_2 layer at 2000 times magnification for Batch #105. The picture was taken at a tilt angle of about 10° with respect to the (010) cleavage plane of the chip. The measured NbO_2 layer thickness is 11 to 12 μm.

4. B.O. Marinder, Ark. Kemi 19, 435 (1963).

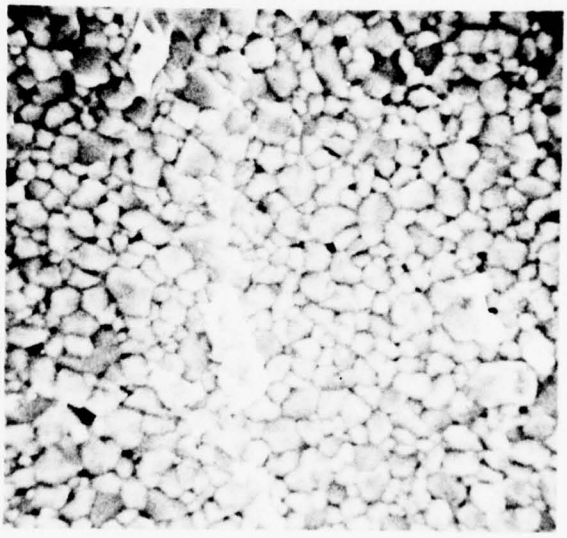
5. N. Terao, Jpn. J. Appl. Phys. 2, 565 (1963).

6. A. Magneli, et al, Acta Chem. Scand. 9, 1402 (1955).



10 μm

Figure 1. S.E.M. photograph. Batch #102.



10 μm

Figure 2. S.E.M. photograph. Batch #104.



Figure 3. S.E.M. photograph.
Batch #105.



Figure 4. Cleaved NbO/NbO_2 chip.
Batch #105.



Figure 5. Batch #105. NbO_2 layer edge on.

Finally, it should be noted that the chips as supplied varied markedly in thickness and diameter. This variety makes device assembly difficult insofar as package size must be compatible with a highly variable chip size. Cleaved chips are probably unsuitable for a completely mechanized manufacturing process.

3. TEST SETUP

We have assembled a fast rise time system to test the switching characteristics of the NbO/NbO_2 devices. The system uses a #503A SKL cable pulser with pulse rise time of about 400 ps. Maximum rated pulse height is 500 V, and pulse width can be varied from 3 to 100 ns. Pulse repetition rates of up to 125 Hz can be achieved. The pulse is fed into a GR-874 system, and, after appropriate attentuation (usually a factor of 1000), the signal is measured with a sampling scope. We are currently using a Tektronix 564B storage scope with a type 3S2 sampling unit. The effective rise time for the detector is 75 ps.

The system response is shown in Figure 6 for a 3 ns pulse. The pulser cable was charged to 1000 V, and a reasonably square pulse (rise time of 400 ps, amplitude of 500 V) is obtained.

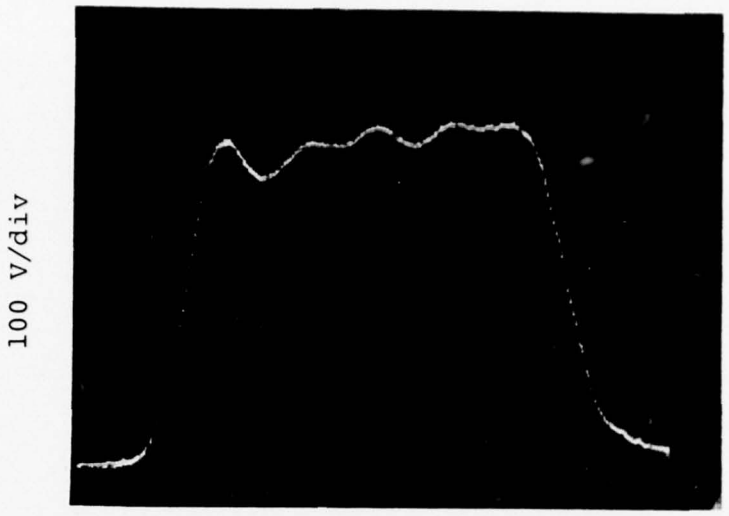


Figure 6. System response for 3 ns pulse.

We have calibrated the system using a coaxial microwave resistor in parallel with the pulser. Figure 7 gives the wave form with a parallel resistance of 5 Ω and the pulser cable charged to 100 V as before. The pulse shape is well preserved, indicating (as expected) no inductive effects for a coaxial shunt resistance. The pulse amplitude is now 80 V, implying a current I of 80/5 = 16 A through the shunt resistance. This value compares well with the calculated value of

$$I = (V_{cable} - 2V_{device})/50$$
$$= (1000-160)/50$$
$$= 16.8 \text{ A}$$

The system has been calibrated with a set of such shunt resistors.

To measure insertion loss of the device in the off state, we are currently using a Hewlett Packard type 431B power meter fed by an appropriately attenuated Hewlett Packard type 608E VHF signal generator. This system has a resolution of better than 0.05 db up to 480 MHz.

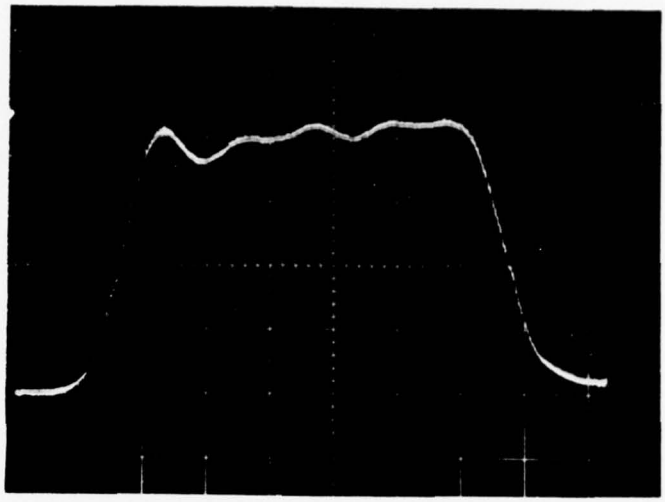


Figure 7. Voltage across 5 Ω coaxial microwave resistor. Applied pulse 500 V, 3 ns.

4. PACKAGING CONFIGURATIONS

Even assuming an ideal device (i.e., a perfect short in the on state), it is clear that inductive effects can cause a voltage spike to occur for a coaxial cable with a noncoaxial short. Consider, for example, the configuration of Figure 8. Here we short the coaxial cable with a foil strip of length 0.6 cm. and width 0.3 cm. The result obtained when pulsed with a 3 ns, 250 V pulse (cable charged to 500 V) is given in Figure 9. The observed voltage spike (30 V) is not surprising if we calculate[7] the inductance L of the foil short. We find $L = 1.6 \times 10^{-9}$ H and hence expect a voltage spike of

$$L \frac{dI}{df} \approx L \frac{V_{cable/50}}{\text{pulse rise time}} = 1.6 \times 10^{-9} \frac{500/50}{0.4 \times 10^{-9}}$$

$$= 40 \text{ V},$$

in good agreement with observation. Of course the magnitude of the inductive spike will be proportional to V_{cable}. Thus, if $V_{cable} = 2000$ V (1000 V pulse), we expect an inductive spike of

7. F.E. Terman, Radio Engineers Handbook, McGraw Hill, New York (1943).

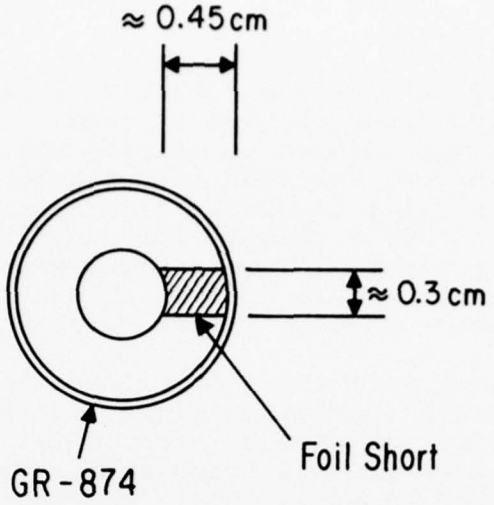
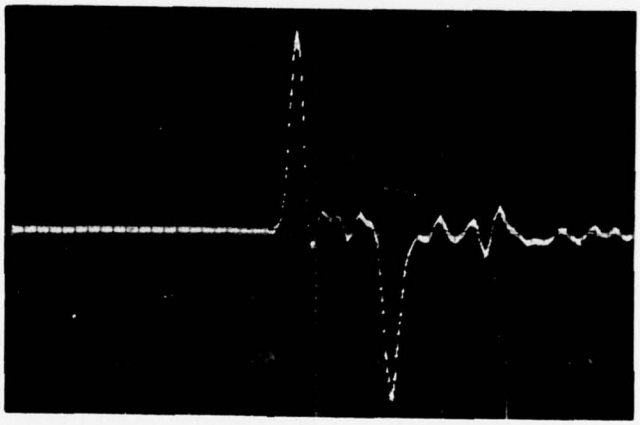


Figure 8. Foil strip between center and outer conductor of GR-874 line.



2 ns/div

Figure 9. Inductive spike from the foil shorting strip of Figure 8. Applied pulse is 250 V, 3 ns.

160 V. We also note that ringing oscillations (~ 4 V, Figure 9) are also present. These oscillations do not occur in a properly matched coaxial system.

In Figure 10 we give the inductive spike resulting when a shorted 1N-23 type diode package is used. In this case the tungsten catswhisker was allowed to contact the package base. The diode package base was inserted into a hole drilled in the center GR-874 line and a pulse of 500 V, 3 ns applied. The resultant inductive spike is 200 V (Figure 10), and it is thus clear that all attempts to protect microwave receivers with this package at a less than 200 V level are futile (unless the system bandwidth is too low to accept such an inductive spike).

It is apparent from the above discussion that it is difficult to avoid significant inductive spikes with a single-sided shunt between center line and ground in a coaxial system subjected to fast rise time, high-voltage transients. Sophisticated solutions to this problem can be envisioned. However, we have chosen to proceed temporarily with a single-sided shunt configuration for our preliminary diode package, since it is our initial goal to characterize the behavior of the NbO/NbO_2 switching material. Where necessary, any background inductive spikes can be subtracted out to display the intrinsic material behavior. The detailed packaging system we have used will be given below.

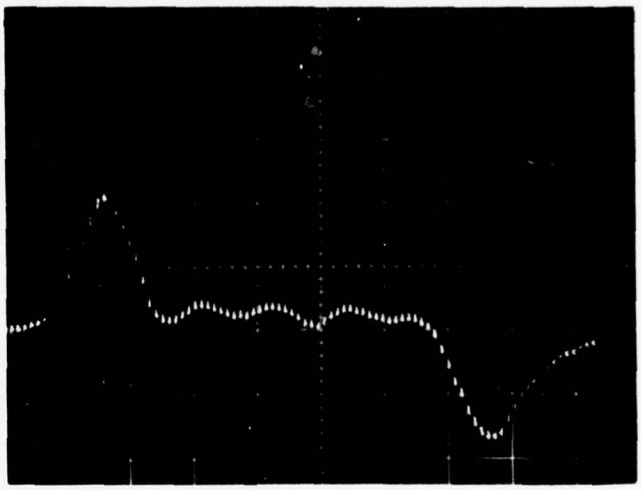


Figure 10. Inductive spike from shorted 1N-23 package (cat whisker type). Applied pulse is 500 V, 3 ns.

5. POINT CONTACT CONFIGURATION

To get some idea of the compatibility of our measurement system with previous work, we have briefly investigated the response of NbO/NbO_2 chips mounted in 1N-23 type diode packages. In this case pressure contact was made to the NbO_2 surface with a tungsten catswhisker.

Contact of the NbO/NbO_2 chip to the package base was made by using the following procedure. The reverse side of the NbO/NbO_2 chip was lapped with a SiC grit/water slurry to expose the conductive NbO. The sample was cleaned in acetone and methanol and dried and bonded with electrically conductive epoxy to the package base stud. The epoxy was cured at 150 °C for 10 min.

Figure 11 gives a typical result for a NbO/NbO_2 chip mounted using a tungsten pressure contact when subject to a 500 V, 3 ns pulse (cable charged to 1000 V). The packaged device switches, reaching its maximum voltage, $V_{th} \approx 500$ V, about 500 ps after the onset of the pulse*. About 200 V of this V_{th} should be attributed to the inductive spike resulting from this kind of sample packaging (see Figure 10). We note also the evident jitter in the trace. This jitter was usually present in point contact samples.

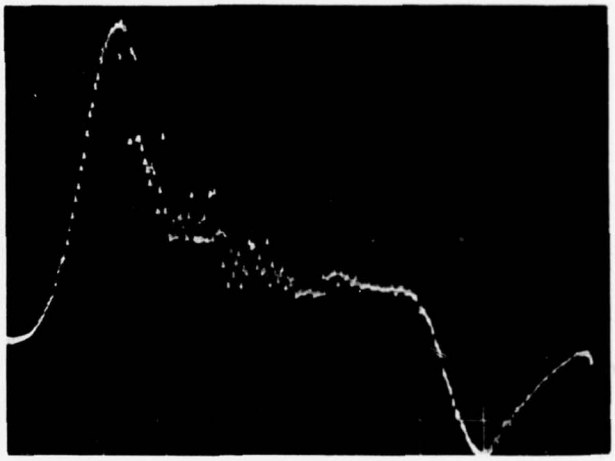


Figure 11. Switching of point contact configuration for NbO/NbO_2 device. Applied pulse 500 V, 3 ns. Sample L-7.

*For a definition of threshold switching voltage as used in this report, see Section 31.

In Table 1 we give dc resistance and insertion loss as a function of the number of pulses. Little insertion loss is evident. The variations observed in the value of the sample attenuation probably results from experimental drift in the power meter.

TABLE 1. PULSE BEHAVIOR OF SAMPLE L-7
(POINT CONTACT CONFIGURATION)
The sample was subjected to repeated pulsing at the 3 ns, 500 V level.

No. of Pulses	DC Resistance (kΩ)	480 MHz Insertion Loss (db)	200 MHz Insertion Loss (db)
0	204	0.06	0.05
10^3	113	0.03	0.04
3×10^3	22	0.09	0.1
5×10^3	7.1	0.06	0.04

Figure 12 gives similar measurements upon a different (L-6) point contact sample. In this case the threshold voltage (including the package) is 380 V. We have digitized this case and the baseline curve of Figure 10 to evaluate the sample response alone,

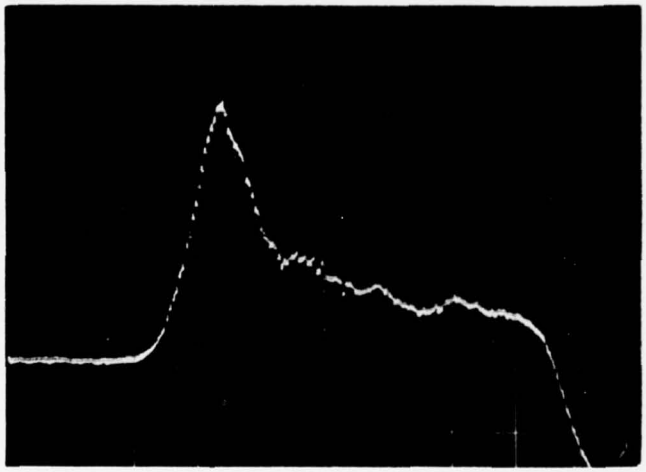


Figure 12. Switch of point contact configuration for sample L-6. 500 V, 3 ns applied pulse.

and this is plotted in Figure 13. As expected, for this sample the threshold voltage (excluding the point contact package) is approximately 200 V.

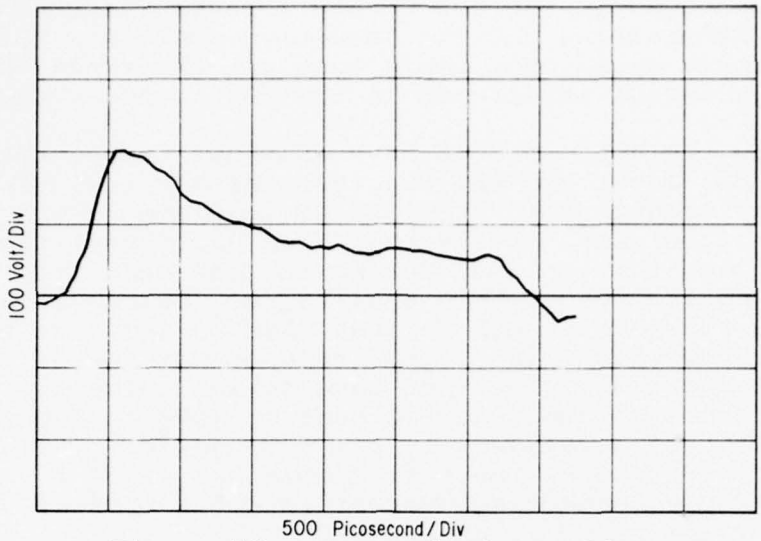


Figure 13. Data of Figure 12 digitized and corrected for package inductance.

In Table 2 we give resistance and insertion loss data for Sample L-6. Note that the insertion loss increased quite substantially after 3000 pulses. Figure 12 was obtained after 3000 pulses.

TABLE 2. PULSE BEHAVIOR OF SAMPLE L-6 (POINT CONTACT CONFIGURATION) The sample was subjected to 500 V, 3 ns pulses.

No. of Pulses	DC Resistance (kΩ)	480 MHz Insertion Loss (db)	200 MHz Insertion Loss (db)
1.5×10^3	3.7	0.06	0.07
3×10^3	0.5	0.6	0.3
4.5×10^3	0.4	0.5	0.5

We may compute the insertion loss α from $\alpha = -20 \log_{10} [2R/(1x2R)]$, where $R = Z/Z_o$. Since it appears we may neglect any capacitative shunting of the packaged device (see, e.g., Table 1) we obtain, after 3000 pulses, $\alpha = 0.4$ db for an off-state resistance of 500 Ω. This agrees well with the data of Table 2.

We may also note at this point that, while quite erratic and variable values were obtained for the sample dc resistance and degradation with pulsing, almost all devices examined exhibited threshold voltages in the 400 to 500 V range (including package effects). Subtracting out the inductive spike due to the cats-whisker package would then imply that the threshold voltage for the NbO/NbO_2 device itself was in the 100 to 200 V range.

Finally, we note that we have examined the contact area between the NbO_2 layer and the tungsten whisker for pulsed samples. A distinctly eroded spot, about 25 μm in diameter was typical of the contact interface. It is therefore clear that the current (whether filamentary or not) during the switching process was restricted to an area of less than 25 μm. We may compute the temperature rise ΔT in such an area when pulsed. We shall assume a pulse of 3 ns width, 200 V amplitude across the switched device. As a good approximation we then have device current $\approx$ 12 A. The high-temperature volume specific heat of NbO_2 is about 3.5 J cm^{-3} $°C^{-1}$ and the X-ray density $\rho = 5.916 gm/cm^2$. Using these values we find: energy input to sample per pulse = 7×10^{-6} J; volume of sample conducting current is $< 5 \times 10^{-9}$ cm^3.

$$\Delta T > \frac{3 \times 10^{-5}}{3.6 \times 5 \times 10^{-9}} \text{ °C} \approx 400\text{°C}$$

Because switching to the metallic state occurs at 800 °C in NbO_2, it is tempting to conclude that the switching observed is in fact thermal. Filament widths of < 25 μm are common in amorphous switching devices, and, if this were the case here, the NbO_2 would clearly reach its metal-semiconductor transition temperature.

6. PACKAGING

To avoid the problems inherent in a point contact packaging configuration, we have attempted to mount devices using evaporated aluminum contacts. The device preparation procedure is as follows:

One side of the NbO/NbO_2 chip is lapped, cleaned, and dried as described in Section 5 to expose the NbO layer. An array of 125 μm aluminum dots is evaporated on the NbO_2 surface. The aluminum layer is 1/2-1 μm thick. The exposed NbO face of the chip is then epoxied to a microwave diode package of the type illustrated in Figure 14.

A connection between the 125 μm aluminum electrode and the rim of the diode package is made by means of a 25 μm fine gold wire. The wire is balled at one end (ball size 50 to 75 μm) and cold-welded to the aluminum dot with pressure and ultrasonic energy.

The completed device is screwed into the holder shown in Figure 15 for pulsing and power loss measurements. The holder is

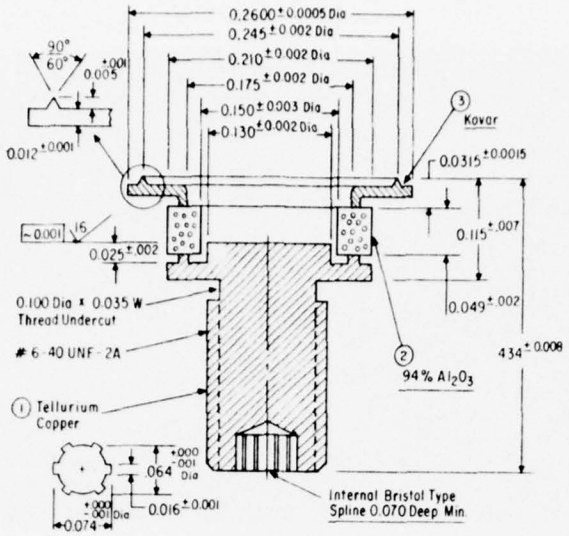


Figure 14. Microwave diode package used for mounting NbO/NbO_2 chip. Various dimensions are available.

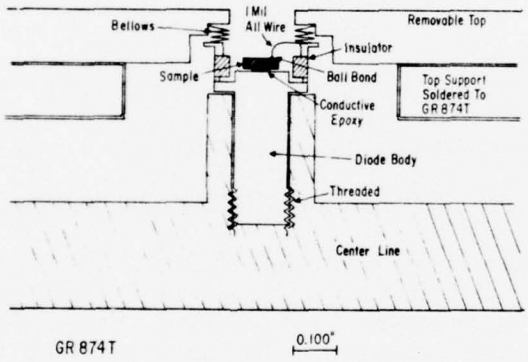


Figure 15. NbO/NbO_2 chip mounted in diode package which fits into a specially adapted GR-874 "tee."

compatible with GR-874 components. Adapters are available to convert the GR-874 "tee" to type N.R.F. fittings.

Figure 16 gives the voltage versus time of such a package with no NbO/NbO_2 chip - i.e., the gold wire is bonded directly to the microwave diode package base. An inductive spike of about 160 V is observed. This is somewhat better than the 1N-23 cats-whisker type configuration, but, as we have emphasized in Section 4, any single-sided short will produce a nonnegligible inductive

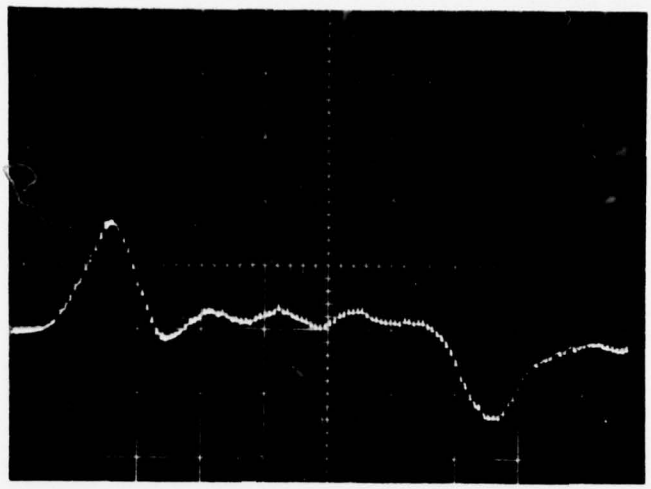


Figure 16. Inductive spike from the shorted diode package of Figure 15. Applied pulse 500 V, 3 ns.

spike for sufficiently fast rise time pulses. We have chosen to use the packages of Figures 14 and 15 and subtract out the package effect where necessary in investigating the NbO/NbO_2 devices.

7. NbO/NbO_2 DEVICES WITH ALUMINUM CONTACTS

The results obtained with the aluminum contacted NbO/NbO_2 devices are quite variable. One measure of the variability is the dc resistance R between the as-evaporated dots on the chip face and the NbO base contact. We have probed this resistance R for a chip mounted on the diode package but not yet wire-bonded. Some results are given in Table 3. We note that the value of R is highly variable, both from sample to sample on the same batch (Yeshiva Lot #110) and even variable on the face of a single sample (X-3-7).

Figure 17 gives the switching curve obtained on a sample (X-3-4B) with aluminum contacts. Threshold voltage was 450V. No jitter is observed. Figure 18 gives the data with the package inductance (Figure 16) subtracted out. The true device threshold voltage is about 300 V, and an "inductive"-type initial peak characteristic of NbO/NbO_2 switching persists. Figures 19 and 20 give the switching behavior (Sample X-2-3) with and without the package inductance, respectively. In this case the device threshold is lower ($\sim$ 150 V). The spike in Figure 19 is largely a package effect.

TABLE 3. VALUE OF DC RESISTANCE R AT VARIOUS POINTS ON THE CHIP FACE FOR THREE NOMINALLY IDENTICAL SAMPLES. An array of 125 μm diameter aluminum dots was evaporated on the sample face.

Dot No.	Sample X-3-6 R (kΩ)	Sample X-3-7 R (kΩ)	Sample X-3-3 R (kΩ)
1	217	15	0.31
2	350	1.2	0.51
3	85	0.45	0.52
4	115	0.47	0.60
5	104	3.4	0.74
6	113	8.4	1.0
7	156	279	-
8	215	641	-
9	135	3.0	-
10	210	1.2	-

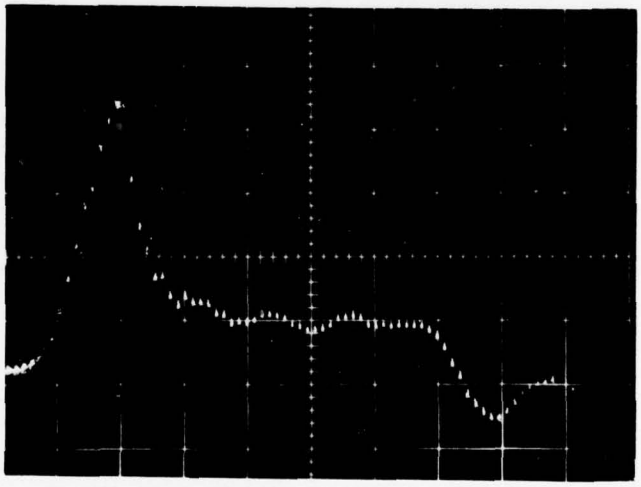


Figure 17. Switching in sample X-3-4B. Applied pulse 500 V, 3 ns.

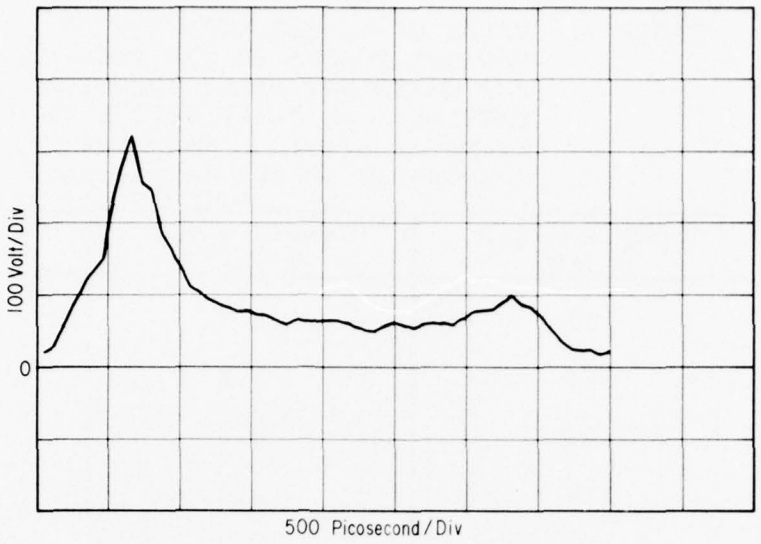


Figure 18. Sample X-3-4B with package inductance removed.

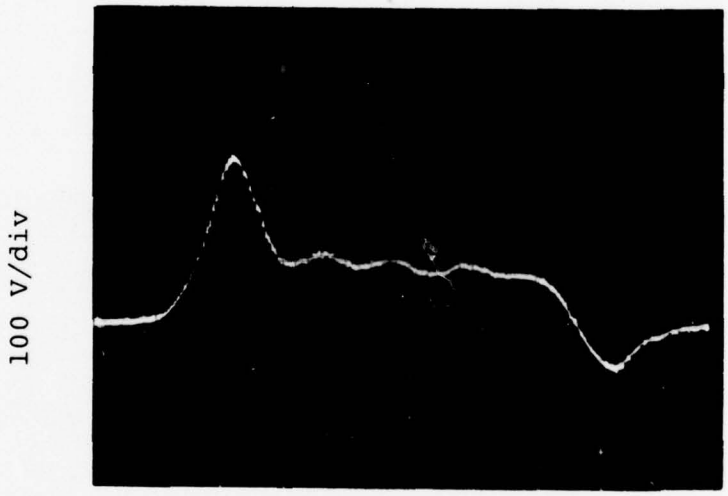


Figure 19. Sample X-2-3. Applied pulse is 500 V, 3 ns.

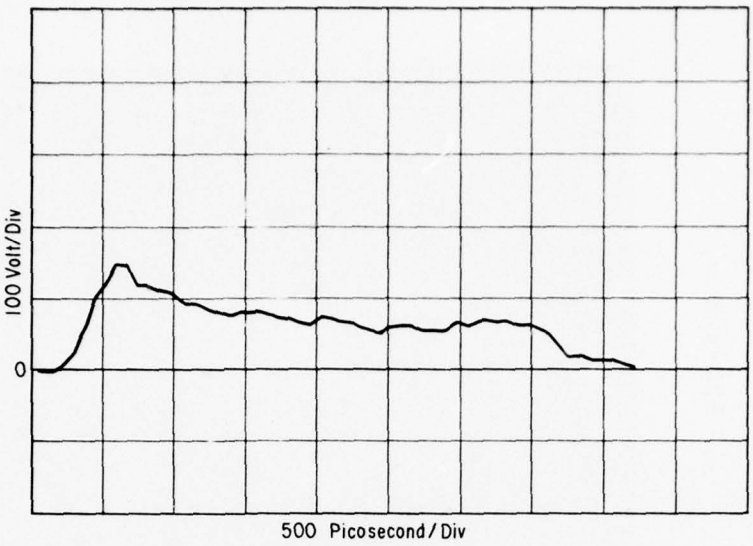


Figure 20. Sample X-2-3 with package inductance removed.

Figure 21 gives the voltage time trace for Sample X-3-4 subjected to a 3 ns, 500 V (cable = 1000 V) pulse. This photograph was taken after 500 pulses had passed the sample. Figure 22 gives the characteristic for this sample with the package inductance subtracted. It is interesting to follow the degradation of this sample with pulsing. In Table 4 we give the resistance and insertion loss at 480 MHz for various types of pulsing. From the data it is clear that the sample undergoes substantially accelerated degradation when the pulse width is increased. This behavior is typical for samples with evaporated aluminum contacts.

TABLE 4. BEHAVIOR OF SAMPLE X-3-4 WITH REPEATED PULSING.

No. of Pulses	Pulse Height (V)	Pulse Width (ns)	DC Resistance (kΩ)	480 MHz Insertion Loss (db)	Comments
0			208	0.1	
250	500	3	1.07	0.09	
250	500	3	95	0.09	
250	250	3	-	-	No Switching
250	250	3	97	0.09	" "
250	375	3	-	-	Partial Switching
250	375	3	-	-	" "
250	500	3	58	0.09	
250	500	10	2.8	0.18	
250	500	10	0.83	0.36	
500	500	50	0.007	8.0	Sample Failed

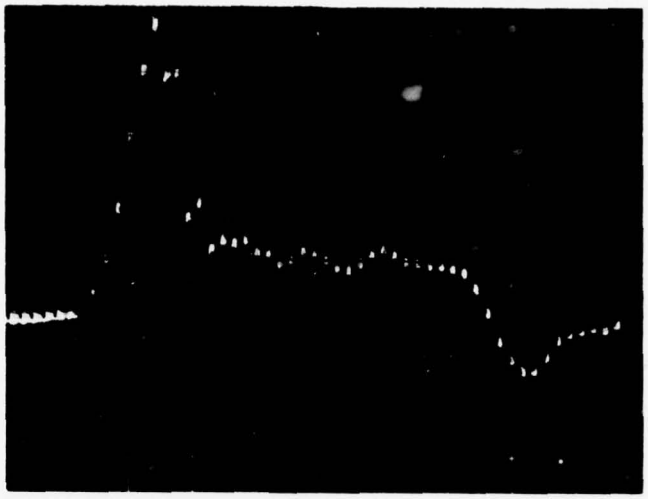


Figure 21. Sample X-3-4. Applied pulse 500 V, 3 ns.

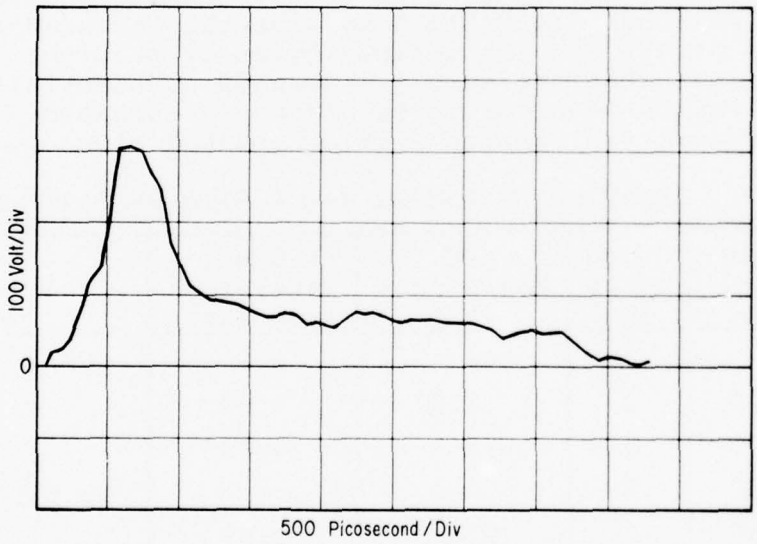


Figure 22. Sample X-3-4 with package inductance removed.

8. EFFECT OF TEMPERATURE

We have evaluated the effect of temperature upon the switching of NbO_2/NbO chips. Samples were mounted with silver epoxy and gold wire bonded to 125 μm diameter evaporated aluminum dots, as described in Section 6. The mounted samples were fixed in the holder previously described (Figure 15), and the holder, in turn, placed in a Statham environmental chamber. The environmental chamber cools using cold CO_2 gas. Heating is resistive in an air ambient. The sample temperature was measured with a thermocouple connected to the ground line of the sample holder.

The sample was connected to our 50 Ω test system using moderately long (1m) flexible cables. Care was taken to ensure that the pulse waveform was not degraded in this setup. Power measurements using this configuration and a power meter were found to be untrustworthy, presumably as a result of imperfect contacts and cable losses. We have therefore chosen to characterize the NbO_2/NbO 500 MHz insertion loss using dc resistance measurements. There is excellent correlation between the dc and 500 MHz measurement techniques, as indicated in Tables 1 and 2.

In Table 5 we give a typical measurement sequence. The pulse applied was 500 V amplitude, 3 ns duration at 50 Hz repetition rate. The virgin sample was measured and found to have resistance 35.8 kΩ at room temperature. This may be compared with a computed value of 48 kΩ, using the literature[8] room temperature resistivity value of 6.3 kΩ parallel to the C axis. Two hundred and fifty pulses reduce R to 1.14 kΩ (Figure 23). (Note that α = 0.4 db corresponds to a shunt resistance of 0.53 kΩ, ignoring capacitive effects.) Raising the temperature to 83 °C then drops R to 0.78 kΩ.

Figure 24 gives the result of pulsing the device at 83 °C. The switching characteristic is basically the same as that of Figure 23, indicating little or no temperature dependence of the switching characteristic.

Further pulsing degrades the sample resistance to 0.42 kΩ. Cooling to -54 °C increases R to 1.43 kΩ, and Figure 25 confirms the basic insensitivity of the switching curve to temperature. Figure 26 gives the switching characteristic upon returning to room temperature.

From Table 5 we conclude that the resistance of a "switched" sample varies only a factor of 3 between +83 and -54 °C. This is surprising in view of the 0.48 eV activation energy[8] for the low field resistivity of NbO_2, which implies a resistance variation of about a factor of 10^4 in this temperature range. We

8. G. Belanger, J. Destry, G. Perluzzo, and P.M. Raccah, Can. J. Phys. 52, 2272 (1974).

TABLE 5. EFFECT OF TEMPERATURE UPON NbO_2/NbO SWITCHING

Experiment Sequence	No. of Pulses Applied	DC Resistance (kΩ)	Temp. °C	Fig. No.
1	Initial	35.8	26	
2	250	1.14	26	23
3	None	0.78	83	
4	250	0.42	83	24
5	None	1.43	-54	
6	250	0.85	-54	25
7	None	0.733	26	
8	250	1.1	26	26

presume that the switched sample is degraded in a way that makes the conducting region more "metallic." We have confirmed this general picture by noting that NbO_2/NbO samples with a higher resistance (whether switched or not) generally exhibit a much greater drop in resistance with increasing temperature.

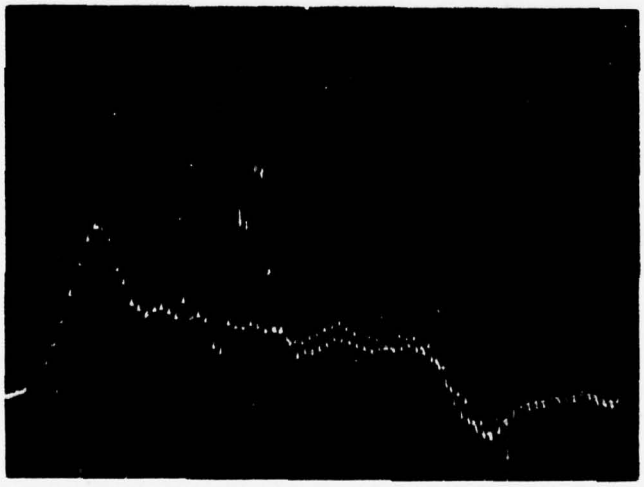


Figure 23. NbO_2/NbO Chip No. X-3-9. Temperature = 26 °C.

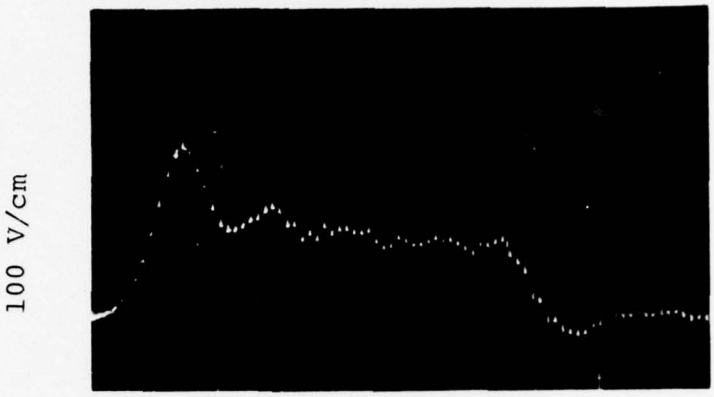


Figure 24. NbO_2/NbO Chip No. X-3-9. Temperature = 83 °C.

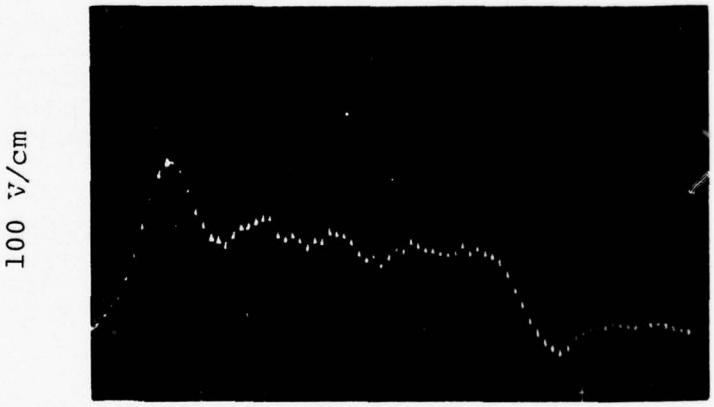


Figure 25. NbO_2/NbO Chip No. X-3-9. Temperature = -54 °C.

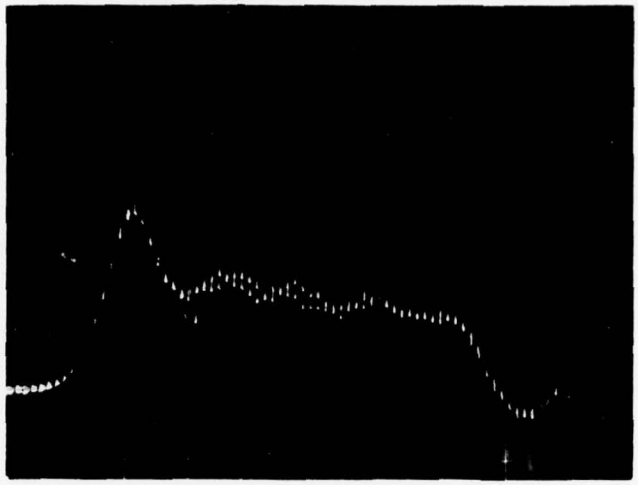


Figure 26. NbO_2/NbO Chip No. X-3-9. Temperature = 26 °C.

9. CONTACT PROCEDURES

It is possible that the rapid deterioration with pulsing (especially for pulses ~50 ns long) of the NbO/NbO_2 chips is a result of an electrode-NbO_2 reaction. To date evaporated aluminum electrodes, approximately 0.5 μm thick, have been used as contact electrodes. An "ideal" electrode system might use niobium metal as the electrode material. Niobium is refractory and very difficult to evaporate. We have therefore utilized a sputtering technique to provide 125 μm diameter contact electrodes to the NbO/NbO_2 chip. The experimental procedure is described below:

1. The as-received chips are examined under a microscope and those with at least one relatively flat surface selected. Ridges, left on the chips during cleaving, preclude the good sample-to-mask contact necessary in the electrode deposition process.

2. The samples are mounted flat side down on a glass plate fastened to a lapping jig. The samples are held securely to the glass by glycol phthalate ($C_{12}H_{12}O_5$, a low melting point (~100 °C) polyester). Mounting is performed with the jig and samples on a hot plate, T ~150 °C.

3. Small glass bars are also secured to the glass plate (using glycol phthalate), which effectively surround the samples as shown in Figure 27. The glass bars (of known thicnkess) are important in the grinding and

polishing step below. They help keep the sample surface flat and are used to estimate the lapped sample thickness.

4. The samples are ground with 280 mesh carborundum grit and polished with 5 μm particle-size carborundum powder. In this step all the NbO_2 is removed from the lapped side. The samples are flat and of uniform thickness ~0.4 to 0.6 mm.

5. The samples are removed from the lapping jig by heating. They are then rinsed three or more times in hot acetone with ultrasonic agitation. This removes all traces of glycol phthalate from the samples.

6. The samples are rinsed in hot methyl alcohol and blown dry in nitrogen.

7. The samples are placed lapped side down on a glass plate in the sputtering apparatus as shown in Figure 28. Each sample is separately covered with a thin molybdenum mask having 125 μm dia. holes on 0.5 mm centers. A pure niobium sputtering target is attached to the high voltage fixture.

8. The sputtering chamber is pumped out with a mercury diffusion pump (no oil contamination). When the chamber attains a vacuum of $\sim 10^{-6}$ torr, the sputtering process can be started.

9. Argon gas is introduced into the sputtering chamber through a needle valve. The flow is adjusted so that the chamber pressure is $\sim 3 \times 10^{-3}$ torr.

10. By means of the dc triode technique, niobium metal is sputtered into the samples through the 125 μm holes in the mask. The sputtering voltage is set at -2000 V and the plasma filament current adjusted to give a sputtering current of 20 mA. (Low-voltage plasma, ~30 V and ~1 A.) Niobium is sputtered for 30 min at a rate of ~7000 Å/30 min.

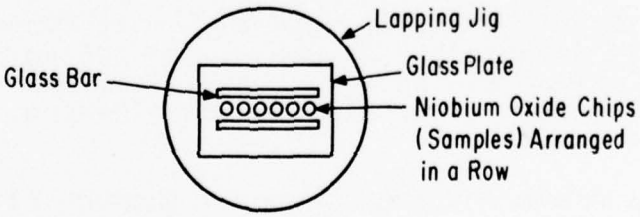


Figure 27. Schematic drawing of sample holder used in grinding and polishing step.

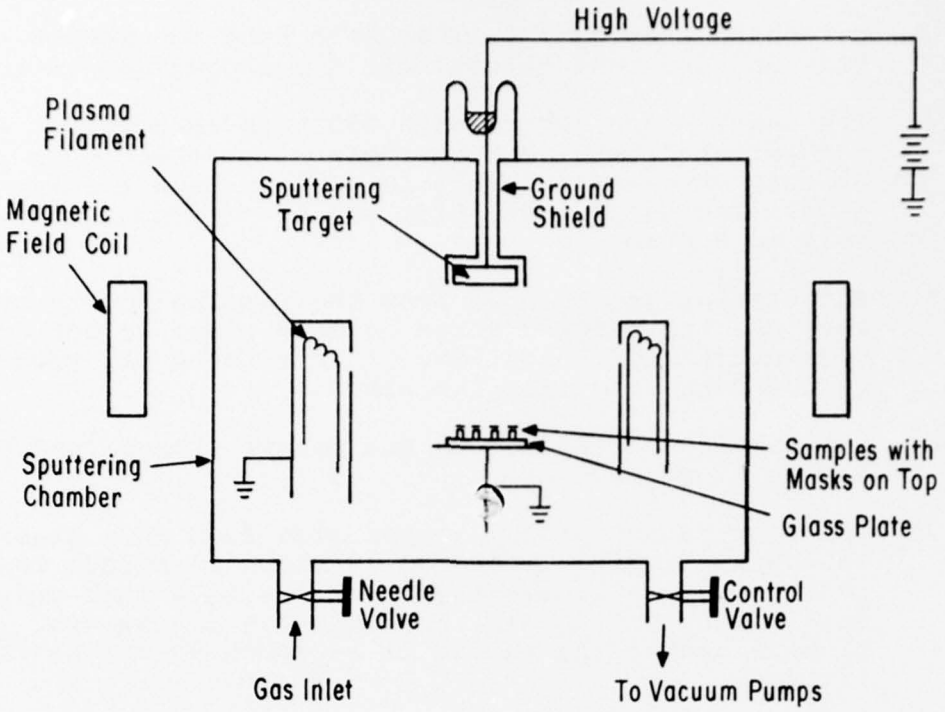


Figure 28. Schematic drawing of sputtering apparatus.

11. After the niobium deposition the pump valve is closed and the chamber back-filled with argon to 1 atm pressure. The chamber is opened and the niobium sputtering target replaced with a gold target. The system is again pumped down and steps 8 and 9 above repeated.

12. The pump valve is throttled until the chamber pressure reaches an equilibrium value of ~40 x 10^{-3} torr of argon. The high voltage is set at V ~ -2000 V, giving a sputtering current of ~14 mA. Gold is sputtered for 10 min. at a rate of ~1.2 μm/10 min. The chamber is back-filled with argon and the samples removed.

13. The samples are mounted in the diode packages by using conducting silver epoxy (on the lapped back side). The epoxy is cured at T ~180 °C for ~10 min.

14. With an ultrasonic gold ball wire bonder, a 25 μm gold wire is attached to one of the 125 μm niobium-gold dots on the sample surface. The other end of the wire is is bonded to the diode package casing. The device is now complete.

[For aluminum contacts, steps 7 through 12 are replaced by a much simpler evaporation procedure. The samples are placed above the aluminum source, front face down on a large mask (125 μm holes - 0.5 mm centers). Hence, much less care is required in obtaining back-side flatness and thickness uniformity.]

Using the above procedure we have electroded a group of NbO/NbO_2 chips (all Batch No. 102) with sputtered Nb/Au contacts. In addition, a control group of samples from Batch No. 102 was electroded with evaporated aluminum contacts.

Table 6 below gives the results of pulsing a sample with Nb/Au contacts. After 500 pulses of 3 ns duration, the resistance decreases from 15.4 to 0.97 kΩ. Further pulsing with a longer pulse width apparently increases the sample resistance. We presume that either part of the electrode has been burned off or that a new filament is now operating in the NbO_2 layer. Figure 29 gives the initial switching characteristic of this sample. We may note that there is great variability among samples regarding the pulse deterioration of the NbO_2/NbO chips. For instance, a sample nominally identical to that of Table 6 with Nb/Au contacts had a virgin dc resistance of 14.1 kΩ, and resistance equal to 1.36 kΩ after 500 pulses of 500 V amplitude, 3 ns duration. However, after 500 pulses of 50 ns duration, the sample had shorted (resistance = 2.6 Ω).

TABLE 6. BEHAVIOR OF NbO_2/NbO CHIP WITH Nb/Au CONTACTS

No. of Pulses	DC Resistance (kΩ)	480 MHz Insertion Loss (db)	Pulse Type
virgin	15.4	0.17	
250	8.8	0.23	500 V, 3 ns
350	0.97	0.4	500 V, 3 ns
500	10	0.22	500 V, 50 ns
500	6.8	0.28	500 V, 50 ns

In Table 7 we give the behavior of a sample from Batch No. 102 with evaporated aluminum contacts. This sample shows basically the same behavior with pulsing as does the sample of Table 6. In Figure 30 we give the initial switching characteristic of the sample of Table 7. We also note that the sample-to-sample variability in degradation characteristics observed for the Nb/Au contact system persists when we use samples with evaporated aluminum contacts. We conclude, then, that the switching characteristics and sample degradation with pulsing of NbO_2/NbO are not a result of the electrode contact system. This behavior is apparently intrinsic to the NbO_2/NbO chip itself.



Figure 29. NbO_2/NbO Chip with Nb-Au contact. Sample No. X-13-4, Batch #102.

TABLE 7. BEHAVIOR OF NbO_2/NbO CHIP WITH ALUMINUM CONTACTS

No. of Pulses	DC Resistance (kΩ)	480 MHz Insertion Loss (db)	Pulse Type
virgin	33.0	0.14	
250	17.3	0.17	500 V, 3 ns
250	20.5	0.17	500 V, 3 ns
500	10.9	0.23	500 V, 3 ns
500	7.7	0.26	500 V, 3 ns



Figure 30. NbO_2/ NbO Chip with aluminum contact. Sample No. X-13-7, Batch #102.

10. FAILURE MODES - SAMPLES WITH ALUMINUM CONTACTS

Since the NbO_2/Nbo chip devices show some degradation with repeated pulsing, it seemed worthwhile to attempt to observe any physical effects due to the pulsing. The aluminum contact pad would obscure any observation of the NbO_2 layer beneath, and we have therefore adopted the following procedure to lay bare the relevant area of NbO_2.

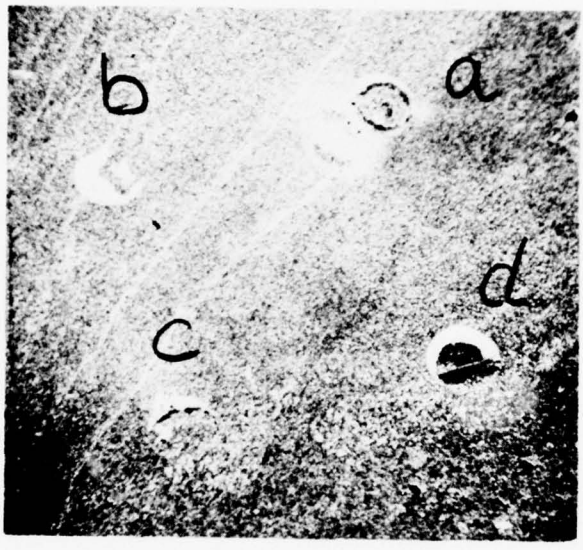
1. The NbO-diode package epoxy bond is mechanically broken to remove the NbO_2/NbO chip from the diode package.

2. With the use of a knife the ball bond pad is popped off the 125 μm diameter aluminum contact evaporated on the NBO_2 layer. This procedure does not remove any aluminum from the NbO_2 layer - i.e., the Al-NbO_2 bond is stronger than the aluminum-gold ball bond.

3. The NbO_2/NbO chip is etched (5 min) in an acid bath (composition: 15 parts HNO_3, 30 parts CH_3COOH, 25 parts H_2O, 380 parts H_3PO_4). This procedure almost completely removes the aluminum contacts.

A control experiment on bonded but unpulsed devices indicated that the etch did not significantly attack the NbO_2 layer. After about 15 min in the bath, bonded but unpulsed devices appeared unblemished in the aluminum contact area. We may thus conclude that the above process is suitable for exposing the NbO_2 layer of pulsed devices.

In Figure 31 we give a low magnification shot of the top of an etched NbO_2/NbO chip. Four partially removed aluminum contact areas are visible. In Table 8, below, we list the pulse history of each area. In Figures 32 through 35 we give high magnification S.E.M. pictures of each of these areas.

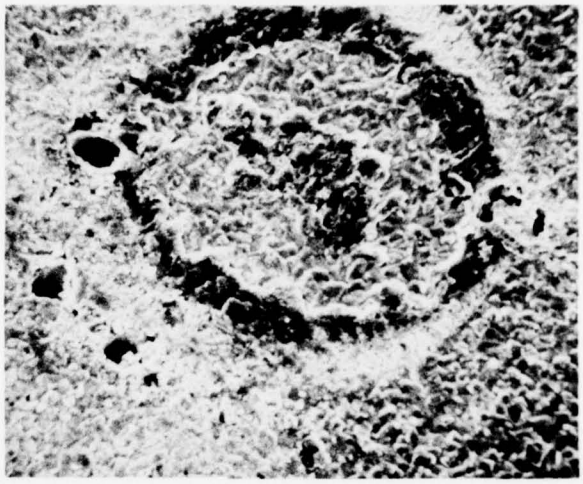


50X

Figure 31. S.E.M. photo of NbO_2 layer after removal of gold contact wires and partial etching of the aluminum contact pads. Four contact areas are visible, and regions a,b,c,d are shown at higher magnification in Figures 32, 33, 34, 35, respectively.

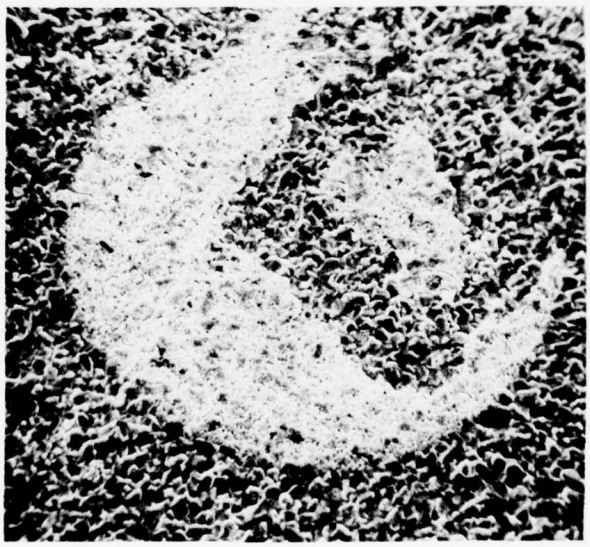
TABLE 8. DAMAGE ANALYSIS - SAMPLE X-14-1

Sample Area	Pulse History	$R_{initial}$ (kΩ)	R_{final} (kΩ)	Observed Damage
a	3000 pulses, 500 V, 3 ns	42	22	4 pits, 5~10 μm dia. 2-8 μm deep - Fig. 32
b	500 pulses, 500 V, 3 ns	37	0.15	None - Fig. 33
c	1000 pulses, 500 V, 3 ns, plus 100 pulses, 200 V, 50 ns	39	0.04	pit, 7 μm deep 10 μm dia. - Fig. 34
d	None - area inadvertently scratched			Fig. 35



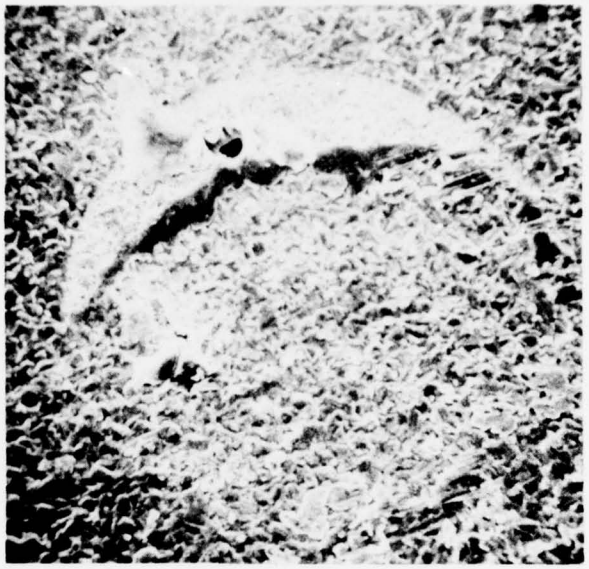
500X

Figure 32. S.E.M. photo of contact area "a" of Figure 31. Four pits are visible. Two are on the periphery of the contact area of the gold ball bond, the deeper pit being 6 μm deep and 13 μm in dia. The two pits close together on the periphery of the aluminum contact area are 7 μm deep.



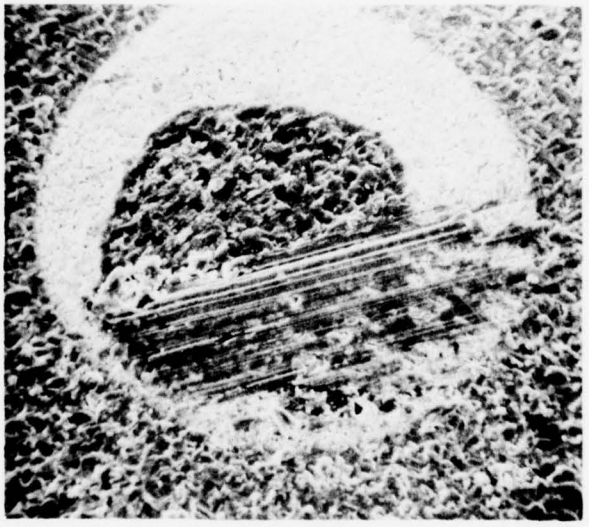
500X

Figure 33. Contact area "b" of Figure 31. No physical damage is visible.



500X

Figure 34. Contact area "c" of Figure 31. Major damage area is pit 10 μm diameter, 7 μm deep, on periphery (between edge of gold ball bond and edge of aluminum contact) of contact area.



500X

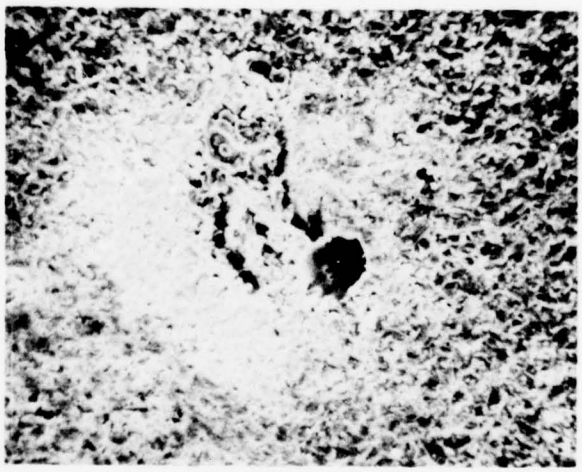
Figure 35. Contact area "d" of Figure 31. This area was inadvertently scratched.

In Table 9 we give particulars on pulse history and observed damage for other NbO_2/NbO devices. Sample X-6-1 was pulsed with a Velonex Pulse Generator. The massive crater formed presumably results from the energy expended during the long (10 μs) applied pulse.

TABLE 9. DAMAGE ANALYSIS NbO_2/NbO CHIPS

Sample No.	Pulse History	$R_{initial}$ (kΩ)	R_{final} (kΩ)	Observed Damage
X-13-8	750 pulses, 500 V 3 ns plus 1000 pulses, 500 V, 50 ns	32	1.0	Pit, 13 μm deep, 16 μm diam. - Fig. 36
X-6-1	3 pulses, 5 A, 10 μs	10	shorted	Crater-extends beyond contact area - Fig. 37
X-6-1A	750 pulses, 500 V 3 ns	2.7	0.2	2 pits, 4 μm deep, 8 μm diam. - Fig. 38

From Tables 8 and 9 and Figures 31 through 38 we conclude that NbO_2/NbO devices with aluminum evaporated contacts suffer substantial degradation on repeated pulsing. The damage is more severe for 50 ns pulses, but some of the devices with numerous 3 ns pulses also exhibit pitting. The multiple pits observed are also consistent with the, at times, erratic behavior of the off-state resistance. Presumably some pits become conducting, short, and burn away from the contact allowing conduction at another location under the electrode.



500X

Figure 36. Sample X-13-8. Major damage is pit 13 μm deep, 16 μm dia. in center of contact area.



200X

Figure 37. Sample X-6-1. This sample was subjected to long duration (10 μs) pulses. The crater formed extends beyond the aluminum contact area.

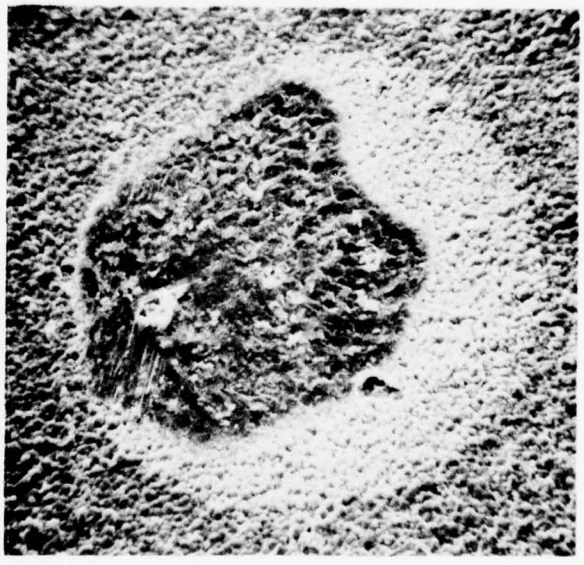


Figure 38. Sample X-6-1A. Two pits about 4 μm deep and 8 μm dia. are visible.

11. BACK-TO-BACK DEVICES

To check whether or not the pulse degradation observed in the aluminum-contacted samples was influenced by the contact procedure, we have constructed "back-to-back devices" as illustrated in Figure 39. The devices are made by removing the NbO_2 layer as usual from one side of a NbO_2/NbO chip and inserting two such chips in a 1N-23 diode package with their NbO_2 layers touching under light pressure. Ohmic contact is made to the exposed NbO on the back of each chip by using conducting epoxy on the NbO crystal.

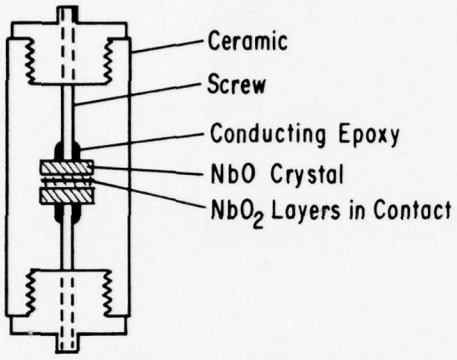


Figure 39. Construction of back-to-back NbO_2/NbO devices.

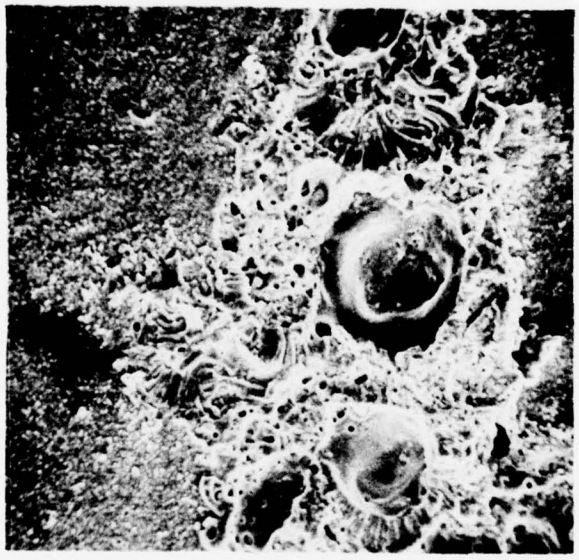
The back-to-back sample would not switch initially under application of a 500 V 3 ns pulse, presumably because of the doubled thickness of the NbO_2 layer. After about 1000 pulses of 50 ns duration, 500 V amplitude, switching of the sample could be induced with 3 ns long pulses. The device was then subjected to about 10 000 pulses of 50 ns duration. This caused the sample offstate resistance to drop from its initial value of 10^6 Ω to 1800 Ω. The device of Figure 39 was then disassembled and the NbO_2 surfaces examined for any evidence of pulse damage.

In Figure 40 we give a low magnification S.E.M. photograph of the NbO_2 face of one of the back-to-back chips. Two areas of damage are evident on the chip periphery with the damage region presumably defined by the point of chip-to-chip contact. In Figures 41a and 41b, we give higher magnification photographs of area "a" marked in Figure 40. Figure 41a corresponds to the same chip as Figure 40. Figure 41b is the adjacent area on the opposing chip. Note the extensive (matching) cratering of the NbO_2 layer. The major crater of Figures 41a and 41b is about 25 μm deep (i.e., it extends into the NbO crystal) and quite wide - about 40 μm. The extensive damage is expected in view of the quite severe pulse schedule to which the device has been subjected. We may also conclude that pitting and cratering of the NbO_2 layer in NbO_2/NbO chip devices is inherent to the device - i.e., it is not a function of the chip contact method. Hundreds of 50 ns pulses or thousands of 3 ns pulses cause severe physical damage. Hundreds of 3 ns pulses cause less evident physical damage, but some deterioration in the device off state resistance is at times evident.



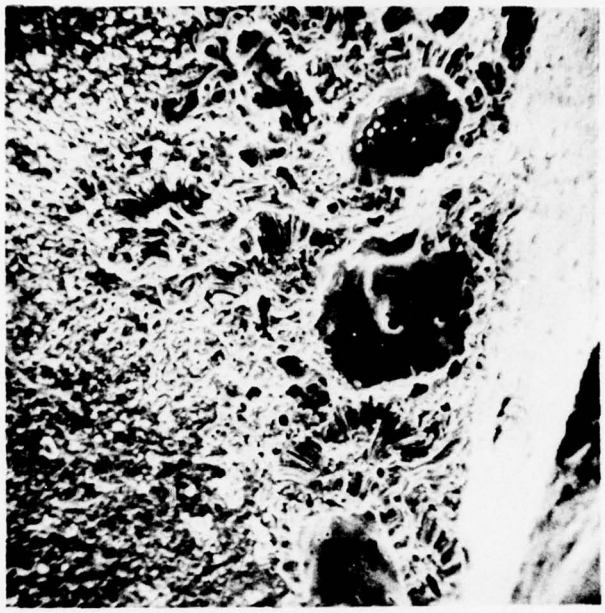
50X

Figure 40. S.E.M. photo of NbO_2 surface of back-to-back device. Two damage areas are indicated.



500X

Figure 41a. Higher magnification photo of damage area "a" of Figure 40. The major crater is about 25 μm deep.



500X

Figure 41b. Area adjacent to damage region of Figure 41a but on opposing chip.

12. FIFTY PRELIMINARY FEASIBILITY MODELS

Fifth mounted coaxial switching devices have been supplied (24 on 10/15/76 and 26 on 12/14/76), which completes item CLIN002.

All devices supplied derive from Batch No. 102 of the as-received NbO/NbO_2 chips. Device construction, which is described in step by step detail in Section 9, is summarized below:

1. Remove NbO_2 layer from one side of NbO/NbO_2 chip to expose NbO.

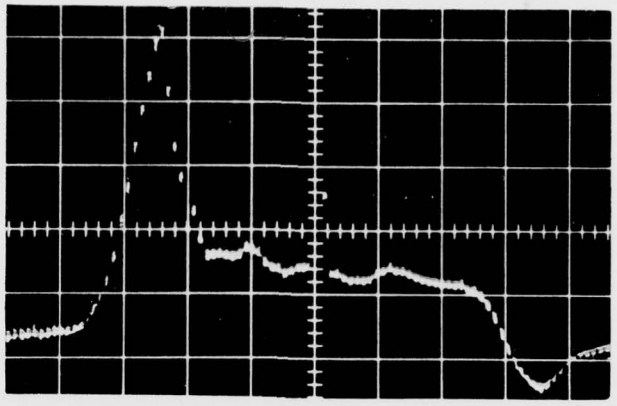
2. Evaporate 125 μm diam. aluminum dot array on NbO_2.

3. Mount exposed NbO surface to microwave diode package with silver epoxy.

4. Bond 25 μm gold wire to one aluminum dot electrode and connect to diode package lip.

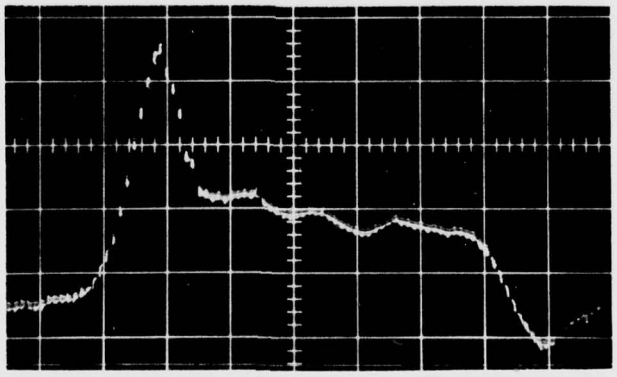
The diode packages and the specially adapted GR-874T fitting into which they are inserted for use in 50 Ω lines are described in Section 6.

All chips were chosen from Batch No. 102. The dc resistance of virgin (unpulsed) samples ranges from 10 to 70 kΩ. Two randomly chosen samples processed simultaneously with the samples supplied have been characterized electrically. Switching characteristics upon application of a 500 V, 3 ns pulse are shown in photographs (Figures 42a and 42b).



500 ps/div

Figure 42a. Pulse response of Sample X-15-31.



500 ps/cm

Figure 42b. Pulse response of Sample X-15-32.

In Table 10 we give data for the devices of Figures 42a and 42b. The 500 MHz insertion loss and final dc resistance were measured after passage of 250 pulses of 500 V amplitude and 3 ns duration. The device voltage drops to 100 to 150 V in less than 1 ns after application of the pulse.

TABLE 10. TYPICAL BEHAVIOR OF PRELIMINARY FEASIBILITY MODELS OF COAXIAL SWITCHING DEVICE

Sample No.	Fig. No.	$R_{initial}$ (kΩ)	R_{final} (kΩ)	500 MHz Insertion Loss (db)	200 MHz Insertion Loss (db)
X-15-31	42a	37	16	0.17	0.10
X-15-32	42b	28	4.8	0.20	0.13

13. NbO_x SINGLE CRYSTALS

Following the visit of G.K. Gaulé to the General Electric Research and Development Center early in January 1977, it was decided to halt temporarily work on NbO/NbO_2 chips. The reasons for this decision lie basically in the observed rapid degradation of the NbO/NbO_2 chips upon repeated pulsing. Since the observed switching takes place in the polycrystalline NbO_2 layer of the NbO/NbO_2 chips, it was felt that it was reasonable to explore switching in single-crystal niobium dioxide. It was thought that the single-crystal material might prove more resistant to pulse degradation.

A set of NbO_x ($2.00 \geq x \geq 1.87$) single-crystal chips was supplied to us by Dr. Gaulé. These crystals were grown by S.H. Shin at Yeshiva University, and, according to Dr. Shin, the stoichiometry designation reflects the Nb:O proportions in the starting materials. Crystals growth was unseeded, and we would expect random crystal orientation. We have verified in one case ("$NbO_{2.00}$") by X-ray diffraction that the material supplied is single-crystal There was no simple relation between the crystal axes and the chip faces.

The supplied single crystals were cut, cleaned, and mounted in the microwave diode packages described in Section 6 of this report. The top faces of the crystals were provided with 125 μm evaporated aluminum electrodes. The bottom face of each chip was bonded to the diode package base with conducting paint. A 25 μm gold wire was then bonded as usual to the top aluminum 125 μm diam. electrode.

14. PULSE RESPONSE OF NbO_x CRYSTALS - CABLE PULSE GENERATOR

The NbO_x crystals tested fell into two broad categories.

(a) Samples with initial off-state resistance > 10 kΩ.

(b) Samples with initial off-state resistance < 10 kΩ.

Type (a) samples had stoichiometry NbO_x with $x \geq 1.89$, while type (b) samples had $x \leq 1.89$. No switching was observed for applied voltages $\leq$ 900 V for type (a) material. The conductive type (b) samples were too lossy for further consideration.

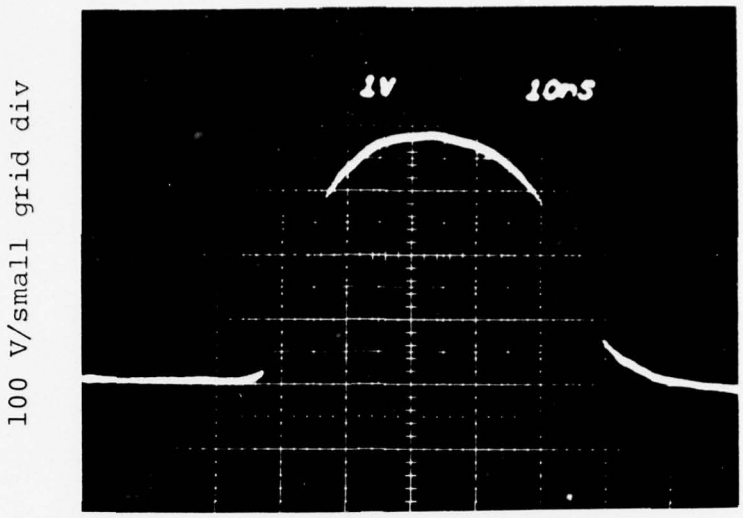
In Table 11 we list some parameters for the single-crystal samples tested. The last entry gives comparable values for the polycrystalline NbO_2 on NbO substrate. From Table 11 we might conclude that the NbO_2 on NbO substrate is nearly stoichiometric. It is also clear that switching of the NbO_x crystals with the available voltage from the cable pulse generator is unlikely, since the maximum applied fields were low compared to the switching field of the NbO_2/NbO chips. In fact, no switching was observed for any of the single-crystal samples of Table 11. To increase the applied field, we can either increase the applied voltage or thin the samples mechanically. Increased applied voltage was obtained with a Velonex pulser, as described in Section 15.

TABLE 11. RESISTANCE AND MAXIMUM APPLIED FIELD FOR THE NbO_x SINGLE-CRYSTAL SAMPLES. The resistivity is computed from the resistance ignoring end effects and is only qualitatively correct.

Sample No.	Sample Type	Batch Date	Initial Resistance kΩ	Initial Resistivity Ω-cm	Max. Applied Field (Volts/μm)
1	$NbO_{2.00}$	9/8/76	104	10^3	3.3
2	$NbO_{1.95}$	7/28/76	142	880	2.8
3	$NbO_{1.90}$	9/17/76	15.8	37	1.0
4	$NbO_{1.89}$	11/4/75	20	24	0.55
5	$NbO_{1.89}$	10/13/76	0.007	0.015	---
6	$NbO_{1.87}$	11/6/75	0.003	0.003	---
	NbO_2 on NbO substrate	---	20-60	2.5×10^3-7.5×10^3	20-40 for switching

15. VELONEX PULSE GENERATOR

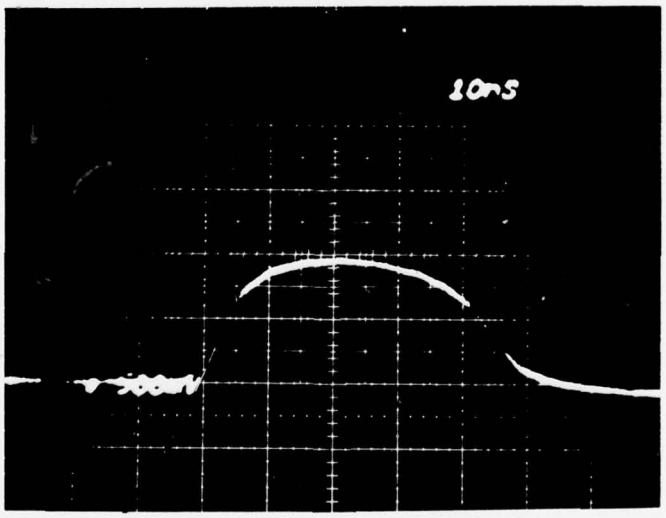
A system capable of 100 ns, 2.5 kV pulses was set up with a Velonex 350 pulse generator and a Tektronix Model 7633 Storage Oscilloscope. Pulse rise time was 30 ns. Voltage and current traces into a 200 Ω carbon resistor are given in Figures 43 and 44, respectively.



100 V/small grid div

10 ns/small grid div

Figure 43. Voltage across 200 Ω resistor-Velonex Pulse Generator.



1 A/small grid div

10 ns/small grid div

Figure 44. Current through 200 Ω resistor-Velonex Pulse Generator.

Attempts were made to switch Samples 2 and 4 (Table 11) using the Velonex Pulse Generator. In both cases no switching was observed below 2 kV. Increasing the voltage above this level produced air breakdown between the top electrode and the diode package. A typical trace is given in Figure 45. Arcing was clearly visible at these voltages. Although it would be possible to suppress arcing by immersing the diode package in, say, oil, we have felt this to be a relatively unprofitable course, since the Velonex Pulse Generator will not produce pulses above 2.5 kV (without transformers, which substantially degrade pulse rise time). It seemed simpler to thin the NbO_x crystals to increase the applied field.

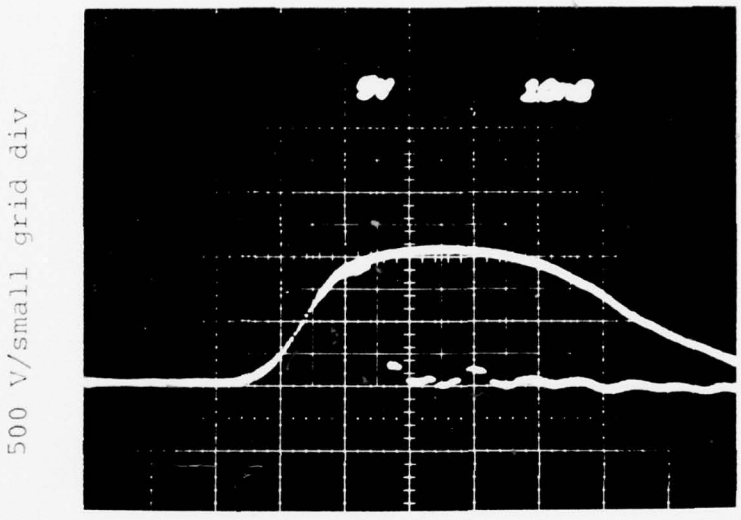


Figure 45. Air breakdown for $V_{applied} > 2$ kV. Sample No. 2, $NbO_{1.95}$.

16. CAT WHISKER CONTACT ON THICK $NbO_{1.87}$ SINGLE-CRYSTAL CHIP

In Section 15 the problems associated with studying thick single-crystal NbO_x materials were discussed. With evaporated contacts to thick crystals, it would be necessary to use large pulse voltages. This, in turn, would necessitate the use of the Velonex Pulse Generator with its rather poor pulse rise time characteristics. It seemed simpler to thin the NbO_x crystals to increase the applied field and thus take advantage of the superior qualities of the fast rise time cable pulser used in the study of NbO_2/NbO polycrystalline devices. Some results, however, were obtained with the cable pulse generator on a thick sample by

utilizing a tungsten cat whisker contact. This study will be briefly discussed here.

A $NbO_{1.87}$ single-crystal chip, ~1.05 mm thick, was observed to switch with an applied pulse of 3 ns length in the range 500 to 1000 V. The switching, which was accomplished in both air and silicon oil environments, was accompanied by continuous sparking in the vicinity of the cat whisker contact. The interesting aspect of this experiment was the observation of rather high initial "resistance" (from cat whisker to backside contact), ~ 350 kΩ, with a material of nominally very low resistance, ~ 0.003 Ωcm (as shown in Table 11, Section 14). After ~ 250 pulses of 3 ns duration, the resistance drops by over a factor of 10^4 to ~ 20 Ω. The switching characteristic in silicon oil is shown in Figure 46. The resulting damage to the crystal surface is shown in Figure 47. The pit located at the point of contact with the cat whisker is ~ 14 μm in diameter and ~ 20 μm deep.

We do not fully understand the origin of the high resistance in the virgin cat whisker contact. However, such contacts are easily damaged, as shown in Figure 47, and we have chosen to do all other single-crystal work with 125 μm evaporated aluminum dots and gold ball bond contacts. Since the field necessary for switching with this type of contact is ~ 20 to 40 V/μm, the remaining single-crystal samples were directly thinned to ~ 25 μm thickness. This rather tedious and exacting procedure is described in detail in the next section.

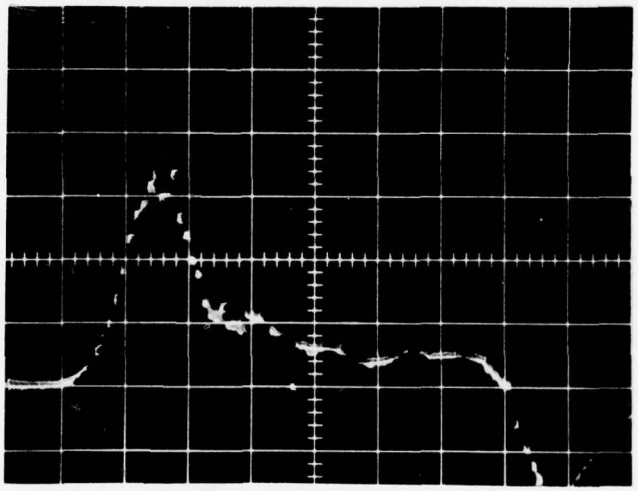


Figure 46. $NbO_{1.87}$ single-crystal chip with cat whisker contact. Applied pulse 1000 V, 3 ns.

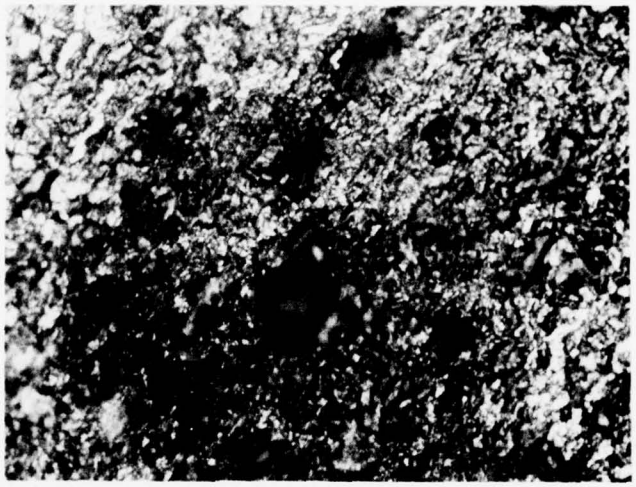


Figure 47. Area of cat whisker contact after 1000 V pulses. The pit is ~ 14 μm across and ~ 20 μm deep.

17. PROCEDURE FOR THINNING NbO_x CRYSTALS

1. Measure thickness and record shape of as-received NbO_x single-crystal samples.

2. Cut the crystals into ~ 2 mm x ~ 2 mm sizes so as to fit into the microwave diode package. This is accomplished by first gluing the sample to a glass plate on the cutting jig (with glycol phthalate). A second glass plate is glued to the top of the sample to prevent chipping of the surface during cutting. The cutting is performed with a diamond saw.

3. Remove sample from cutting jig and clean in hot acetone with ultrasonic agitation.

4. Mount sample on a lapping jig with glycol phthalate making sure sample is in good contact with the jig as the glycol phthalate cools and hardens.

5. Lap sample on a glass lapping plate using 3 μm alumina powder, distilled water, and shaving cream as the lapping medium. Lap until surface is flat.

6. Remove sample from lapping jig and clean in hot acetone with ultrasonic agitation. Blow dry.

7. Mount sample on a flat tungsten disk ~ 0.4 mm thick and ~ 3 mm in diameter with a drop of silver epoxy (EpoTek, H-31 conducting silver epoxy).

8. Clean the sample and disk in hot acetone with ultrasonic agitation and then remount on the lapping jig. In addition, three pieces of slide glass or silicon wafer, thicker than the total of sample plus disk and spaced ~ 120° apart, are also set in place with glycol phthalate. This arrangement, shown in schematic in Figure 48 helps keep the sample flat during lapping.

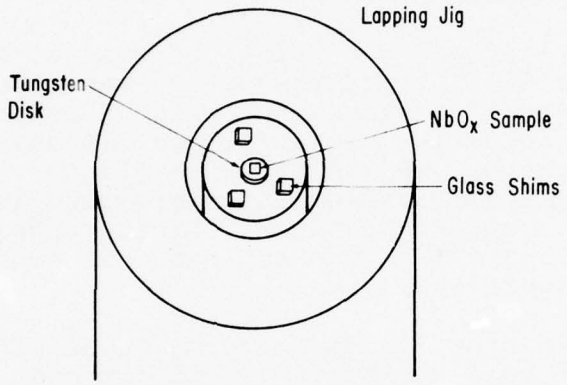


Figure 48. Schematic drawing of lapping jig with NbO_x sample mounted on a tungsten disk surrounded by three glass shims.

9. Lap the sample on a glass plate using 5 μm alumina powder, distilled water, and shaving cream. When the sample is ~ 50 μm thick, clean the lapping jig and sample in Ivory soap and distilled water.

10. Use 3 μm alumina powder for the final lapping to ~25 μm. The lapping rate is about half of that for 5 μm powder.

11. Remove the sample (and attached disk) from the lapping jig and wash 3 or 4 times in hot acetone ultrasonically agitated.

12. Mount the sample on a mask with 125 μm diameter holes and evaporate aluminum of thickness ~ 1 μm onto the sample through the holes (in an appropriate vacuum chamber).

13. Mount the disk (and sample) in a microwave diode package using DuPont (#201231) Air Dry Silver Paint.

14. Attach 25 μm gold wire to one of the 125 μm aluminum dots using an ultrasonic gold ball wire bonder (Mech-El, NU823). Bond the other end of the wire to the diode package casing. The device is now ready for testing.

The above procedure involves a large number of "hand" operations. As we shall see below in Section 19, switching in 25 μm-thick samples occurs at applied voltages in the 500 to 1000 V range (for 3 ns pulse lengths). If practical devices necessitate lower switching voltages, the crystals would require thinning to thicknesses less than 25 μm. While this can be done in the laboratory on a one-at-a-time basis, it is probably not a procedure easily amenable to high-volume, low-cost processing.

18. ENVIRONMENTAL TEST CHAMBER

In the next section, the pulse response of NbO_x crystals of ~ 25 μm thickness will be discussed. It was also desirable to investigate the sparking phenomenon which frequently accompanies switching and to determine the influence, if any, of the device environment. A chamber was built which allowed the pressure and type of ambient gas surrounding the microwave diode package and test fixture to be quickly changed. Photographs of the test set up are shown in Figure 49. The apparatus is schematically illustrated in Figure 50.

A glass cylinder ~ 7.5 cm in diameter and 18 cm long was fitted with thick rubber stoppers on either end. The GR fittings were assembled with vacuum-sealed coaxial connectors for sealing the centerline and insulator portions. The external parts of the GR fittings were tightly sealed into a hole in the stopper with O-rings. Additional holes were placed in the stoppers to accommodate an ionization gauge, an inlet pipe for rough vacuum, and one for air, freon, etc. A "high vacuum" tubulation was placed in the side of the chamber and connected through a valve to an oil diffusion pump with a substantial liquid nitrogen trap. A vacuum of ~ 5×10^{-4} torr could be maintained within the chamber during testing.

In the freon experiments, the valve of the freon container was directly connected to the chamber line. The chamber was first exhausted of air using the rough vacuum line and then back-filled with freon. This process was repeated several times to ensure that the device environment was free from air contamination.

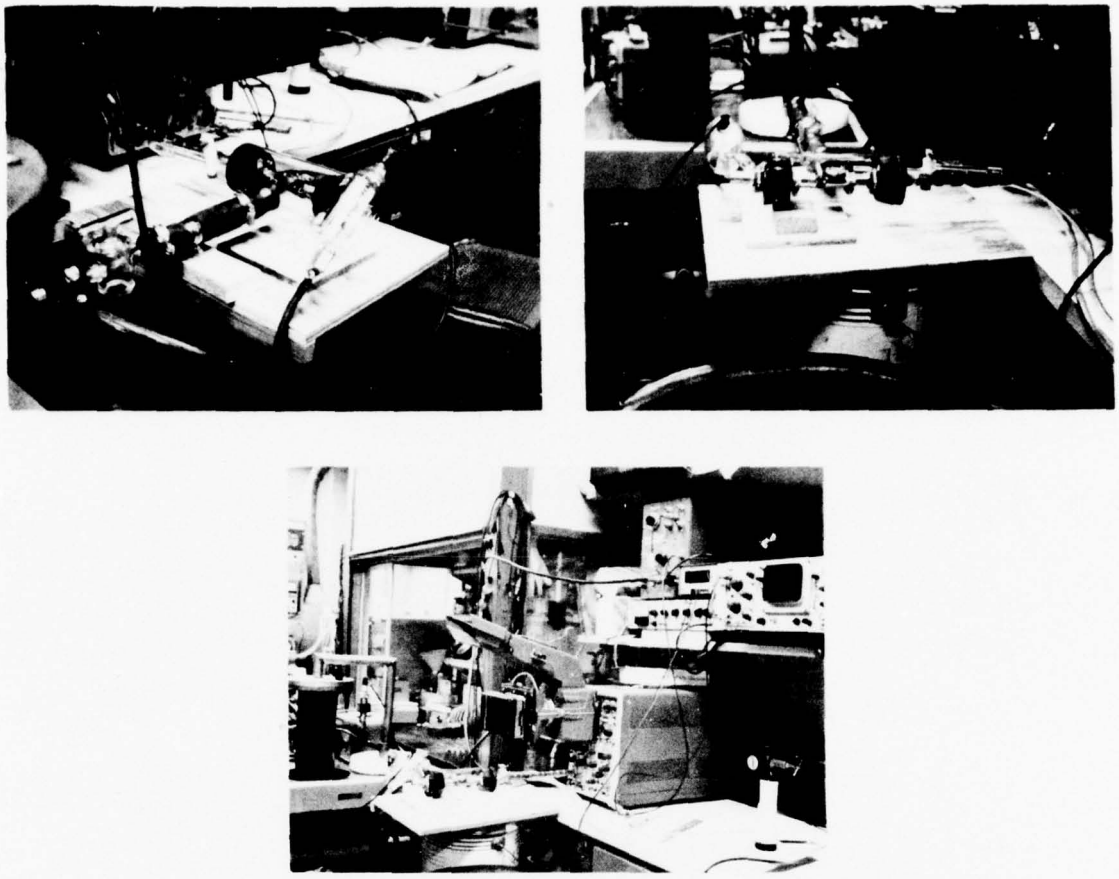


Figure 49. Photographs of environmental test chamber.

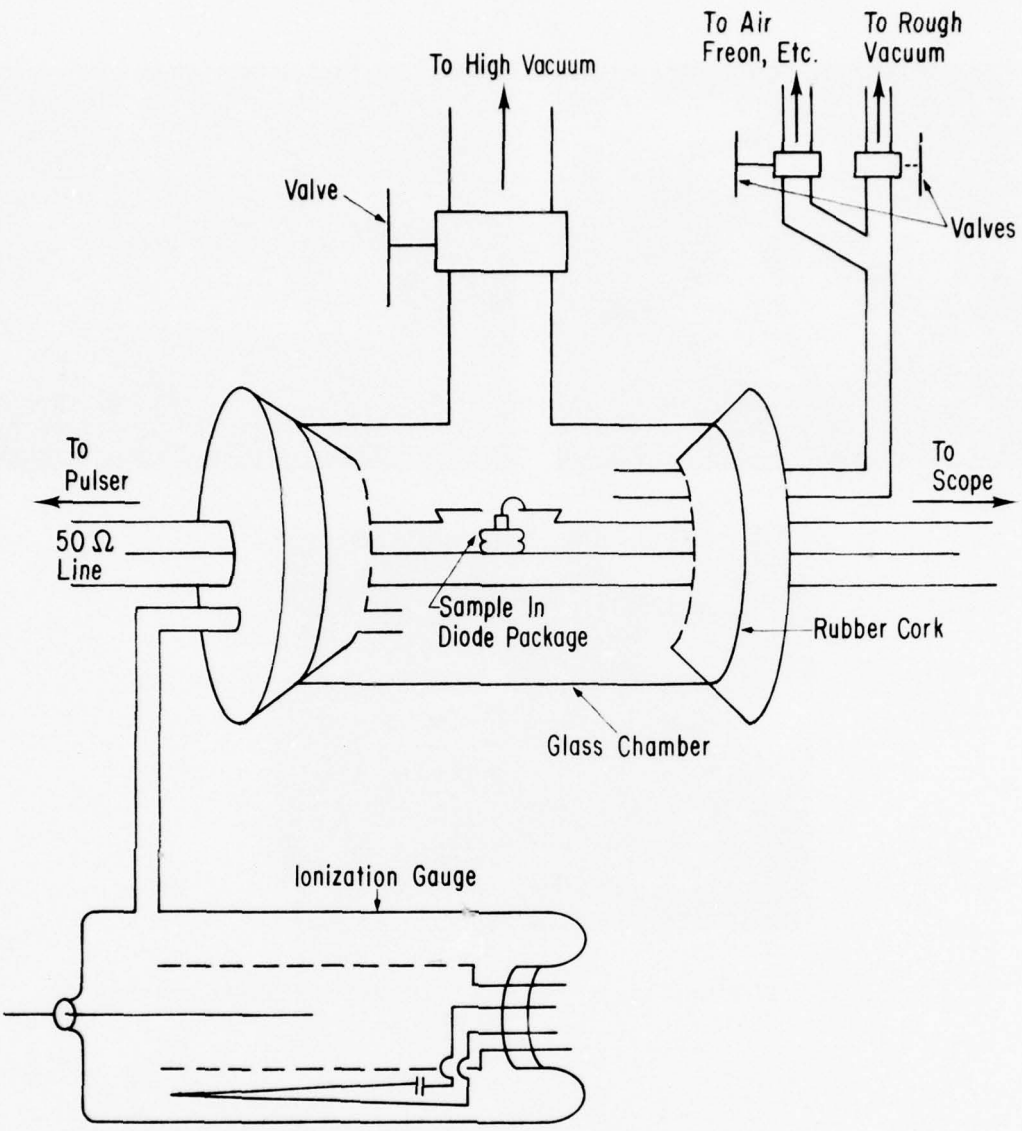


Figure 50. Schematic diagram of environmental test chamber.

19. PULSE RESPONSE OF THINNED NbO_x CRYSTALS

In Tables 12, 13, and 14, concise electrical histories are given for three NbO_x crystals thinned to ~ 25 μm thickness. The samples were tested in air, freon 12, and vacuum environments. All of the individual tests were performed in a time of 5 s and at a pulse repetition rate of 50 pulses per second. Thus, each listing in the tables corresponds to the application of 250 pulses.

TABLE 12

ELECTRICAL BEHAVIOR OF THINNED $NbO_{1.89}$ CRYSTAL IN VARIOUS AMBIENT GASES

Pulse Voltage V	Pulse Length ns	DC Resistance After Pulsing kΩ	Ambient Gas	Remarks	Oscilloscope Trace
250	3	28.1	Freon	No switching, no sparks	
500	3	16.8	Freon	No switching, no sparks	
750	3	21.3	Freon	Switched, continuous sparks	Fig. 51a
500	3	22.7	Freon	No switching, no sparks	
500	50	21.0	Freon	Switched, continuous sparks	Fig. 51b
250	3	33.7	Air	No switching, no sparks	
500	3	33.1	Air	No switching, no sparks	
750	3	28.2	Air	Switched, continuous sparks (glow)	Fig. 51c
250	3	29.3	Freon	No switching, no sparks	
500	3	26.2	Freon	No switching, no sparks	
750	3	20.8	Freon	Switched, initial sparking then stopped	Fig. 51d
250	3	19.7	Vacuum	No switching, no sparks	
500	3	19.9	Vacuum	Switched, no sparks	Fig. 51e
750	3	19.4	Vacuum	Switched, no sparks	Fig. 51f
500	3	22.0	Air	Switched, no sparks	Fig. 52a
500	3	24.0	Freon	No switching, no sparks	
250	50	22.2	Vacuum	Switched, no sparks	Fig. 52b
250	3	25.8	Vacuum	No switching, no sparks	
500	50	13.7	Vacuum	Switched, big bursts, sparking, streamers	Fig. 52c
250	3	15.3	Vacuum	No switching, no sparks	
250	3	17.4	Air	No switching, no sparks	
250	50	19.5	Air	Partial switch, flickering sparks	Fig. 52d
500	50	17.1	Air	Switched, occasional bursts then low level	Fig. 52e
500	50	18.0	Air	Switched, small sparking, flash at end	Fig. 52f
500	50	18.2	Air	Switched, bright low, then bright sparks at end	
500	50	20.1	Air	Switched, high and low sparking with bursts	
250	3	22.7	Air	No switching, no sparks	

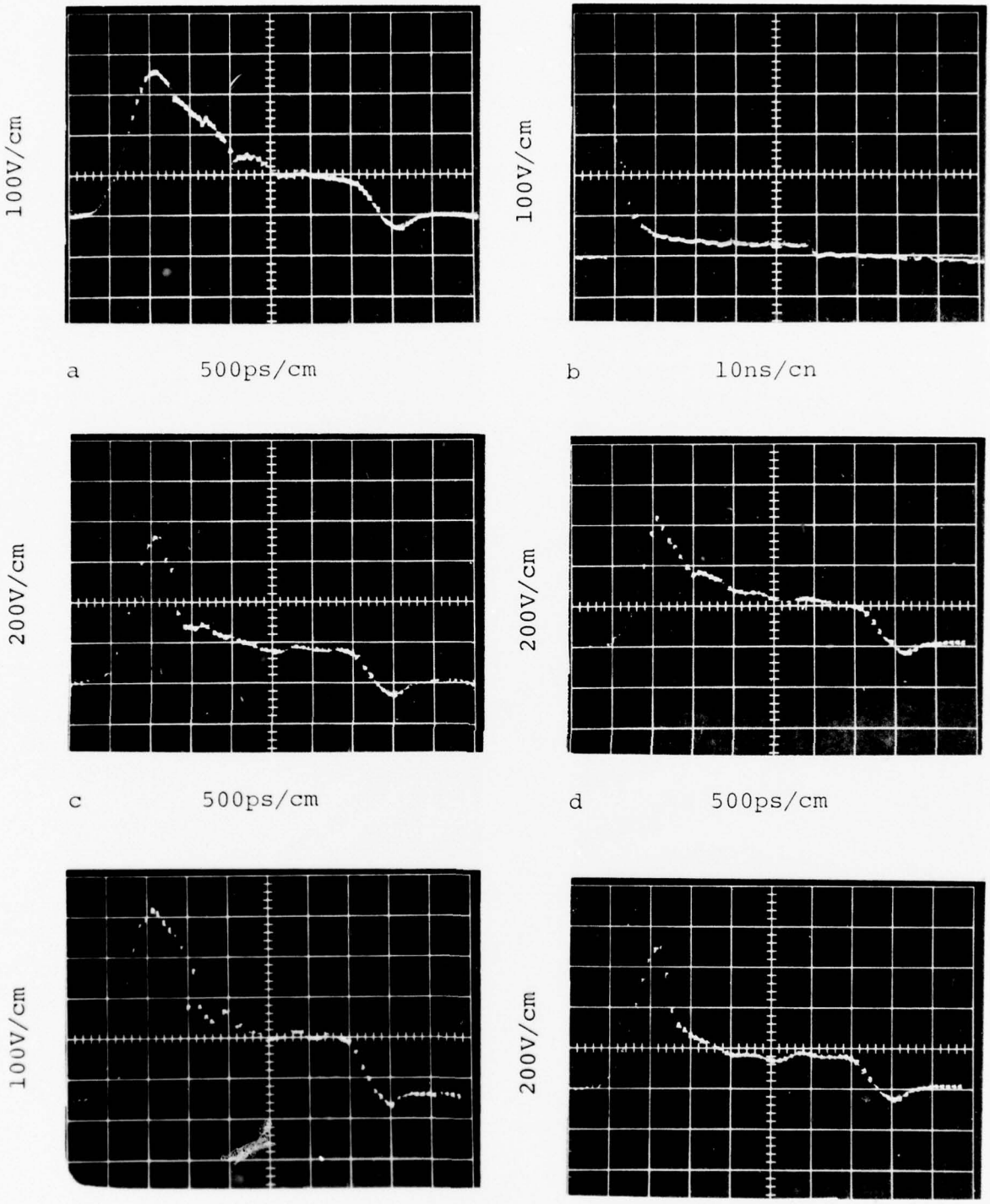


Figure 51. Switching in thinned $NbO_{1.89}$ sample. See Table 12.

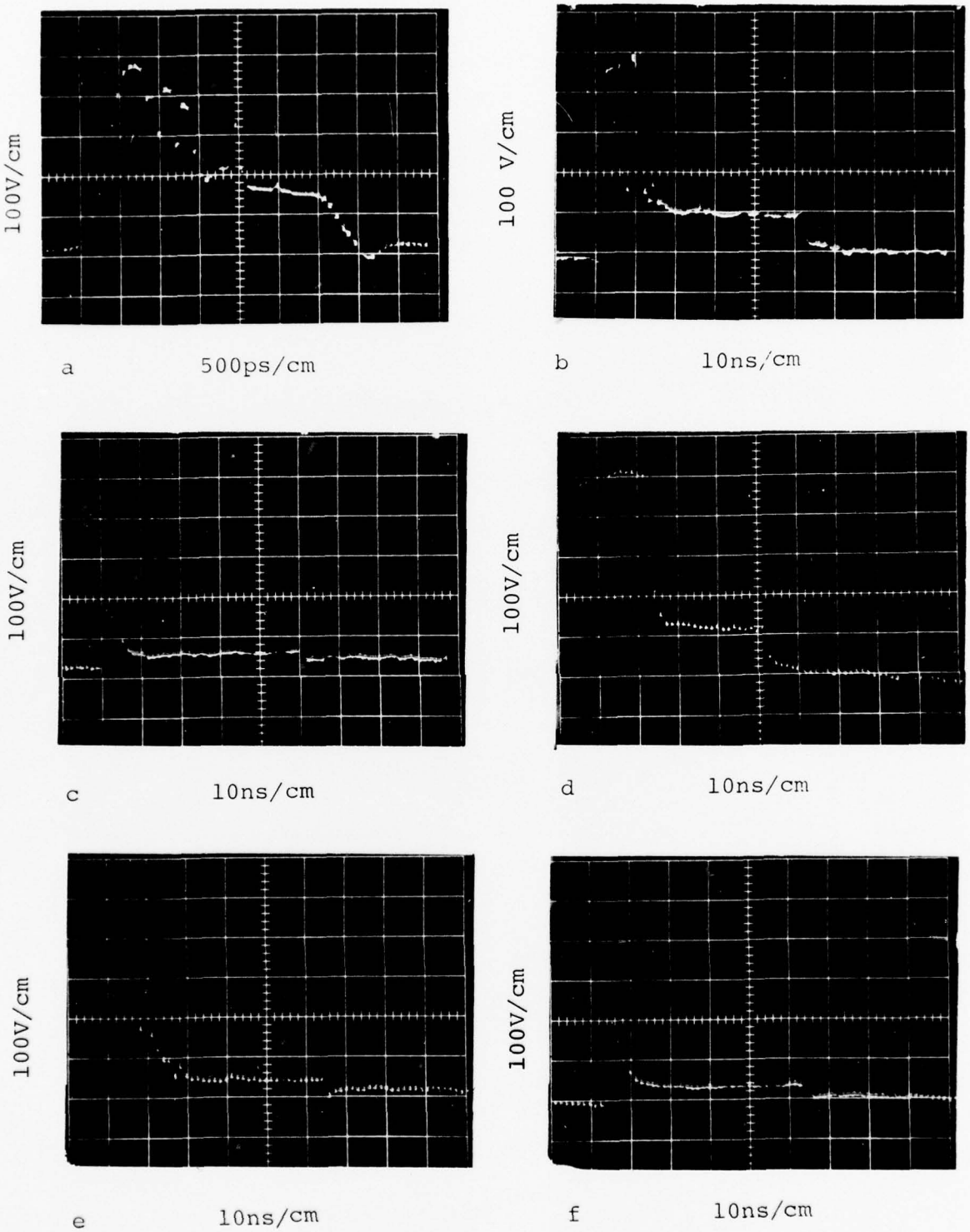


Figure 52. Switching in thinned $NbO_{1.89}$ sample. See Table 12.

TABLE 13

ELECTRICAL BEHAVIOR OF THINNED $NbO_{1.90}$ CRYSTAL IN VARIOUS AMBIENT GASES

Pulse Voltage V	Pulse Length ns	DC Resistance After Pulsing kΩ	Ambient Gas	Remarks	Oscilloscope Trace
250	3	89.2	Freon	No switching, no sparks	
500	3	29.4	Freon	No switching, no sparks	
750	3	28.8	Freon	Switched, continuous sparks	Fig. 53a
500	3	27.7	Freon	No switching, no sparks	
500	3	27.2	Air	No switching, no sparks	
500	3	27.6	Air	No switching, no sparks	
550	3	27.9	Air	No switching, no sparks	
600	3	29.2	Air	No switching, no sparks	
650	3	28.0	Air	No switching, no sparks	
700	3	26.0	Air	No switching, no sparks	
700	3	28.8	Freon	Switched, faint continuous sparks	Fig. 53b
700	3	25.7	Air	No switching, no sparks	
750	3	35.2	Air	Partial switch, no sparks	Fig. 53c
800	3	27.4	Air	Partial switch, no sparks	
800	3	32.9	Freon	Switched, continuous sparks	Fig. 53d
800	3	33.9	Helium	Partial switch, no sparks	Fig. 53e
900	3	42.5	Helium	Switched, no sparks	Fig. 53f
900	3	46.9	Freon	Switched, continuous sparks	Fig. 54a
900	3	43.3	Air	Partial switch, no sparks	Fig. 54b
900	3	29.3	Poor Vacuum	Switched, large glow, then continuous sparks	Fig. 54c
250	3	51.2	Air	No switching, no sparks	
500	3	53.8	Air	No switching, no sparks	
750	3	49.8	Air	Partial switch, intermittent sparks not localized	Fig. 54d
250	3	53.7	Freon	No switching, no sparks	
500	3	54.9	Freon	No switching, no sparks	
750	3	55.9	Freon	Partial switch, continuous sparks	Fig. 54e
250	3	60.9	Vacuum	No switching, no sparks	
500	3	58.4	Vacuum	No switching, no sparks	
750	3	53.3	Vacuum	Partial switch, continuous low level sparks	Fig. 54f
1000	3	28.6	Vacuum	Partial switch, continuous sparking, large burst towards end	Fig. 55a
750	3	39.5	Vacuum	No switching, light sparking but appeared to jump around	Fig. 55b
1000	3	36.0	Vacuum	Switched, continuous sparking occasional burst	Fig. 55c
1000	3	35.5	Vacuum	Switched, low-level continuous sparks	
500	3	39.4	Air	No switching, no sparks	
750	3	41.6	Air	Partial switch, continuous sparks	
1000	3	48.5	Air	Switched, low-level continuous sparking	Fig. 55d
+1000	3	52.9	Air	Switched, low level of sparking intermittent at end	Fig. 55e
-1000	3	32.7	Air	Switched, intermittent (of different character from above?)	Fig. 55f

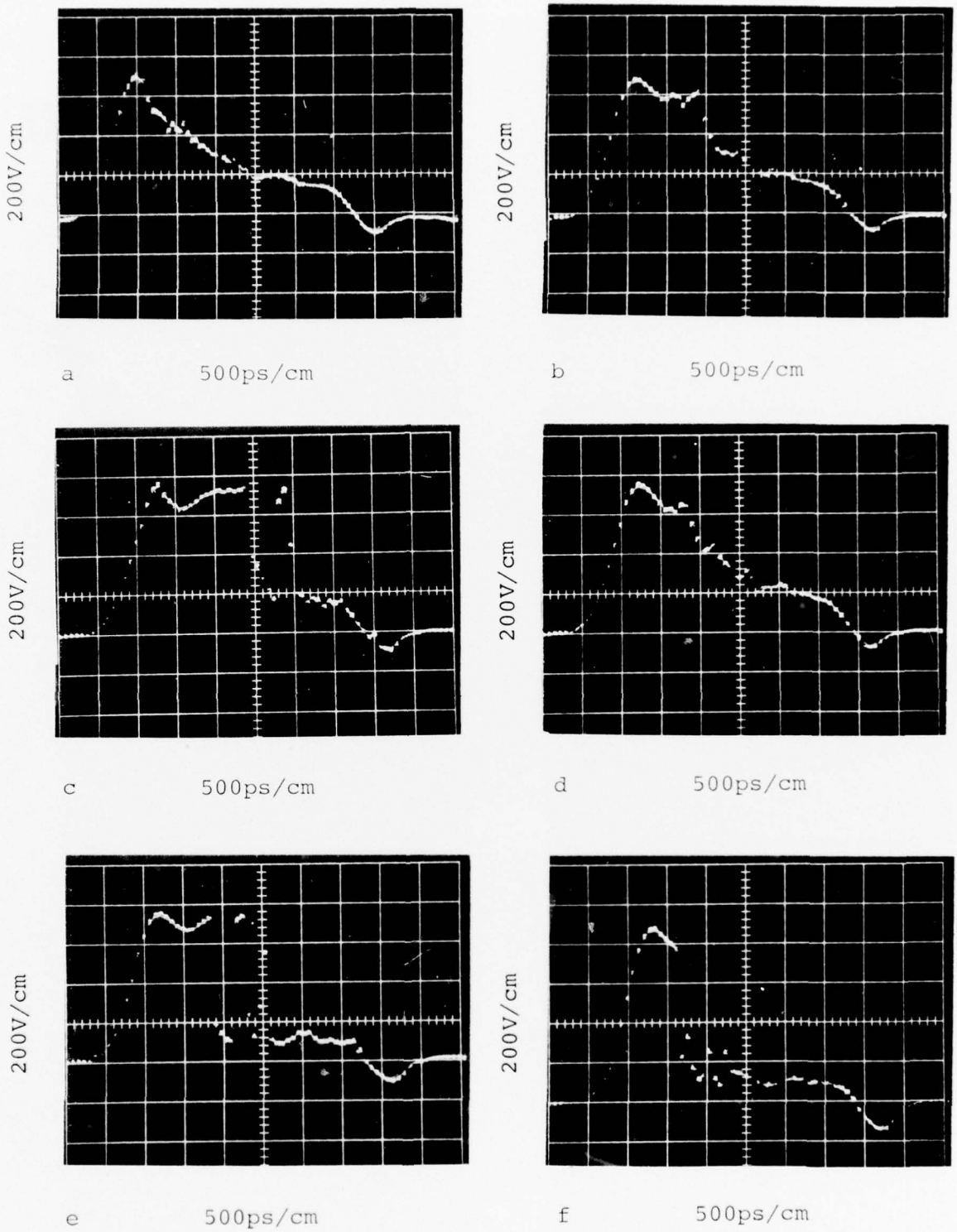


Figure 53. Switching in thinned $NbO_{1.90}$ sample. See Table 13.

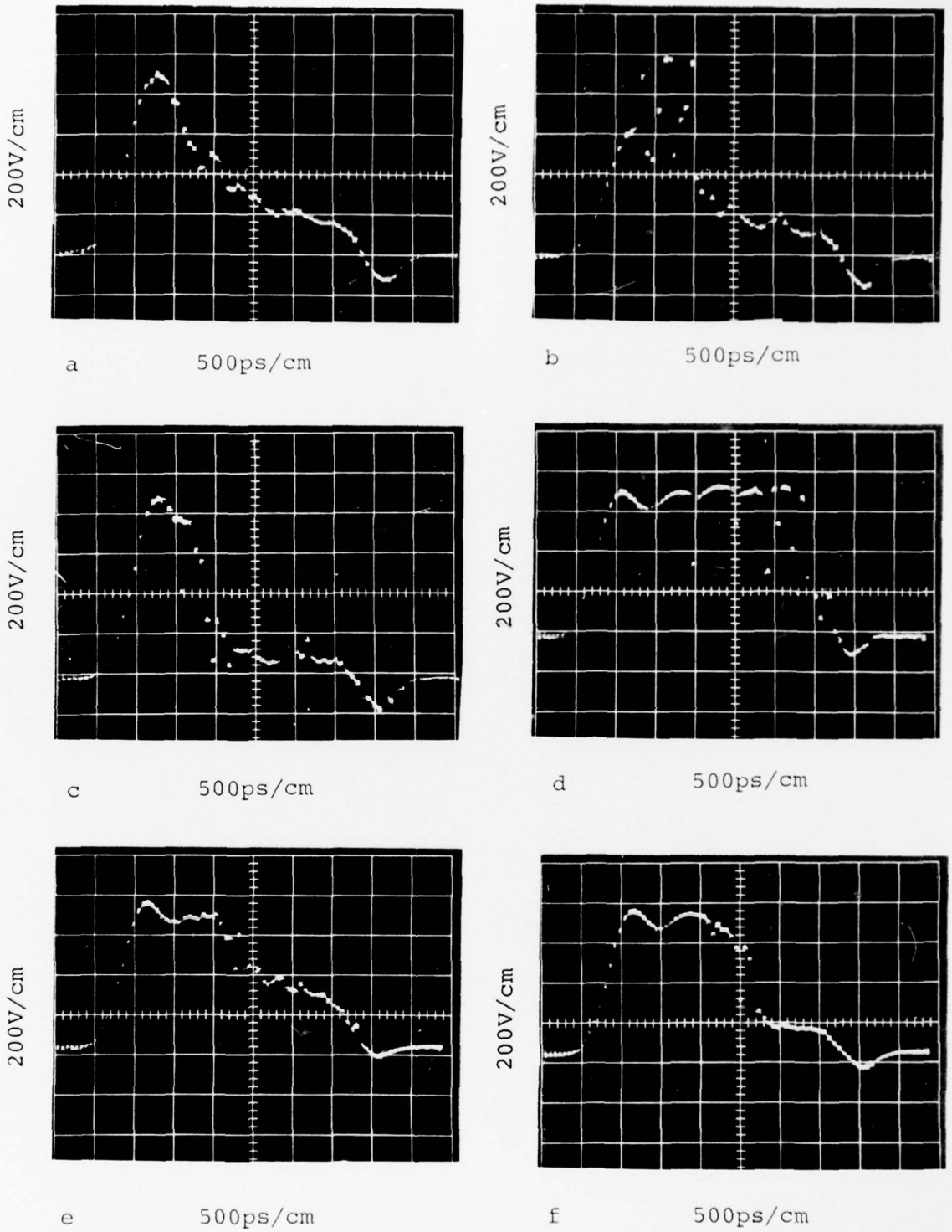


Figure 54. Switching in thinned $NbO_{1.90}$ sample. See Table 13.

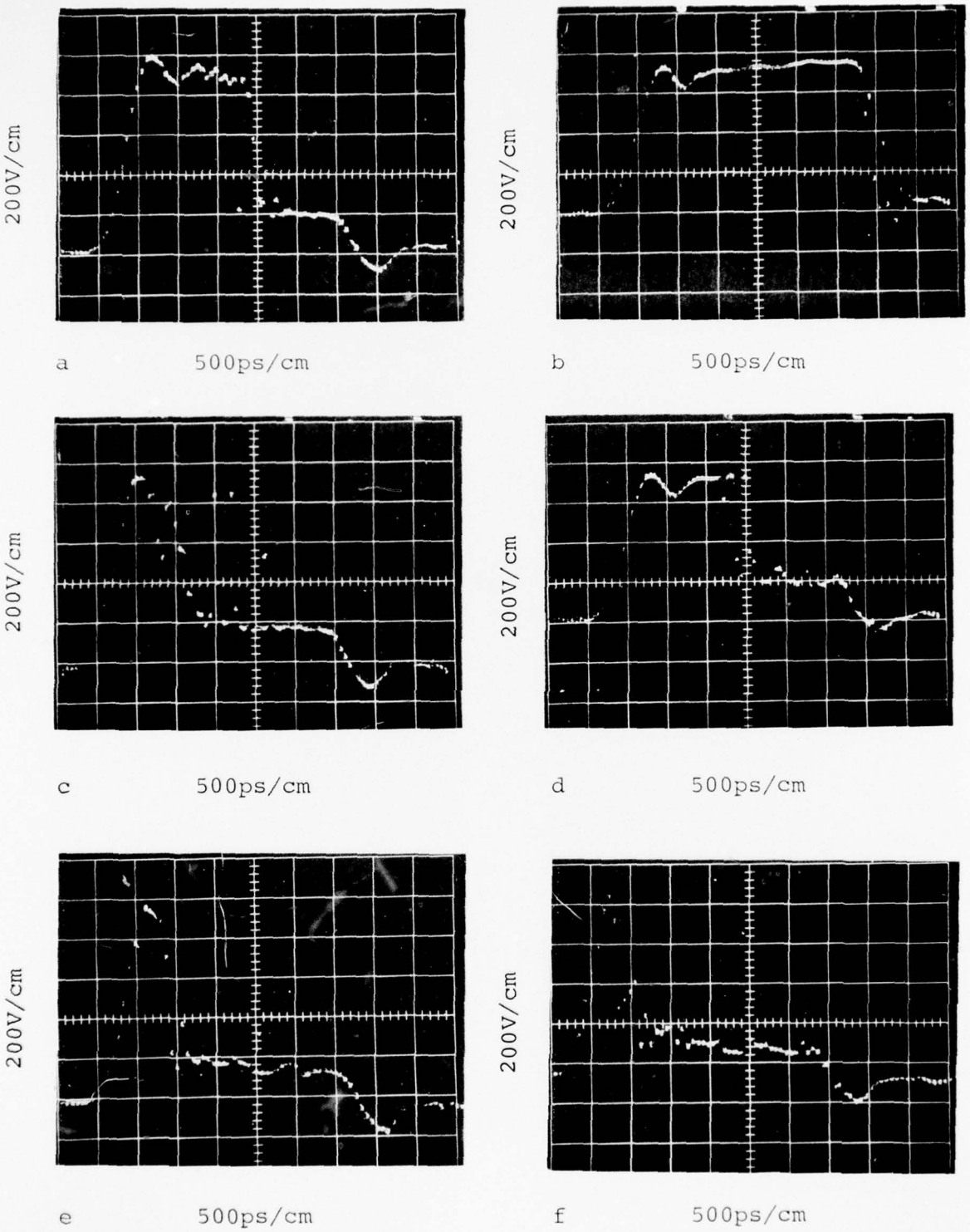


Figure 55. Switching in thinned $NbO_{1.90}$ sample. See Table 13.

TABLE 14

ELECTRICAL BEHAVIOR OF THINNED $NbO_{1.95}$ CRYSTAL IN VARIOUS AMBIENT GASES

Pulse Voltage V	Pulse Length ns	DC Resistance After Pulsing kΩ	Ambient Gas	Remarks	Oscilloscope Trace
500	3	161	Air	Switched, no sparks	
500	3	244	Freon Air	Partial switch, many faint sparks	
500	3	297	Freon	No switching, no sparks	
750	3	266	Freon	Switched, continuous sparking	Fig. 56a
1000	3	225	Freon	Switched, continuous sparking	Fig. 56b
750	3	237	Freon	Switched, low-level continuous sparking	
750	3	266	Air	Switched, initial low level sparking then no sparks	Fig. 56c
500	3	59.6	Air	No switching, no sparks	
750	3	59.2	Air	Switched, no sparks	
500	3	58.5	Air	No switching, no sparks	
250	3	60.4	Vacuum	No switching, no sparks	
500	3	23.1	Vacuum	Partial switch, no sparks	Fig. 56d
750	3	22.8	Vacuum	Switched, no sparks	Fig. 56e
750	3	54.5	Air	Switched, no sparks	
250	3	59.1	Freon	No switching, no sparks	
500	3	58.8	Freon	No switching, no sparks	
750	3	32.8	Freon	Switched, initially no sparks, then continuous sparking	Fig. 56f
500	3	---	Air	No switching, no sparks	
500	3	34.7	Air	No switching, no sparks	

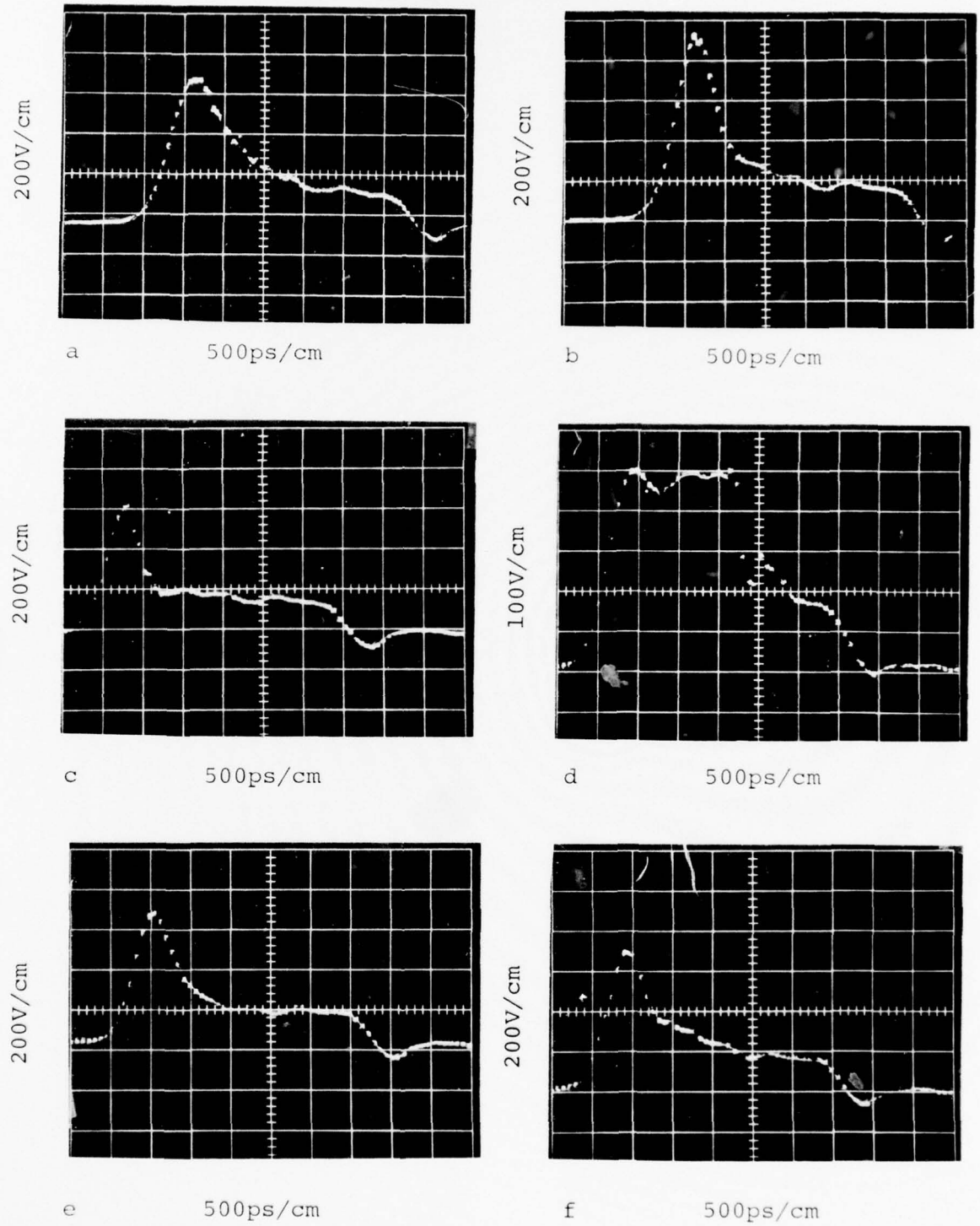


Figure 56. Switching in thinned $NbO_{1.95}$ sample. See Table 14.

Some oscillograph traces of the switching characteristic are also given in the accompanying Figures. The 25 μm thick crystals switch between 500 and 750 V for 3 ns pulses. This corresponds to a field of ~ 20 to 30 V/μm, which is comparable to that observed in polycrystalline NbO_2 on NbO substrates discussed in earlier sections. The switching field is lower by a factor of perhaps 2 for 50 ns pulses.

The main purpose of the above experiments was to examine the sparking phenomenon which frequently occurs during switching. In each of the individual tests listed in the above tables, a subjective response is given concerning the nature of the sparking, if any. These observations were made by eye in a darkened room.

The presence or absence of sparking during switching was not related to the dielectric strength of the gas environment. In several cases sparking was observed in freon gas and not in room air for the same applied voltage pulse.

The magnitude of the voltage pulse applied to cause switching is insensitive to device environment. For the $NbO_{1.90}$ sample described in Table 13, small differences in the threshold switching voltage were noted between freon and air environments. The threshold switching voltage was slightly lower for the crystal held in freon. The relation of this result and the apparent increase in sparking in freon compared to air environment is not obvious. However, the observation of sparking in a vacuum environment does give us an important clue as to its origin.

The mean free path for electrons is many centimeters at 10^{-3} torr of pressure.[9] Hence, it is difficult to initiate or sustain a gas discharge at these pressures in dimensions of the order of 0.1 cm or less. The pressure in our chamber as measured on an ionization gauge is ~ 5×10^{-4} torr. The sparks are thus most probably associated with particles "boiled away" from the NbO_x crystal at local hot spots associated with the switching process. The amount of sparking and the observations of "bursts of sparks" are more prevalent in 50 ns pulses than in 3 ns pulses of the same voltage. Thus, the sparking phenomena is associated with the amount of energy in the applied pulse. Even more convincing is the presence of holes around the periphery of the ball bond contact, especially in severely pulsed samples, indicating that material has been boiled away from the crystal surface. This evidence is presented in the next section.

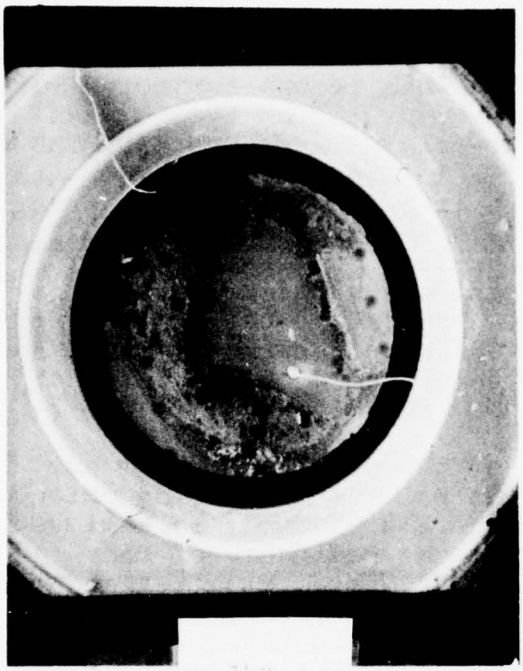
9. S. Dushman, Vacuum Technique (John Wiley, New York, 1949), p. 42.

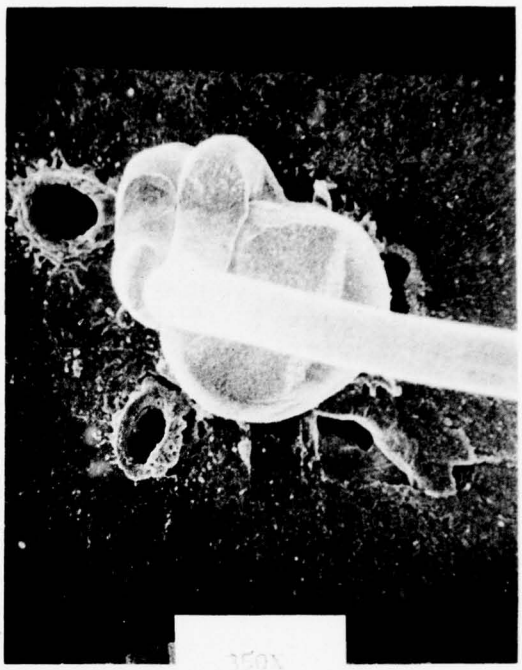
20. S.E.M. STUDIES OF DEVICE DAMAGE

The $NbO_{1.89}$ sample described in Table 12 was subjected to a number of 50 ns pulses. Three S.E.M. pictures of this crystal taken at different magnifications are shown in Figure 57. The 14X picture shows the crystal mounted in the diode package with the ball bond gold wire lead. There is a general "light" area around the ball bond contact, which we believe to be material spewed from the periphery of this contact. Several holes or pits are observed around the bond perimeter, which are seen in greater detail in the 350X picture. The pit in the upper left of this picture is also shown at 1400X magnification. The diameter of these holes is ~ 30 μm. The depth of these holes, which can be determined in the light microscope, is ~ 20 μm.

Similar S.E.M. pictures taken of the $NbO_{1.90}$ crystal are shown in Figure 58. We again wish to point out the ring which surrounds the ball bond contact in the 35X picture; we believe this ring is material spewed out from the periphery of the contact. The largest visible pit is ~ 20 μm in diameter and ~ 22 μm deep. The $NbO_{1.95}$ crystal, which was not tested as vigorously as were the other samples, was also examined. Minor damage was found around the periphery of the ball bond contact.

It is important to point out that each of the above three samples is still in "working order" in spite of the observed damage. It would appear that the crystal samples are substantially more stable than the polycrystalline NbO_2 on NbO substrate samples, which do not hold up very well, especially for pulses of 50 ns length or longer. These latter samples fail mostly by becoming short circuits. However, the crystal samples are about twice as thick as, or thicker than, the polycrystalline layers (which are ~ 10 μm in thickness) of NbO_2 that make up these devices. The pits observed in crystalline samples are ~ 20 μm deep and possibly do not quite "punch through" to the base contact. Such a crater in a polycrystalline NbO_2/NbO sample would reach the conducting NbO substrate and could cause the device to short out.





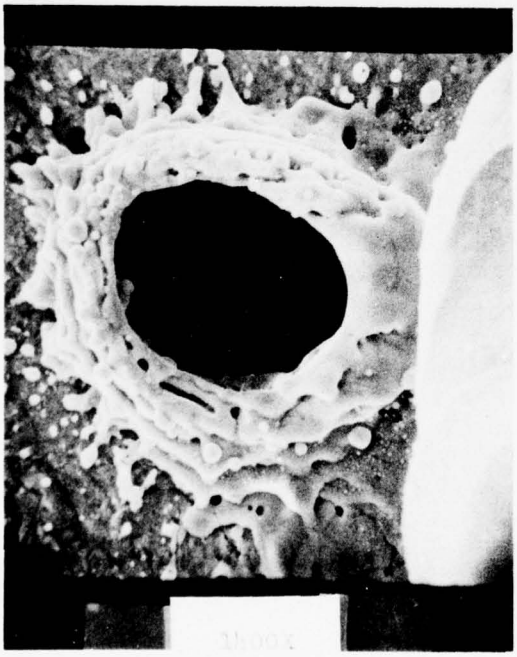
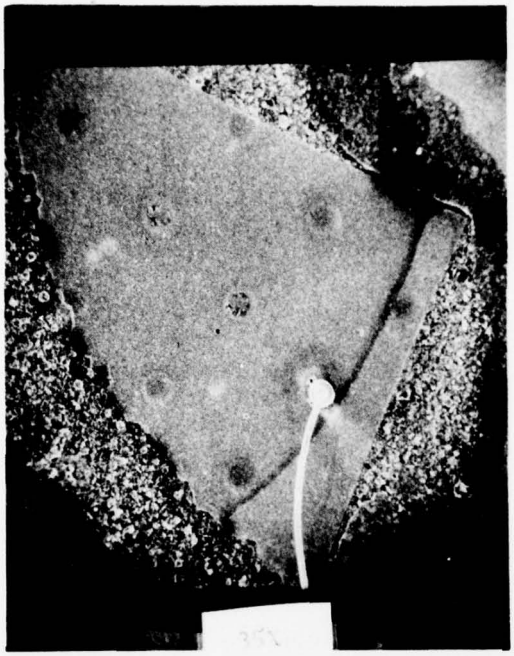


Figure 57 S.E.M. pictures at 14X, 350X, and 1400X of the $NbO_{1.89}$ sample after the experiments described in Table 12. The pits are of diameter ~ 30 μm and depth ~ 20 μm.





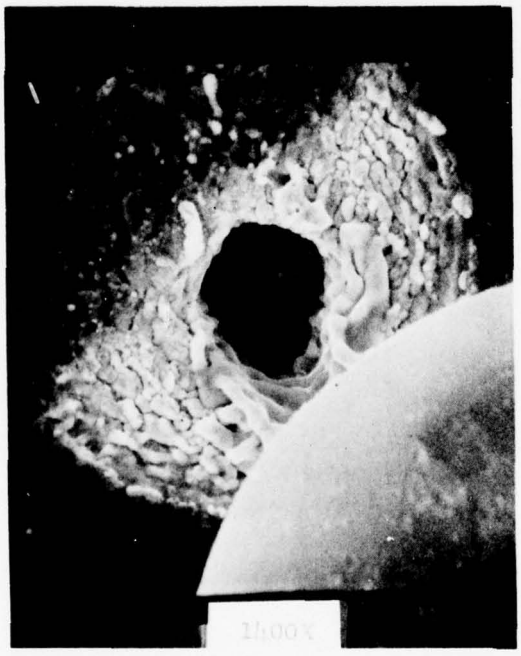


Figure 58. S.E.M. pictures at 35X, 350X, and 1400X of the $NbO_{1.90}$ sample after the experiments described in Table 13. The largest visible pit is ~ 20 μm in diameter and ~ 22 μm deep.

21. EFFECTS OF CRYSTAL STOICHIOMETRY

As discussed in Section 14, the supplied single-crystal materials fell into two broad categories: (a) samples with initial off state resistance > 10 kΩ and (b) samples with initial off state resistance < 10 Ω. Type (a) samples had stoichiometry NbO_x with $x \geq 1.89$, while type (b) samples had $x \leq 1.89$. The conductive type (b) samples were too lossy for further device consideration.

Three sample stoichiometries studied in Section 19 ($NbO_{1.89}$, $NbO_{1.90}$, and $NbO_{1.95}$) and described in Tables 12, 13, and 14, respectively, show similar switching voltages and switching characteristics. The initial resistances of the devices do increase with increasing oxygen content. However, after the pulsing tests described above, the contact-to-base resistance of all samples was a relatively consistent 20 to 35 kΩ. Hence, there does not appear to be any advantage or superiority of one stoichiometry over another for $1.89 \leq x \leq 1.95$.

22. ENVIRONMENTAL TESTS ON NbO_2/NbO POLYCRYSTALLINE DEVICES

Environmental tests were also made on NbO_2/NbO polycrystalline device from the same batch as the prelinary feasibility models furnished to ECOM. Pertinent electrical data are shown in Table 15. Sparking which accompanies switching was observed in both air and freon environments. The sparking seen for this sample was quite weak except for that occurring during the first switching pulse. In previous tests of similar devices, no sparking was found. However, observations for its occurrence were made on a somewhat random basis during pulse testing, and it is very possible that some sparking did take place which was not recorded. S.E.M. pictures taken after testing are shown in Figure 60. No appreciable damage is observed after the relatively light testing schedule.

TABLE 15

ELECTRICAL BEHAVIOR OF A POLYCRYSTALLINE NbO_2/NbO SAMPLE (NO X-15-33) IN VARIOUS AMBIENT GASES

Pulse Voltage V	Pulse Length ns	DC Resistance After Pulsing kΩ	Ambient Gas	Remarks	Oscilloscope Trace
100	3	33.2	Air	No switching, no sparks	
200	3	41.9	Air	No switching, no sparks	
300	3	27.9	Air	No switching, no sparks	
400	3	27.7	Air	No switching, no sparks	
500	3	27.5	Air	No switching, no sparks	
600	3	23.8	Air	Switched, continuous sparks	Fig. 59a
300	3	23.3	Freon	No switching, no sparks	
400	3	10.6	Freon	Switched, very weak continuous sparking	Fig. 59b
400	3	16.8	Air	Switched, very weak continuous sparking	Fig. 59c
400	3	8.1	Vacuum	Switched, no sparks	Fig. 59d
400	3	15.1	Air	Switched, one faint spark	Fig. 59e
400	3	13.8	Poor Vacuum	Switched, no sparks	Fig. 59f

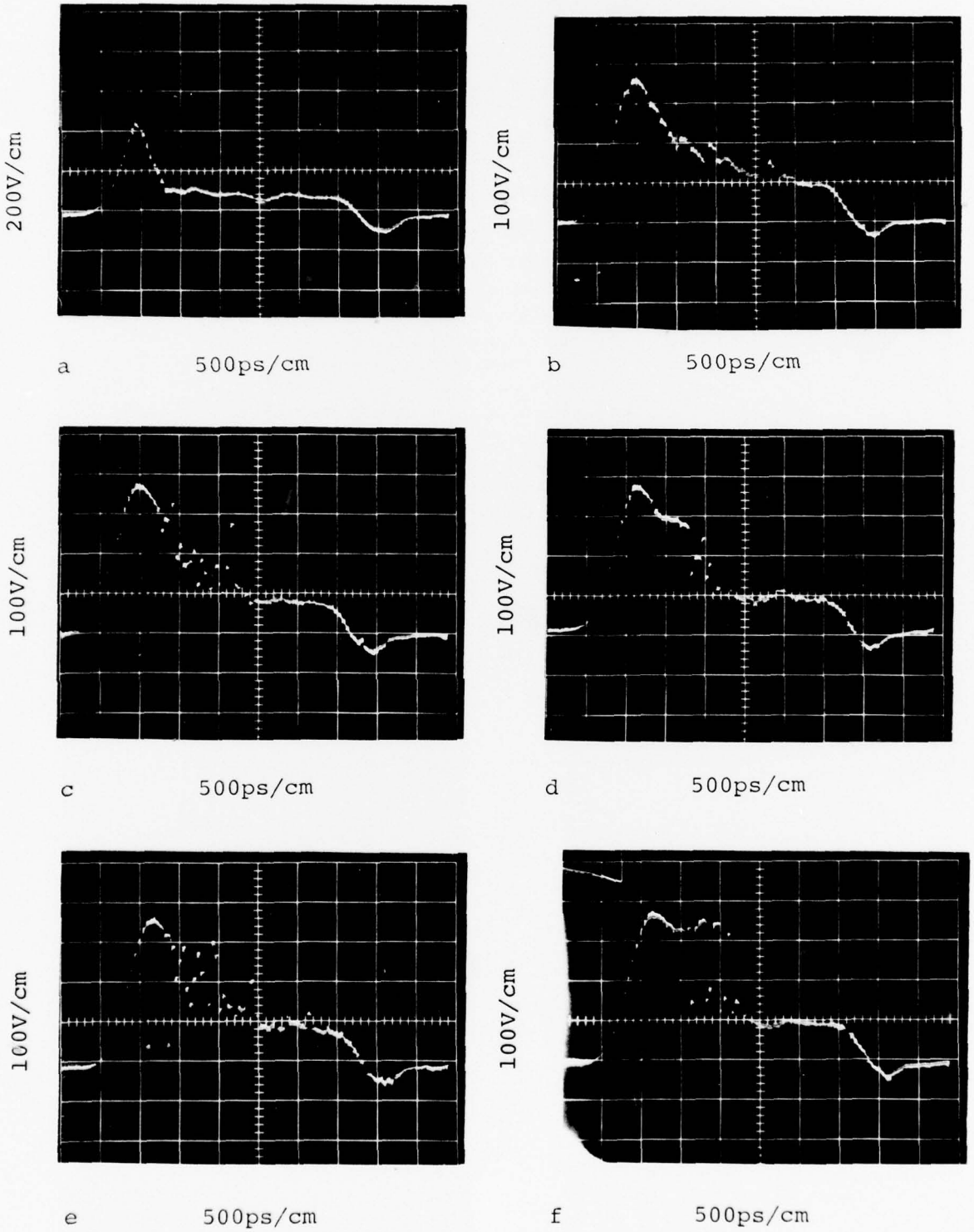


Figure 59. Switching in a polycrystalline NbO_2/NbO sample (No. X-15-33). See Table 15.

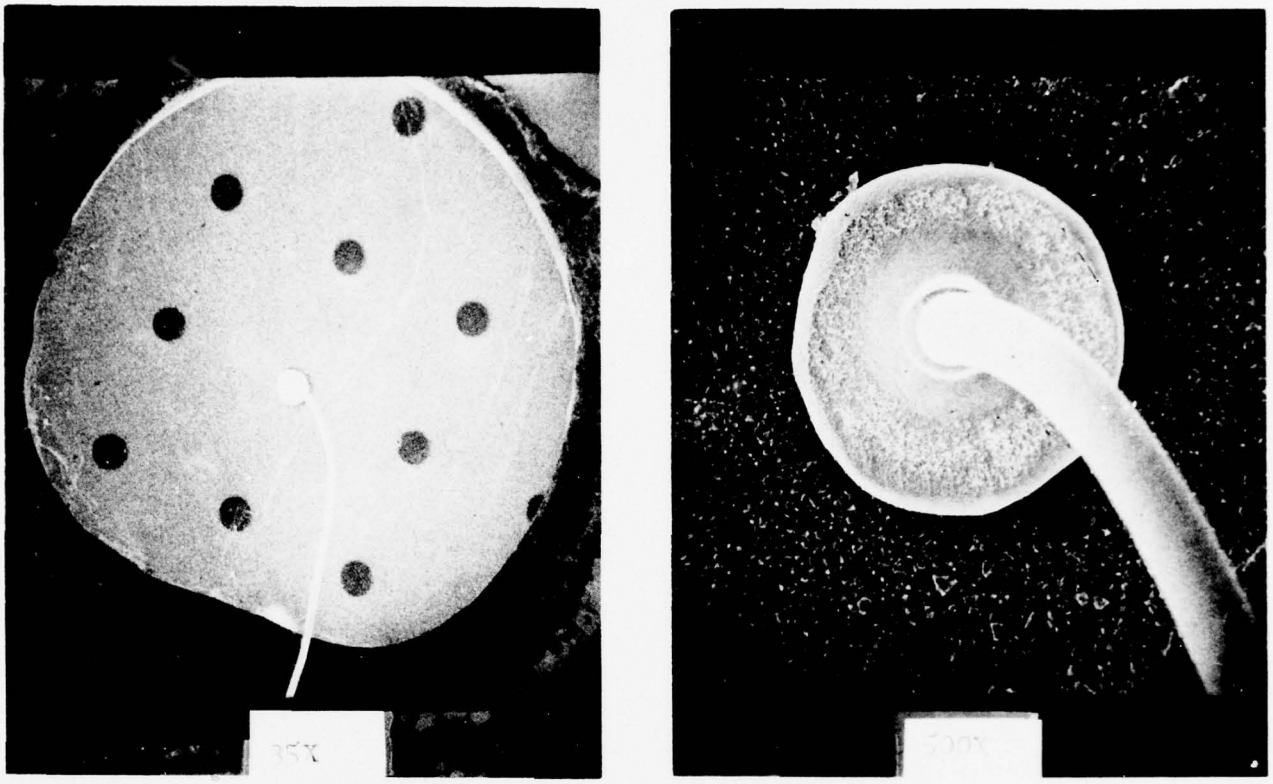
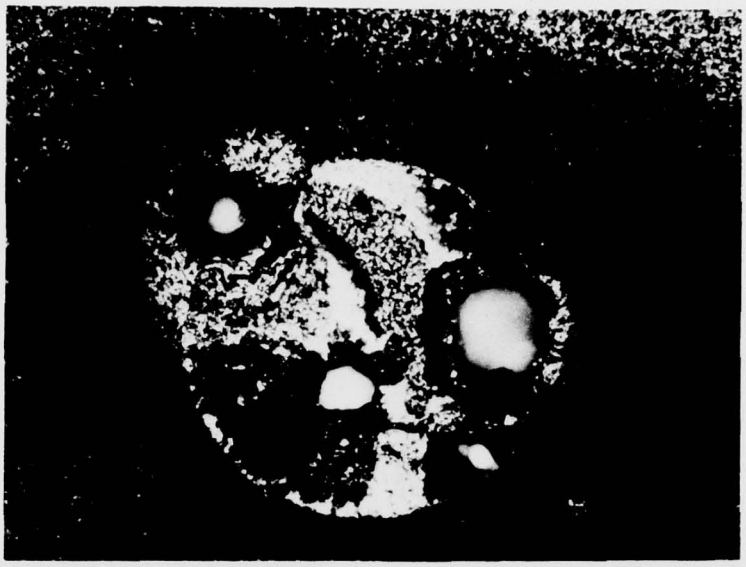


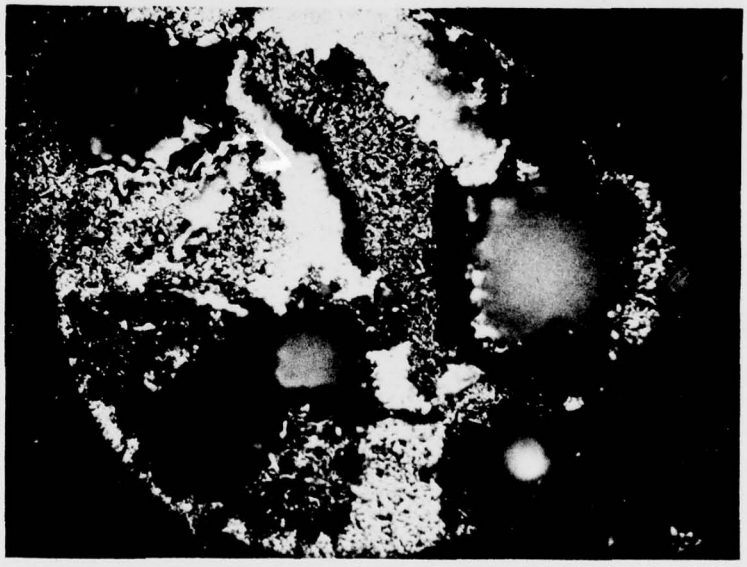
Figure 60. S.E.M. pictures at 35X and 500X of a polycrystalline NbO_2/NbO sample (No. X-15-33) after the experiments described in Table 15.

23. FURTHER STUDIES OF SINGLE-CRYSTAL DEVICE DAMAGE

In Section 20 scanning electron microscopic (S.E.M.) studies were discussed concerning damage in the vicinity of the ball bond contact of pulsed single-crystal samples. In severely pulsed samples, pits ~ 25 μm across and ~ 20 μm deep were observed around the periphery of the contact. The ball bonds of the $NbO_{1.89}$ and $NbO_{1.90}$ crystals were removed and the samples re-examined in the optical microscope. The results are shown in Figures 61 ($NbO_{1.89}$) and 62 ($NbO_{1.90}$) and should be compared with Figures 57 and 58, respectively, of Section 20. We note that little additional damage occurred underneath the ball bond contact area. For each sample only one additional pit smaller in diameter than those previously found around the edge of the contact is seen. This pit is located at the outer part of the contact area. Possibly the contact of the gold ball to the crystal surface is made nearer the center of the ball and

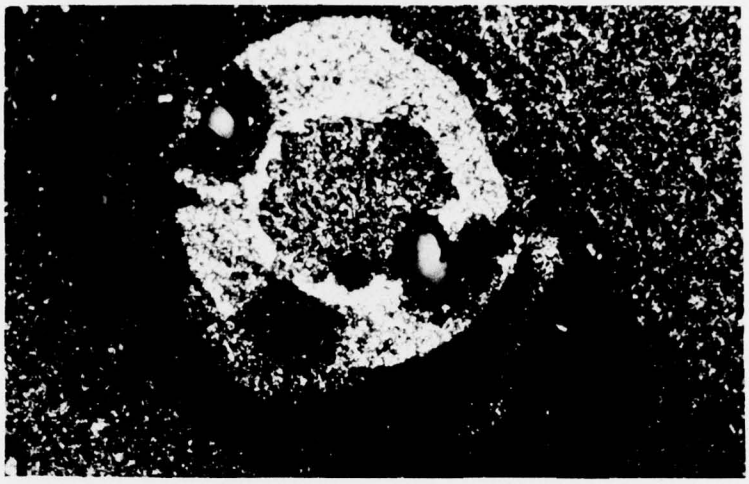


375X



750X

Figure 61. Light microscope pictures at 375X and 750X of the $NbO_{1.89}$ sample after removal of the ball bond contact.



375X



750X

Figure 62. Light microscope pictures at 375X and 750X of the $NbO_{1.90}$ sample after removal of the ball bond contact.

the additional pits occur where the ball is slightly lifted from the sample.

We have related the presence of pits to localized heating which occurs during the switching process and causes material to be spewed from the crystal surface. We may speculate that where the metal ball is in intimate contact with the crystal surface, heat may be conducted away from any "switching filaments," and/or material from the crystal surface may be physically held in position by the contact, thereby preventing the pits from forming. It is thus conceivable that the damage shown in the S.E.M. and light microscope pictures could be reduced or eliminated by employing a buried contact. One way in which this might be accomplished is by covering the contact and the crystal surface in the vicinity of the contact by an insulating layer (for example, epoxy cement, sputtered SiO_2, various silicones, etc). More elaborate schemes, including "diffused" contacts, could also be used. Since electrical degradation and the presence of physical damage appear to be correlated, the life of and applications for NbO_2 devices might be extended through the use of buried contacts.

24. PULSE RESPONSE OF A THINNED NbO_2 + 5% Ti CRYSTAL

A NbO_2 + 5% Ti crystal when thinned to ~ 20 μm thickness was observed to switch at ~ 875 V. The results are summarized in Table 16. The ambient gas was air. Each test was performed in a time of 5 s and at a pulse repetition rate of 50 pulses per s (250 pulses in all). Partial switching accompanied by sparking was initially observed at a pulse voltage of ~ 750 V, but when this pulse sequence was reapplied, no switching was observed. Attempts to switch the crystal with 1000 V, 3 ns pulses at crystal thicknesses of ~ 0.3 mm and ~ 75 μm failed, and hence the necessity for final thinning to ~ 20 μm. Although the dc resistance of the Ti-doped crystal is appreciably lower than those of the undoped crystals previously studied, the switching field is comparable. There thus appears to be little advantage to working with doped material, although it is not known whether doping aids or hinders device degradation associated with repeated pulsing. The present sample was not subjected to any additional pulse testing in order to preserve its "near virgin" status. It is included as one of the 100 coaxial switching devices delivered to ECOM under the terms of the contract.

TABLE 16

ELECTRICAL BEHAVIOR OF THINNED NbO_2 + 5% Ti CRYSTAL

Pulse Voltage V	Pulse Length ns	DC Resistance After Pulsing kΩ	Ambient Gas	Remarks	Oscilloscope Trace
100	3	7.5	Air	No switching, no sparks	
200	3	4.8		No switching, no sparks	
300	3	3.7		No switching, no sparks	
400	3	3.2		No switching, no sparks	
500	3	2.8		No switching, no sparks	
750	3	2.2		Partial switch; continuous sparking, intermittent at end	Fig. 63a
750	3	2.2		No switching, one little spark	Fig. 63b
875	3	2.0		Switched, burst of sparks, then nothing	Fig. 63c

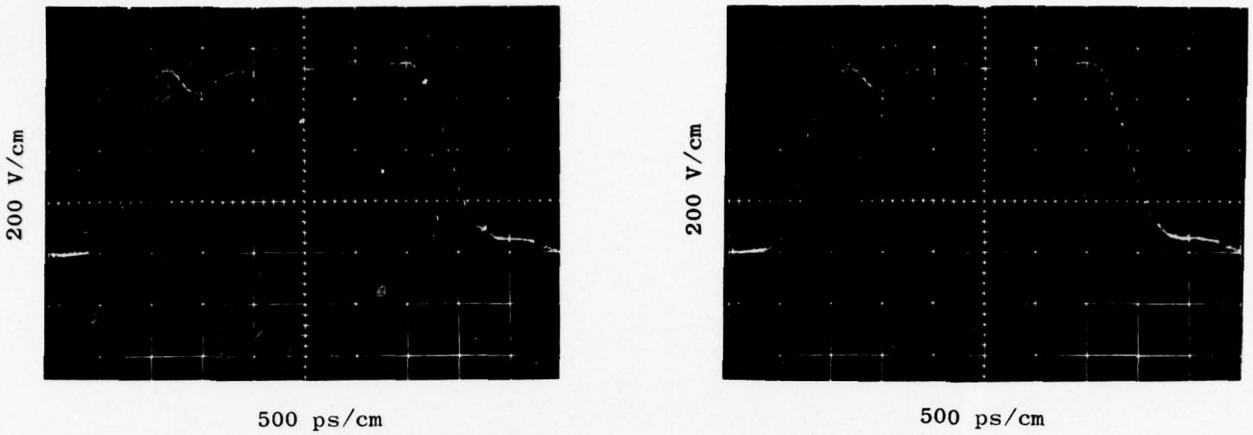


Figure 63. Switching in Thinned NbO_2 + 5% Ti. See Table 16.

25. X-RAY STUDIES OF AS-RECEIVED NbO_x CRYSTALS

Single crystals of NbO_2 can be grown from the melt[10] at about[11] 1915 °C. The crystals can apparently be grown[10] with a range of NbO_x compositions from x = 1.90 to x = 2.10. Generally,

10. S.H. Shin, T.H. Halpern, and P.M. Raccah, Mater. Res. Bull. 10, 1061 (1975).
11. R.P. Elliott, Trans. Am. Soc. Met. 52, 990 (1960).

the homogeneity range of such a crystal decreases with decreasing temperature[12]. At 1000 °C Marucco et al[12], found a range of x of $2.000 \leq x \leq 2.003$. The range found by Jannick and Whitmore[13] at 1100 °C was $1.997 \leq x \leq 2.003$.

The crystals used in the present study, which were grown at Yeshiva University[10], have a claimed range of x from $1.87 \leq x \leq 2.00$. It is not known whether these stoichiometries were determined from the starting ingredients of the melt or by some measurement on the grown crystals themselves. We examined these crystals by X-rays to find out if they were single-phase as delivered and if there was any variability in the lattice parameters of the tetragonal "NbO_2" phase. The five different crystals studied all showed identical lattice parameters with:

$$a_o = 13.693 \pm 0.003 \text{ Å}$$

$$c_o = 5.985 \pm 0.002 \text{ Å}$$

These values are in fairly good agreement with those found in the literature for "NbO_2." A tabulation of such measurements is given in Table 17. It is noted that the literature values tend to be equal to or smaller than the present numbers. We believe that the lattice parameters we determined are those for stoichiometric NbO_2 at $x = 2.000$. If the "NbO_2" crystals can actually be oxygen-rich, i.e., $x > 2.000$ by replacing some Nb^{4+} with Nb^{5+} and metal vacancies, then one would expect some lattice shrinkage as x increases above 2.000. Such deviations would be in agreement with the findings of Marucco et al.[12]

As pointed out above, the lattice parameters of all the crystals we measured were identical. This result is not to be expected if each of the crystals is single-phase with the labeled stoichiometry. Indeed, we found that the crystals of labeled stoichiometry $x = 1.87$ and 1.89 also showed lines corresponding to crystalline NbO. Although we could not quantitatively determine the amount of NbO from these data, these samples are obviously two-phase, with inclusions of NbO inside the bulk crystals. On the basis of the work cited in References 12 and 13 and the "constant" lattice parameter values we found, it is also conceivable that all of the as-received crystals with $x < 2.000$ are two-phase. The resistivity values

---

12. J.F. Marucco, R. Tetot, P. Gerdanian, and C. Picard, J. Solid State Chem. 18, 97 (1976).

13. R.F. Jannick and D.M. Whitmore, J. Phys. Chem. Solids 27, 1183 (1966).

TABLE 17

LITERATURF REFERENCES FOR THE LATTICE PARAMETERS OF "NbO_2" AT ROOM TEMPERATURE

a_o Å	c_o Å	c_o/a_o	Year	Reference
13.693 ± .003	5.985 ± .002	0.4371 ± .0003	1977	Present Work
13.660	5.964	0.4366	1976	(14)
13.71	5.985	0.4365	1972	(15)
13.675	5.964	0.4361	1967	(16)
13.681	5.976	0.4368	1963	(17)
13.71	5.985	0.4365	1963	(18)
13.71	5.985	0.4365	1955	(19)

14. R. Pynn, J.D. Axe, and R. Thomas, Phys. Rev. B13, 2965 (1976).

15. T. Sakata, K. Sakata, G. Höfer, and T. Horiuchi, J. Crys. Growth 12, 88 (1972)

16. T. Sakata, K. Sakata, and I. Nishida, Phys. Status Solidi 20, K155 (1967).

17. N. Terao, Jap. J. Appl. Phys. 2, 565 (1963).

18. B.O. Marinder, Ark. Kemi 19, 435 (1963).

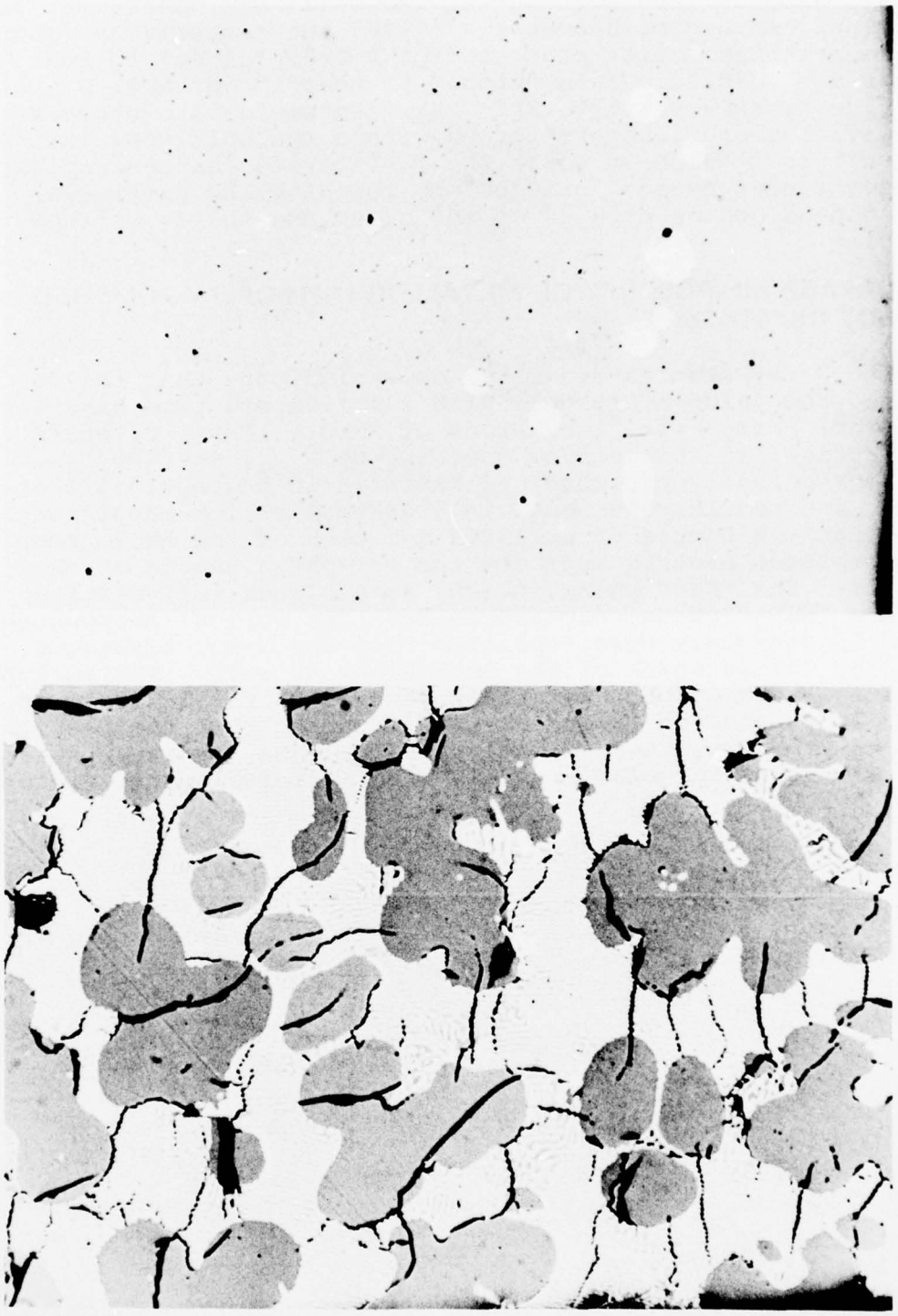
19. A. Magneli, G. Andersson, and G. Sundkvist, Acta Chem. Scand. 9, 1402 (1955)

of these samples (see Section 14, Table 11) are consistent with this view. At a stoichiometry x ~ 1.89 the resistivity (plotted on a logarithmic scale) changes from values "close" to that of NbO_2 at x = 1.90 to values "close" to that[20] of NbO, $\rho \sim 1.4 \times 10^{-5}$ Ω-cm, at x = 1.87. This behavior would take place if NbO particles or filaments formed within the bulk NbO_2 lattice. The specific x value at which the resistivity changes rapidly (the electrodes become "bridged" by touching NbO particles) would depend on the details of the sizes and shapes of these particles.

26. SURFACE MICROSCOPY OF METALLOGRAPHICALLY POLISHED NbO_x CRYSTALS

The X-ray studies described above indicate that the as-received NbO_x single crystals with x < 1.90 are two-phase and consist of "NbO_2" with inclusions of "NbO." Three crystals with labeled stoichiometries $NbO_{1.87}$, $NbO_{1.89}$, and $NbO_{1.90}$ were metallographically polished and examined in the optical microscope. The results are shown in Figure 64 at low magnification, ~ 230X, and in Figure 65 at 1320X for each of the above samples. These pictures clearly indicate the two-phase nature of the crystals. The "NbO" phase, which has a higher reflectivity than the "NbO_2" phase, appears white. The optical microscope method is obviously more sensitive than the X-ray technique, revealing the patterns of the inclusions as well. The switching characteristics of NbO_x materials studies so far indicate no strong dependence on stoichiometry (assuming that the resistance is above some minimum practical value). Thus, there appears to be no advantage in using crystals with a stoichiometry different from x = 2.00.

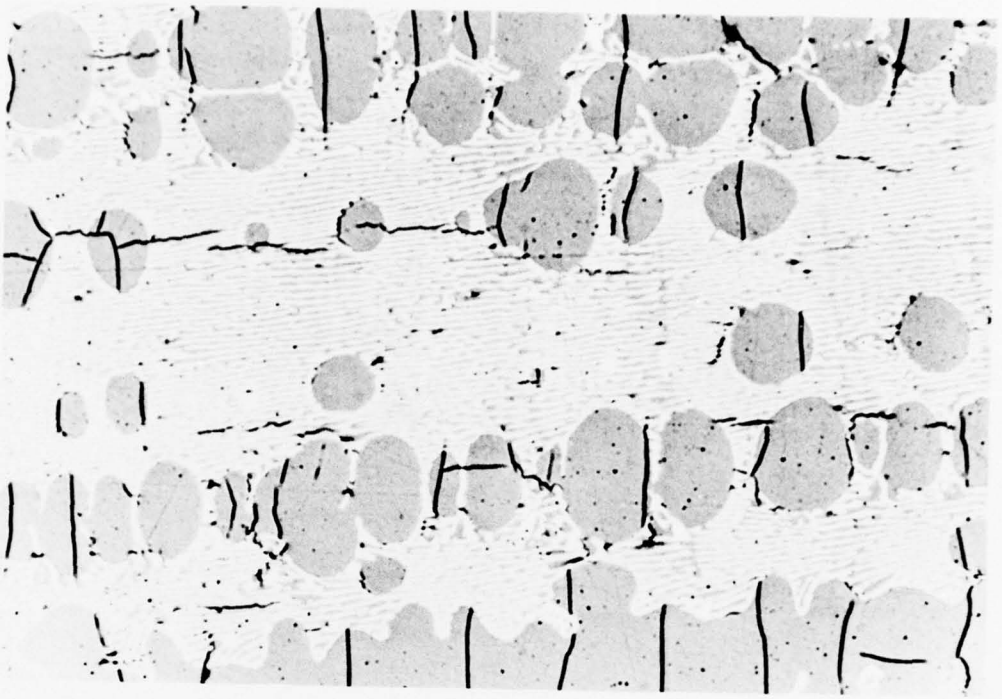
20. G.V. Chandrashekar, J. Moyo, and J.M. Honig, J. Solid State Chem. 2, 528 (1970).



(a)

(b)

Figure 64. Microscope pictures at 230X of metallographically polished NbO_x crystal surfaces for stoichiometry. (a) x = 1.90, (b) x = 1.89, and (c) x = 1.87.

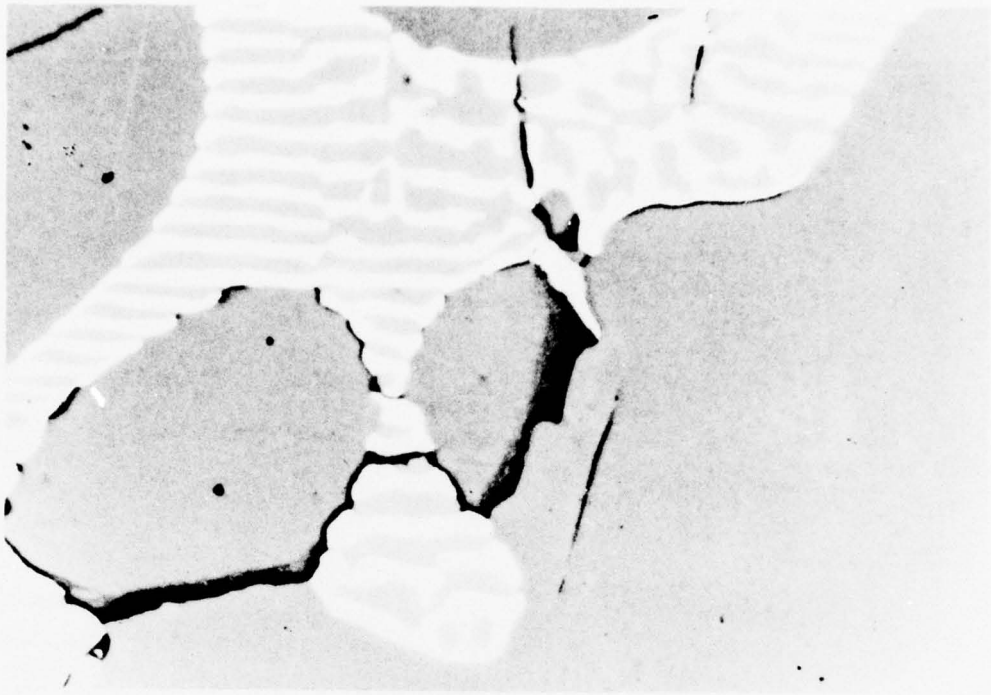


(c)

Figure 64. (Cont'd)

(a)

Figure 65. Microscope pictures at 1320X of metallographically polished NbO_x crystal surfaces for stoichiometry. (a) x = 1.90, (b) x = 1.89, and (c) x = 1.87.



(b)



(c)

Figure 65. (Cont'd)

27. GROWTH OF POLYCRYSTALLINE NbO_2 LAYERS ON NbO CRYSTALS

The polycrystalline niobium oxide chips used in switching devices described and discussed in detail earlier in this report were grown at Yeshiva University on single-crystal NbO substrates. The ~ 10 μm thick NbO_2 layers were made by exposing the cleaved NbO crystals to an oxidizing atmosphere at an average temperature of ~ 850 °C for ~ 48 hr. The actual temperatures used varied from 800 °C to 1000 °C for various time periods (see Section 2 for growth details). The oxidizing atmosphere was supplied by a mixture of Nb_2O_5 powder and NbO_2 powder sealed inside an isothermal fused quartz tube with the NbO crystals. Thermodynamic calculations on the niobium-oxygen system based on the data of Reed[21] are shown in Figure 66. At 850 °C, the partial pressure of oxygen over NbO_2 produced by a mixture of Nb_2O_5 and NbO_2 is ~ 10^9 times higher than the equilibrium pressure over stoichiometric NbO_2. This difference leads to rapid growth of the NbO_2 layer and perhaps to poor layer perfection.

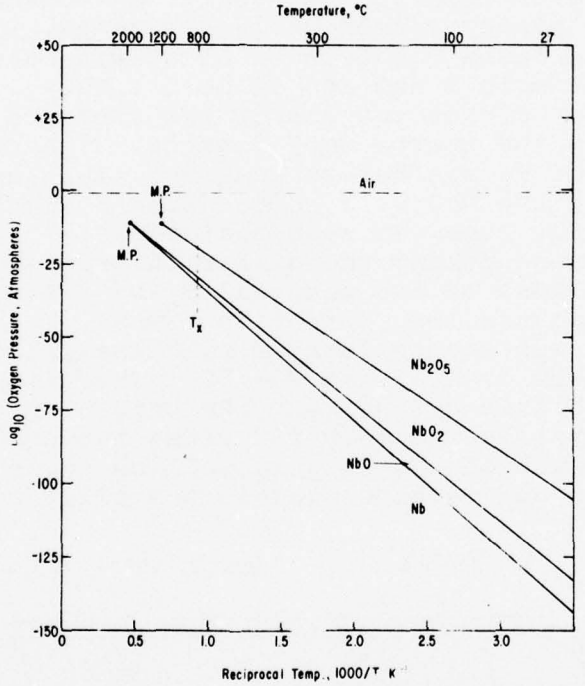


Figure 66. The oxygen partial pressure over the various two-phase regions of the niobium-oxygen system as a function of temperature. The lowest line indicates the oxygen pressure in equilibrium with a mixture of niobium metal and NbO. The semiconductor-metal transition in NbO_2 occurs at T_x. The melting points are indicated by "M.P."

21. T.B. Reed "Free Energy of Formation of Binary Compounds" (M.I.T Press, Cambridge, 1971).

A somewhat different isothermal technique was used here in preparing some polycrystalline NbO_2 layers on NbO substrates. The substrates were those initially furnished us. The original NbO_2 layers were removed by grinding. Our growth technique differed from that at Yeshiva University in several respects: (1) the oxide was grown at constant temperature; (2) hydrogen gas was used as a catalyst; and (3) carefully polished NbO surfaces rather than as-cleaved ones were oxidized. It was hoped that a denser grain structure in the polycrystalline layer would result, which in turn might produce a device with an improved pulse stability. However, devices made in the above fashion (electrical characteristics are briefly described in the next section) behaved in a manner similar to that of the as-received chips grown at Yeshiva University, except that the dc resistance of the new samples was lower.

A second technique was also used to oxidize polished NbO crystal surfaces, using again as starting material the NbO chips received from Yeshiva University. A schematic of this two-temperature process is shown in Figure 67. The NbO crystals were sealed in a fused quartz tube along with a pressed pellet consisting of 10 mole % NbO and 90 mole % NbO_2. In this method the crystals are held at one end of the tube and the pellet at the other end by the quartz wool inserts. The tube is filled with ~ 1/5 atm of H_2 gas before sealing. This H_2 gas aids in the oxidation of the NbO as a combination buffer and catalyst. The outside of the tube was also contained in H_2 gas at one atmosphere pressure during the oxidation process. This external H_2 prevents any loss of the internal H_2 by diffusion through the quartz during the long oxidation times. The quartz tube was heated in a resistance furnace with the pellet end held at 950 °C and the NbO crystals at 850 °C. The time at temperature was 48 hr. With this arrangement the partial pressure of oxygen over the NbO crystals was only 10^3 times the equilibrium value, and thus the growth of the polycrystalline oxide, it was thought, should be slower and perhaps contain a smaller concentration of

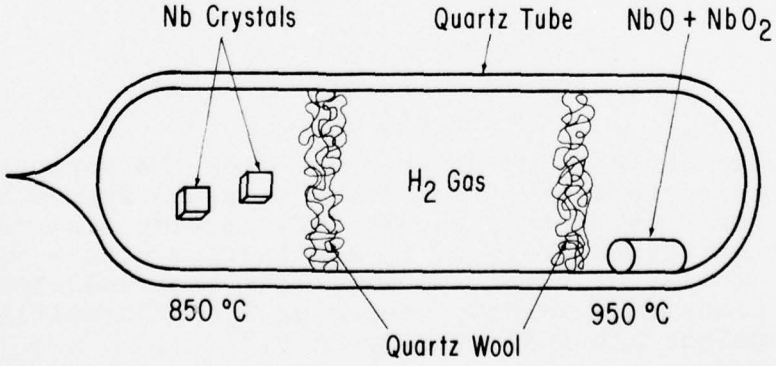


Figure 67. Schematic diagram of a two-temperature technique for oxidizing polished NbO crystal surfaces.

oxygen compared to the isothermal growth described earlier. If the isothermal growth with its larger oxygen overpressure corresponds to $x > 2.00$, then this growth might be closer to $x = 2.00$ and show increased resistivity. However, if the isothermal growth is close to $x = 2.00$, then the reduced oxygen overpressure could result in a stoichiometry $x < 2.00$ and a decreased resistivity.

Unfortunately, the latter situation prevailed, and, while the growth was much slower as predicted, the resulting resistivity was only ~ 150 Ω cm corresponding to stoichiometry $x < 2.00$. The switching characteristics of a device made from such a chip are also briefly described in the next section.

28. PULSE RESPONSE OF NbO_x POLYCRYSTALLINE LAYERS ON NbO SUBSTRATES

In Section 27 two different growth techniques were described and used for producing NbO_x/NbO chips. The switching characteristics of each are shown in Tables 18 and 19 for the isothermal and two-temperature processes, respectively. The latter device has a relatively thin NbO_x layer of thickness, ~ 5 μm, and may have a stoichiometry $x < 2.0$. It switched with only 100 V applied and after 250 pulses of length 3 ns each was degraded to 18 Ω resistance. We have not studied the dependence of device degradation on layer thickness. It is quite probable, however, that such degradation proceeds much more rapidly in thin layers.

TABLE 18

ELECTRICAL BEHAVIOR OF NbO_x LAYERS GROWN BY ISOTHERMAL PROCESS

Pulse Voltage V	Pulse Length ns	DC Resistance After Pulsing kΩ	Ambient Gas	Remarks	Oscilloscope Trace
100	3	7.3	Air	No switching, no sparks	
200	3	7.3		No switching, no sparks	
300	3	7.3		No switching, no sparks	
400	3	7.3		No switching, no sparks	
500	3	3.0		Switched, no sparks	Fig. 68a
500	3	1.4		Switched, no sparks	
400	3	0.4		Switched, no sparks	
300	3	1.4		Switched, no sparks	Fig. 68b
200	3	3.0		Partial switch, no sparks	Fig. 68c
500	3	1.3		Switched, no sparks	
500	3	2.5		Switched, no sparks	
500	3	1.4		Switched, no sparks	
500	3	1.2		Switched, no sparks	
500	50	0.0045		Switched, no sparks	
500	3	0.0048		Switched, no sparks (short circuit)	Fig. 68d

TABLE 19

ELECTRICAL BEHAVIOR OF NbO_x LAYERS GROWN BY TWO-TEMPERATURE PROCESS

Pulse Voltage V	Pulse Length ns	DC Resistance After Pulsing kΩ	Ambient Gas	Remarks	Oscilloscope Trace
100	3	0.317 (before) 0.0178	Air	Switched, no sparks	Fig. 69

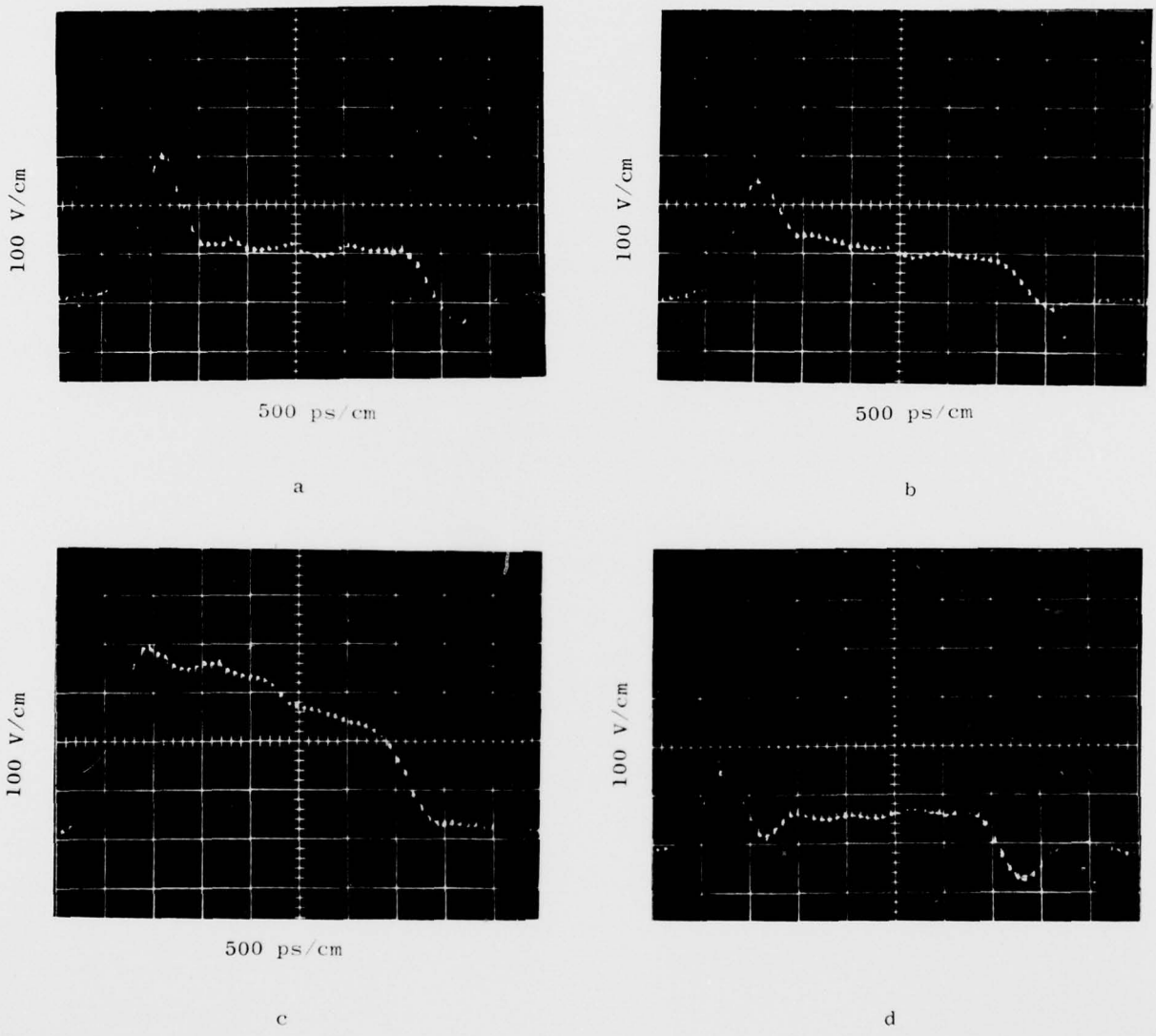


Figure 68. Switching in NbO_x layers grown by isothermal process. See Table 18.

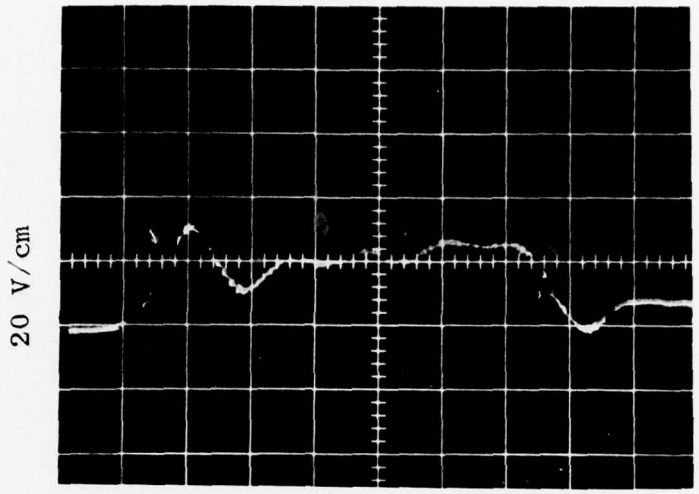


Figure 69. Switching in NbO_x layers grown by a two-temperature process. See Table 19.

29. ONE HUNDRED FINAL FEASIBILITY MODELS OF PROTECTIVE COAXIAL SWITCHES

One hundred final feasibility models of a protective coaxial switching device have been supplied, which completes item CLIN 0003. The basic device construction has been thoroughly described in previous sections of this report. All contain 25 μm gold wires, ball bonded to 125 μm dia. evaporated aluminum contacts on the device surface. The diode packages and the specially adapted GR-874T fitting into which they are inserted for use in 50 Ω lines has also been described in previous sections.

The NbO_2/NbO device chips were chosen mainly from as-received Batch #102. These number 91 in total and are labeled X-16-(1-49, 52-56), X-17-(2-24), and X-18-(1-14). The pulse characteristics of a typical sample are described in Table 15 of Section 22. Seven devices are made with NbO chips oxidized here according to procedures described for isothermal growth in Section 27. These are labeled G-2(3-9). The pulse characteristics of a typical G-2 chip are described in Table 18. Two devices were made with single-crystal chips. The one labeled $NbO_{1.95}A_2$ is described in Table 14 of Section 19 and the one labeled NbO_2 + Ti 5%A is described in Table 16 of Section 24. A listing of all device numbers and their resistance are given below in Table 20.

TABLE 20
RESISTANCE VALUES OF 100 FINAL FEASIBILITY MODELS OF PROTECTIVE COAXIAL SWITCHES

NUMBER	RESISTANCE kΩ	NUMBER	RESISTANCE kΩ
X-16-1	29.8	X-16-53	14.9
X-16-2	22.4	X-16-54	19.5
X-16-3	23.3	X-16-55	28.1
X-16-4	13.7	X-16-56	12.8
X-16-5	28.4	X-17-2	31.1
X-16-6	26.4	X-17-3	27.9
X-16-7	79.4	X-17-4	23.7
X-16-8	7.1	X-17-5	13.9
X-16-9	12.6	X-17-6	14.1
X-16-10	18.8	X-17-7	24.1
X-16-11	20.6	X-17-8	22.9
X-16-12	18.6	X-17-9	40.8
X-16-13	20.4	X-17-10	29.1
X-16-14	15.4	X-17-11	21.8
X-16-15	25.4	X-17-12	22.1
X-16-16	14.8	X-17-13	24.6
X-16-17	32.1	X-17-14	20.1
X-16-18	13.3	X-17-15	20.7
X-16-19	25.2	X-17-16	22.7
X-16-20	26.9	X-17-17	19.3
X-16-21	38.3	X-17-18	56.6
X-16-22	20.5	X-17-19	24.5
X-16-23	26.8	X-17-20	19.3
X-16-24	25.2	X-17-21	36.6
X-16-25	28.2	X-17-22	23.8
X-16-26	19.2	X-17-23	20.1
X-16-27	14.3	X-17-24	20.3
X-16-28	26.1	X-18-1	29.6
X-16-29	17.3	X-18-2	27.1
X-16-30	25.4	X-18-3	29.3
X-16-31	27.4	X-18-4	18.8
X-16-32	24.3	X-18-5	22.2
X-16-33	21.1	X-18-6	24.1
X-16-34	27.9	X-18-7	22.0
X-16-35	18.9	X-18-8	25.7
X-16-36	27.3	X-18-9	26.7
X-16-37	15.6	X-18-10	33.2
X-16-38	22.4	X-18-11	36.8
X-16-39	27.0	X-18-12	30.5
X-16-40	27.0	X-18-13	22.9
X-16-41	25.6	X-18-14	105.0
X-16-42	21.7	G-2-3	13.7
X-16-43	20.1	G-2-4	15.4
X-16-44	14.2	G-2-5	8.7
X-16-45	15.2	G-2-6	8.5
X-16-46	19.7	G-2-7	6.0
X-16-47	21.7	G-2-8	8.9
X-16-48	32.0	G-2-9	6.9
X-16-49	27.4	$NbO_{1.95}A_2$	34.7
X-16-52	16.0	$NbO_2Ti5\%A$	2.02

AD-A047 732 GENERAL ELECTRIC CO SCHENECTADY N Y RESEARCH AND DEV--ETC F/G 9/1
PROTECTIVE COAXIAL SWITCHING DEVICES.(U)
OCT 77 L M LEVINSON, H R PHILIPP, G A SLACK DAAB07-76-C-1331

UNCLASSIFIED SRD-77-158 ECOM-76-1331-F NL

2 OF 2
ADI
A047 732



END
DATE
FILMED
1 -78
DDC

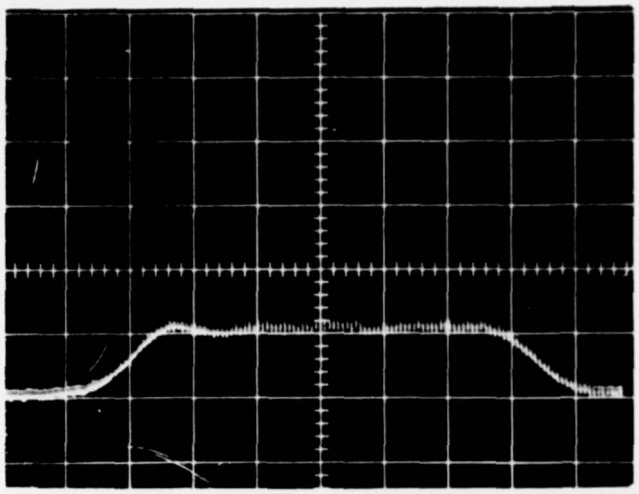
30. FINAL STATEMENT OF MANUFACTURING FEASIBILITY

Mounted coaxial switching devices which utilize as-received NbO/NbO_2 chips can be made according to the procedures outlined in Section 12 and described in detail in Section 6. A number of hand operations are presently required, owing in particular to the differences in physical nature of the as-received chips. However, all procedures are straightforward and make use of common, generally available processing and manufacturing equipment and other readily purchasable items such as diode packages. For use in 50Ω GR lines, a specially adapted GR-874T "tee" is used into which the diode package is inserted. It is described in Section 6. If large numbers of these are required, special arrangements with the manufacturer of GR fittings to produce such modified units could probably be made.

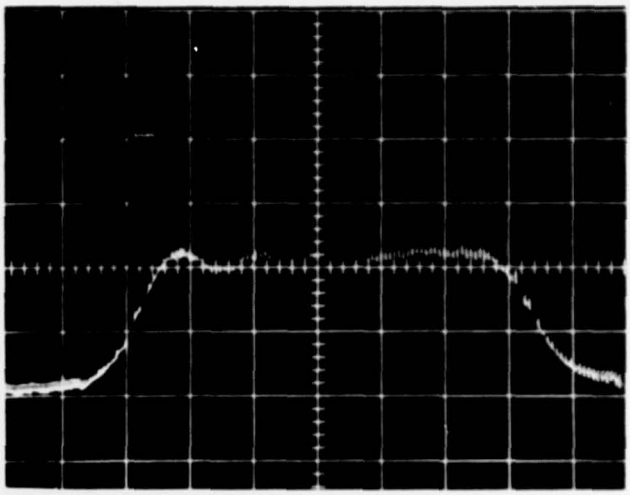
Devices which utilize as-received NbO_x single-crystal material require a cutting and thinning procedure which is described in detail in Section 17. As stated there, this procedure is tedious and involves a number of operations which are not easily amenable to high-volume, low-cost processing techniques.

31. THRESHOLD SWITCHING VOLTAGE

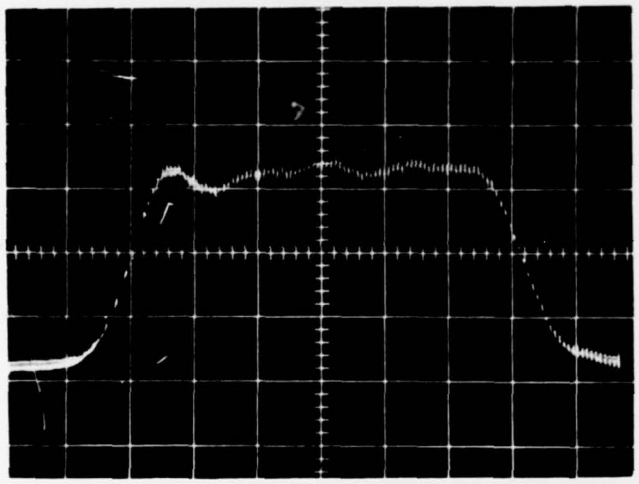
Throughout this report we have used the term "threshold switching voltage," V_{th}, to denote the maximum voltage which appears across the device (in response to a voltage pulse) in its low impedance or switched state. This definition follows from Figure 1 of *Technical Guidelines DAA1307-76-Q-1335*. For the devices made from ECOM chips and described in this report, the threshold switching voltage is typically 100 to 300 V (when corrected for package inductance) and occurs within the first nanosecond of the applied voltage pulse. However, the voltage necessary to switch the material to its low impedance state may be considerably larger than the threshold switching value. This is illustrated in Figure 70 where the device response is shown for 3 ns pulses of 100, 200, 300, 400, and 500 V. As is clearly evident the device remains in its high impedance state for pulse voltages of at least 400 V, and thus any circuit in parallel with this device will, under these conditions, experience the full pulse voltage. When the pulse voltage is further increased to 500 V, the device switches to its low impedance state in less than one nanosecond, and the maximum voltage observed, the threshold switching voltage, is ~ 200 V (when account is also taken of inductive effects). It is very important to recognize that circuit protection may not be obtained even for input voltage pulses considerably in excess of the threshold switching voltage as measured and described in this report. The device must switch before circuit protection for voltages of value V_{th} is achieved.



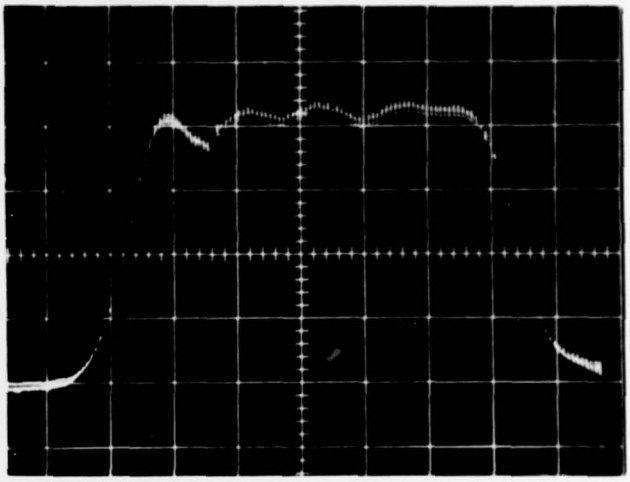
a



b



c



d

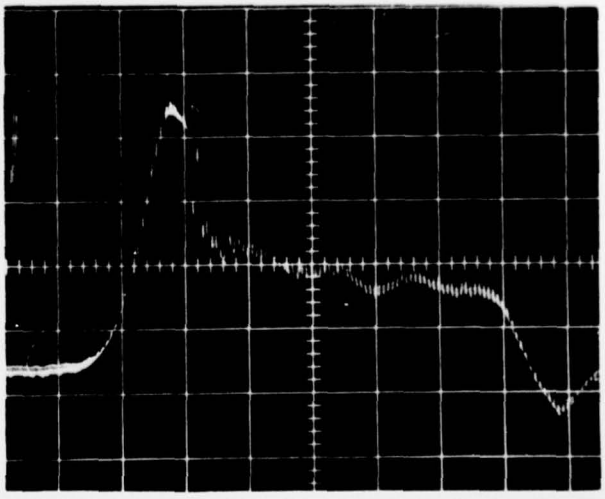


Figure 70. The response of chip No. X-15-29 to input voltage pulses of 100, 200, 300, 400, and 500 V. The device does not switch into its low impedance state until the applied voltage exceeds 400 V.

32. CONCLUSIONS

The primary conclusions are as follows. The NbO/NbO_2 chips supplied by ECOM do exhibit switching with a delay time of less than 1 ns. The electrical parameters of these chips, however, do not meet the specifications listed in Technical Guidelines DAAB07-76-Q-1335. The threshold switching voltage is typically 100 to 300 V and not < 100 V, as specified. Switching characteristics and off-state resistance are highly variable among chips and even from place to place on a single chip. Device degradation with repeated pulsing is observable for 3 ns pulse width, and degradation is markedly accelerated for larger pulse widths. Samples subjected to long (50 ns) pulses or extensive pulsing (thousands of 3 ns pulses) exhibit deep channels through the NbO_2 layer to the NbO substrate. Samples with less severe pulsing show less physical damage, but deterioration is sometimes observed in device off-state resistance. There is no clear correlation between physical damage and device off-state resistance. The switching characteristics and degradation with pulsing of the devices do not appear to be a function of the electrode material. Polycrystalline NbO_x layers prepared by oxidizing NbO single-crystal surfaces probably have stoichiometry $x < 2.0$ when the available "oxygen" pressure is reduced compared to that used by Yeshiva University in preparing the NbO_2/NbO chips received at the onset of the present work.

The single-crystal devices exhibit switching at approximately the same field, 20 to 30 V/μm, as found for the NbO_2/NbO polycrystalline devices. The electrical stability of the thicker single-crystal devices is, however, much better. Switching and device degradation are not dependent on the crystal stoichiometry, NbO_x for $1.89 \leq x \leq 2.0$. Sparking frequently accompanies device switching. This sparking is not related to the dielectric strength of the gas environment but rather, is probably associated with a thermal volatilization of material from the NbO_x upon pulsing. Damage in the form of pits ~ 25 μm in diameter and ~ 2 μm deep is observed around the periphery of the ball bond contact in pulsed single-crystal samples. The amount of damage is correlated with the severity (number and length) of the applied pulses. Damage also occurs under the ball bond contact but is not nearly as pronounced. The switching characteristics of Ti-doped (5%) single-crystal NbO_2 samples are similar to those of the undoped crystal; however, the resistance is lower. X-ray studies of as-received NbO_x single-crystal samples with labeled stoichiometries of 1.89 and 1.87 indicate that they are two-phase and consist of NbO_2 with inclusions of NbO. This two-phase nature is clearly confirmed by microscopic examination.

33. RECOMMENDATIONS

1. Polycrystalline NbO_2 on NbO

Coaxial switching devices made from the polycrystalline NbO_2 on NbO chips supplied by ECOM (physically described in

Section 2) do not fulfill requirements for NEMP protective devices as described in the Detailed Requirements Section (3.2.1 to 3.2.10) of Technical Guidelines DAAB07-76-Q-1335. It is stated therein that the device must have sufficiently high impedance in the off state to ensure minimum insertion loss (less than 0.4 db at 200 MHz), while in the on state the device voltage should never exceed 100 V with a corresponding delay time of less than 1 ns and, in addition, should withstand 1000 switching cycles of 100A for 1 μs or 20 A for 5 μs without suffering a significant change in protection capabilities.

It was found, however, that, although the device did exhibit switching, the switching voltages were typically 100 to 300 V and not < 100 as specified and that device degradation took place for pulses of 50 ns duration and even for extensive pulsing in the 3 ns range.

If the NbO_2 layers of the ECOM chips were made thinner, the switching threshold could be reduced to the required level. However, a device made from such a chip might show an increased insertion loss and most probably would degrade even faster than one fabricated from the as-supplied chips.

If the Detailed Requirements set forth in DAAB07-76-Q-1335 are firm and polycrystalline chips are desirable, then it is recommended that alternative work plans be initiated which show better prospects of meeting the NEMP requirements. Areas for further investigation are outlined below:

(a) Extend the evaluation of NbO_2/NbO chips on which the grain size and structure of the NbO_2 layer is altered by changes in the oxidation procedures.

(b) Evaluate NbO_2/NbO chips which utilize buried contacts (for example, In diffusion in NbO_2 layer). This may reduce surface deterioration and hence improve device stability.

2. Single-Crystal NbO_x

Coaxial switching devices made from thinned (~ 25 μm) single-crystal chips supplied by ECOM switch at essentially the same electric field but exhibit far superior pulse stability compared to the polycrystalline devices which have thinner NbO_2 layers. To meet the switching voltage requirement (~ 100 V), however, the crystals would have to be thinned to ~ 8 μm or less. Such thin single-crystal devices have not been fabricated, and hence their pulse stability is not known. It would appear, nevertheless, that work on single-crystal materials rather than poly-crystalline layers is a preferred approach toward the eventual satisfaction of some or all of the requirements for NEMP protective devices

using niobium dioxide. Recommended areas for further investigation are outlined below.

(a) Evaluate NbO_2 single-crystal devices which utilize buried contacts.

(b) Evaluate NbO_2 single-crystal devices which have been "preformed" by controlled prepulsing. This might allow thicker crystalline chips to be used, thus eliminating certain fabrication difficulties. Device stability may also be enhanced.

(c) Examine new structures and methods (for example, epitaxial growth of crystalline NbO_2 on conducting substrates) for fabricating devices which eliminate thinning procedures.

It is also of importance to affirm that the NbO_2 devices studied here do have unique properties as fast response switches. Thus, applications should be sought, in addition to NEMP protection, which take advantage of the unique properties and present capabilities of NbO_2 devices. As a longer term project, basic studies of the mechanisms of switching in materials such as NbO_2 should be undertaken. Such work would help to determine the ultimate potential of these devices and would aid in the discovery of possible material alternatives to NbO_2.

3. *Other Materials*

There are other types of devices, such as metal oxide varistors[22] which also exhibit fast response time and are useful in many applications where it is desirable to "clamp" the voltage at some predetermined value in the presence of line transients. Devices made from metal oxide varistor materials were fabricated and mounted in the diode package described and used in this report for the NbO_2 study. For a thickness of ~ 0.25 mm, the clamp voltage was ~ 100 V, and the device showed excellent pulse stability. The insertion loss for ~ 6×10^{-4} cm^2 contacts was 3 db at 480 MHz and ~ 1 db at 200 MHz. It is thus recommended that alternative devices such as metal oxide varistors be examined for NEMP and other applications.

22. See L.M. Levinson and H.R. Philipp, J. Appl. Phys. 46, 1332 (1975) and cited references.

34. REFERENCES

1. A.L. Bowman, et al, Acta Crystallogr. 21, 843 (1966).

2. G. Braver and H. Morawietz, Anorg. Allg. Chem. 317, 13 (1962).

3. G. Anderson and A. Magneli, Acta Chem. Scand. 11, 1065 (1957).

4. B.O. Marinder, Ark. Kemi 19, 435 (1963).

5. N. Terao, Jpn. J. Appl. Phys. 2, 565 (1963).

6. A. Magneli, et al, Acta Chem. Scand, 9, 1402 (1955).

7. F.E. Terman, Radio Engineers Handbook (McGraw Hill, New York 1943).

8. G. Belanger, J. Destry, C. Perluzzo, and P.M. Raccah, Can. J. Phys. 52, 2272 (1974).

9. S. Dushman, Vacuum Technique (John Wiley, New York, 1949), p. 42.

10. S.H. Shin, T.H. Halpern, and P.M. Raccah, Mater. Res. Bull. 10, 1061 (1975).

11. R.P. Elliott, Trans. Am. Soc. Met. 52, 990 (1960).

12. J.F. Marucco, R. Tetot, P. Gerdanian, and C. Picard, J. Solid State Chem. 18, 97 (1976).

13. R.F. Jannick and D.M. Whitmore, J. Phys. Chem. Solids 27, 1183 (1966).

14. R. Pynn, J.D. Axe, and R. Thomas, Phys. Rev. B13, 2965 (1976).

15. T. Sakata, K. Sakata, G. Höfer, and T. Horiuchi. J. Crys. Growth 12, 88 (1972).

16. T. Sakata, K. Sakata, and I. Nishida, Phys. Status Solidi 20, K155 (1967).

17. N. Terao, Jap. J. Appl. Phys. 2, 565 (1963).

18. B.O. Marinder, Ark. Kemi 19, 435 (1963).

19. A. Magneli, G. Anderson, and G. Sundkvist, Acta Chem. Scand. 9, 1402 (1955).

20. G.V. Chandrashekar, J. Moyo, and J.M. Honig, J. Solid State Chem. 2, 528 (1970).

21. T.B. Reed "Free Energy of Formation of Primary Compounds" (M.I.T. Press, Cambridge, 1971).

22. See L.M. Levinson and H.R. Philipp, J. Appl. Phys. 46, 1332 (1975) and cited references.

DISTRIBUTION LIST

101 Defense Documentation Center
Attn: DDC-TCA
Cameron Station (Bldg 5)
*012 Alexandria, VA 22314

103 Code R123, Tech Library
DCA Defense Comm Engrg Ctr
1860 Wiehle Ave
001 Reston, VA 22090

104 Defense Communications Agency
Technical Library Center
Code 205 (P.A. Tolovi)
001 Washington, DC 20305

200 Office of Naval Research
Code 427
001 Arlington, VA 22217

203 Gidep Engineering &
Support Dept
TE Section
PO Box 398
001 Norco, CA 91760

205 Director
Naval Research Laboratory
Attn: Code 2627
001 Washington, DC 20375

206 Commander
Naval Electronics
Laboratory Center
Attn: Library
001 San Diego, CA 92152

207 CDR, Naval Surface Weapons
Center
White Oak Laboratory
Attn: Library, Code WX-21
001 Silver Spring, MD 20910

210 Commandant, Marine Corps
Hq, US Marine Corps
Attn: Code LMC
002 Washington, DC 20380

211 Hq, US Marine Corps
Attn: Code INTS
001 Washington, DC 20380

212 Command, Control &
Communications Division
Marine Corps Development
& Educ Comd
001 Quantico, VA 22134

301 Rome Air Development Center
Attn: Documents Library
(TILD)
001 Griffiss AFB, NY 13441

307 Hq ESD (DRI
L.G. Hanscom AFB
001 Bedford, MA 01731

314 Hq, Air Force Systems
Command
Attn: DLCA
Andrews AFB
001 Washington, DC 20331

403 CDR, US Army Missile Command
Redstone Scientific Info
Center
Attn: Chief, Document
Section
002 Redstone Arsenal, AL 35809

404 Commander
US Army Missile Command
Attn: DRSMI-RE (Mr. Pittman)
001 Redstone Arsenal, AL 35809

405 Commander
US Army Aeromedical
Research Lab
Attn: Library
001 Fort Rucker, AL 36362

406 Commandant
US Army Aviation Center
Attn: ATZQ-D-MA
003 Fort Rucker, AL 36362

407 Director, Ballistic Missile
Defense
Advanced Technology Center
Attn: ATC-R, PO Box 1500
001 Huntsville, AL 35807

*Decrease to 2 copies if report is not releasable to public.
See ECOMR 70-31 for types of reports not to be sent to DDC.

408 Commandant
US Army Military Police School
Attn: ATSJ-CD-M-C
003 Fort McClellan, AL 36201

417 Commander
US Army Intelligence Center & School
Attn: ATSI-CD-MD
002 Fort Huachuca, AZ 85613

418 Commander
Hq Fort Huachuca
Attn: Technical Reference Div
001 Fort Huachuca, AZ 85613

419 Commander
US Army Electronic Proving Ground
Attn: STEEP-MT
002 Fort Huachuca, AZ 85613

420 Commander
USASA Test & Evaluation Center
Attn: IAO-CDR-T
001 Fort Huachuca, AZ 85613

421 Commander
Hq US Army Communications Center
Attn: CC-OPS-SM
001 Fort Huachuca, AZ 85613

437 Deputy for Science & Technology Office,
Assist Sec Army (R&D)
001 Washington, DC 20310

438 HQDA (DAMA-ARP/DR. F.D. Verderame)
001 Washington, DC 20310

455 Commandant
US Army Signal School
Attn: ATSN-CTD-MS
001 Fort Gordon, GA 30905

470 Director of Combat Developments
US Army Armor Center
Attn: ATZK-CD-MS
002 Fort Knox, KY 40121

473 Commandant
US Army Ordanance School
Attn: ATSL-CD-OR
002 Aberdeen Proving Ground, MD 21005

475 CDR, Harry Diamond Laboratories
Attn: Library
2800 Powder Mill Road
001 Adelphi, MD 20783

477 Director
US Army Ballistic Research Labs
Attn: DRXBR-LB
001 Aberdeen Proving Ground, MD 21005

481 Harry Diamond Laboratories,
Dept of Army
Attn: DRXDO-RCB (Dr. J. Nemarich)
2800 Powder Mill Road
001 Adelphi, MD 20783

482 Director
US Army Materiel Systems Analysis Acty
Attn: DRXSY-T
001 Aberdeen Proving Ground, MD 21005

499 Commander
US Army Tank-Automotive Command
Attn: DRDTA-RH
001 Warren, MI 48090

507 CDR, US Army Aviation Systems Command
Attn: DRSAV-E
PO Box 209
001 St. Louis, MO 63166

511 Commander, Picatinny Arsenal
Attn: SARPA-FR-S
Bldg 350
002 Dover, NJ 07801

512 Commander
Picatinny Arsenal
Attn: SARPA-ND-A-4 (Bldg 95)
001 Dover, NJ 07801

513 Commander
Picatinny Arsenal
Attn: SARPA-TS-S #59
001 Dover, NJ 07801

515 Project Manager, Rembass
Attn: DRCPM-RBS
002 Fort Monmouth, NJ 07703

517 Commander
US Army Satellite
Communications Agcy
Attn: DRCPM-SC-3
002 Fort Monmouth, NJ 07703

518 TRI-TAC Office
Attn: TT-SE (Dr. Pritchard)
001 Fort Monmouth, NJ 07703

531 CDR, US Army Research Office
Attn: DRXRO-IP
PO Box 12211
001 Research Triangle Park, NC
27709

532 CDR, US Army Research Office
Attn: DRXRO-PH
(Dr. R. J. Lontz)
PO Box 12211
001 Research Triangle Park, NC
27709

533 Commandant
US Army Inst for Military
Assistance
Attn: ATSU-CTD-MO
001 Fort Bragg, NC 28307

537 CDR, US Army Tropic Test
Center
Attn: STETC-MO-A
(Tech Library)
Drawer 942
001 Fort Clayton, Canal Zone 09827

543 Division Chief
Meteorology Division
Counterfire Department
002 Fort Sill, OK 73503

554 Commandant
US Army Air Defense School
Attn: ATSA-CD-MC
001 Fort Bliss, TX 79916

555 Commander
US Army Nuclear Agency
001 Fort Bliss, TX 79916

556 Commander, Hq Master
Technical Information
Center
Attn: Mrs. Ruth Reynolds
001 Fort Hood, TX 76544

564 CDR, US Army Security
Agency
Attn: IARDA-IT
Arlington Hall Station
001 Arlington, VA 22212

568 Commander
US Army Mobility Eqp
Res & Dev Cmd
Attn: DRXFB-R
001 Fort Belvoir, VA 22060

569 Commander
US Army Engineer
Topographic Labs
Attn: ETL-TD-EA
001 Fort Belvoir, VA 22060

572 Commander
US Army Logistics Center
Attn: ATCL-MC
002 Fort Lee, VA 22801

602 Director, Night Vision
Laboratory
US Army Electronics Command
Attn: DRSEL-NV-D
001 Fort Belvoir, VA 22060

603 CDR/DIR, Atmospheric
Sciences Laboratory
US Army Electronics Command
Attn: DRSEL-BL-SY-S
001 White Sands Missile Range,
NM 88002

604 Chief
Ofc of Missile Electronic Warfare
Electronic Warfare Lab, ECOM
001 White Sands Missile Range, NM 88002

606 Chief
Intel Material Dev & Support Ofc
Electronic Warfare Lab, ECOM
001 Fort Meade, MD 20755

680 Commander
US Army Electronics Command
000 Fort Monmouth, NJ 07703

1	DRSEL-PL-ST
1	DRSEL-NL-D
1	DRSEL-WL-D
1	DRSEL-VL-D
3	DRSEL-CT-D
1	DRSEL-BL-D
1	DRSEL-TL-DT
*3	DRSEL-TL-M
1	DRSEL-TL-M (Ofc of Record)
1	DRSEL-TE
1	DRSEL-MA-MP
**2	DRSEL-MS-TI
1	DRSEL-GG-TD
1	DRSEL-PP-I-PI
1	DRSEL-GS-H
1	DRSEL-CG
2	DRSEL-PA
1	DRSEL-RD
1	DRSEL-TL-D
1	USMC-LNO
1	TRADOC-LNO
25	DRSEL-TL-MD

700 CINDAS
Purdue Industrial Research Park
2595 Yeager Road
001 W. Lafayette, IN 47096

701 MIT - Lincoln Laboratory
Attn: Library (Rm A-082)
PO Box 73
002 Lexington, MA 02173

703 NASA Scientific & Tech Info Facility
Baltimore/Washington Intl Airport
001 PO Box 8757, MD 21240

704 National Bureau of Standards
Bldg 225, Rm A-331
Attn: Mr. Leedy
001 Washington, DC 20231

705 Advisory Group on Electron Devices
201 Varick Street, 9th Floor
002 New York, NY 10014

706 Advisory Group on Electron Devices
Attn: Secy, Working Group D (Lasers)
201 Varick Street
002 New York, NY 10014

707 TACTEC
Battelle Memorial Institute
505 King Avenue
001 Columbus, OH 43201

709 Plastics Tech Eval Center
Picatinny Arsenal, Bldg 176
Attn: Mr. A.M. Anzalone
001 Dover, NJ 07801

710 Ketron, Inc.
Attn: Mr. Frederick Leuppert
1400 Wilson Blvd, Architect Bldg
002 Arlington, VA 22209

711 Metals and Ceramics Inf Center
Battelle
505 King Avenue
001 Columbus, OH 43201

---

* Or number specified in contract. Add COTR's mail symbol.
** Unclassified reports only.

712 Yeshiva University
Belfer Graduate School of Science
2495 Amsterdam Avenue
New York, New York 10033
001 Attn: Dr. Pollack

713 Rutgers University
The State University of New Jersey
New Jersey Ceramic Research Station
New Brunswick, New Jersey 08903
001 Attn: Professor Edward J. Smoke

714 Rutgers University
The State University of New Jersey
Electrical Engineering Department
New Brunswick, New Jersey 08903
001 Attn: Dr. Lalevic

715 Honeywell Corporation
1885 Douglas Drive, North
Attn: Wm. B. Harrison
Orlen F. Rice
001 Minneapolis, Minn 55422

717 Bell Telephone Laboratories
Murray Hill, New Jersey
001 Attn: Dr. J. Williams

718 State University of New York
College of Ceramics at Alfred University
Alfred, New York 14802
001 Attn: Dr. Edward E. Mueller

719 Owens-Illinois Inc
South Technical Center
1510 North Westwood Avenue
Toledo, OH 43601
001 Attn: Dr. J.M. Woulbrown

720 University of Illinois
Physics Dept.
Chicago Circle - Box 4348
Chicago, IL 60680
001 Attn: Dr. Paul Raccah

721 Los Alamos Scientific Laboratory
Group AP - 1
Mail Station 566
Los Alamos, NM 87545
001 Attn: Mr. Walt Willis

721 CDR Harry Diamond Laboratories
Woodbridge Facility
2800 Powder Hill Road
Adelphi, MD 20753
001 Attn: Dr. R.E. McCoskey

Applied Physics Laboratory
The Johns Hopkins University
Laurel, MD 20810
Attn: Dr. Charles Feldman